Founded 1905

Process Parameter Optimization for Direct Metal Laser Sintering (DMLS)

BY

NingYu

(B. Eng.)

A DISSERTATION SUBMITTED

FOR THE DEGREE OF DOCTOR OF PHILOSOPHY

DEPARTMENT OF MECHANICAL ENGINEERING

NATIONAL UNIVERSITY OF SINGAPORE

2005

ACKNOWLEDGEMENT

I would like to express my sincere appreciation to my supervisors, Assoc. Prof. Jerry Fuh and Assoc. Prof. Wong Yoke San, for their invaluable guidance, insightful comments, strong encouragements and personal concerns both academically and otherwise throughout the course of the research. I benefit a lot from their comments and critiques. I will also like to thank Assoc. Prof. Loh Han Tong, who has given me invaluable suggestions for this research.

Thanks are also given to my colleagues in CIMPAS lab for their significant helps and discussions: Mr. Yang Yong, Mr. Mani Mahesh, Ms. Zhu Haihong, Dr. Tang Yaxin and Ms. Wang Xinhua. They have provided me with helpful comments, great friendship and a warm community during the past few years in NUS.

I would also like to thank all my friends with whom I enjoyed my research and social life at NUS and all my well-wishers, who have extended their support in one way or another.

I would like to thank the National University of Singapore for providing me with research scholarship to support my study.

Finally, my deepest thanks go to my parents, for their encouragements, moral supports and loves.

Summary

Compared with traditional material subtractive manufacturing technologies, rapid prototyping is a layer-based material additive process and can produce a 3-D freeform object with a CAD-defined geometric model directly. It offers rapid, cost-effective and low-volume manufacturing of physical parts. As one of the advanced rapid prototyping and manufacturing processes, the direct metal laser sintering (DMLS) process gives designers the possibility to build parts of almost any complexity in a wide range of metallic materials. However, as a relatively new technique, it is still in the development stage as the resulting properties of the sintered metallic parts are not yet strong enough for many industrial applications.

The aim of this research is to improve the overall performance of the DMLS process by optimizing the control of process parameters that have very strong influence on the quality of the built part. An intelligent parameter selection (IPS) system has been implemented involving artificial neural network, design of experiment (DOE), and multi-objective optimization. The set of process parameters can be determined according to different requirements using the IPS system. A test part was built to verify that the IPS optimization strategy is satisfactory in achieving the better part quality.

The sintered material is known to be anisotropic because of its dependency on the hatch direction and part orientation. Besides the direction dependency, the properties of the material in each layer are also not homogenous. The length of the hatch line is one significant factor that affects the quality of the final part. Short hatch length and its corresponding short scanning time result in material heterogeneity in the part,

which has a negative effect on the part quality because the hatch line changes with the variation of the 2D-layer geometric shapes. The negative effect of short hatch lines on part accuracy and mechanical properties was quantitatively analyzed with a designed experimental method. A layer-based hatch optimization method using a genetic algorithm (GA) approach has been developed to determine the hatch direction with the minimum number of short hatch lines. A rotor shade model was built with the optimized hatch direction to demonstrate the effectiveness of the proposed method.

To further reduce the effect of the residual short lines, a speed compensation (SC) method that includes experimental data collection method and statistical analysis was developed. Based on the SC method, the negative effect of the short hatch lines can be reduced significantly. It improves the part homogeneity effectively and makes further quality improvement.

TABLE OF CONTENTS

List of Illustrations

List of Tables

List of Notation

[Chapter 2]

An	Andrew number
$K1, K2$	coefficient factors of the strength model

[Chapter 3]

D	focus distance of the lens
e	distance between the center of X and Y mirrors
θ_x, θ_y	projection angles of the beam with the XZ and YZ planes
f_r	the travel length of the beam from the center of the X mirror to the focus point
s	length of the vector from the target point to the origin
K	calibration factor
x, y, z	coordinate values
$\Delta x, \Delta y$	errors in x, y values
K_x, K_y	calibration factors in the X-direction and Y-direction
L	set length of the scan line
L^1	measured length of the scan line
L^1_{ave}	average measured length
K_x^1 , K_y^1	optimized calibration factor in the X-direction and Y-direction

[Chapter 4]

T_m	melting-point of the binder
T_g	glass transition temperature of amorphous polymer
I_0	energy intensity in the center point of the laser beam
r	distance from the point to the center of the laser beam
w_0	distance in which the laser energy equals to 1/e of I_0
e	base of natural logarithms
P	laser power
E	irradiation
dA	differential area
R	radius of the zone of influence
E_{absorb}	actual energy absorbed by the powder
α_R	absorptivity
S_{Scan}	scan speed
HS	hatch space
t_{eff}	time for the powder to absorb the 99.99% laser energy
t_{Total}	denotes the total build time
TH	layer thickness
V_{Parts}	total part volume
$V_{Cavities}$	cavity volume in the part
H_{Height}	part height
S_{Jump}	jump-scan speed
t_{Layer}	building time taken from each layer

ΔL	thermal shrinkage
μ	linear thermal expansion coefficient
ΔT	temperature gradient
R_a	arithmetic mean deviation
T	layer thickness
θ	angle between the digital model surface and the build direction
dl	differential length along the layer contour
de_i	sectional area of ΔABC
σ_0	strength of fully dense material
C	empirical material constants
m	empirical material constants
p	fractional density
Ra	surface roughness

[Chapter 5]

k	non-input unit
$x_1, x_2, ..., x_m$	input values of NN
$\omega_{k1}, \omega_{k2}, ..., \omega_{km}$	weights
e_j	error between the network output with the target output of output unit j
$\hat{y}_j$	network output of output unit j
y_j	target output (given by experimental data) of output unit j
$\varphi(.)$	activation function
θ_j	bias of unit j

η	learning factor
o_i	output of the preceding unit *i*
RMSE	Root-Mean-Square Error
N	total number of sample pairs
$\bar{y}$	average value of the corresponding target outputs
V	input of normalization
A	normalized value
D_{Hatch}	default hatch value
$D_{Thickness}$	default thickness value
$L_{Scanlines}$	distance of each produced scan line
$L_{Jumplines}$	distance between the endpoint of the first scan line, with the start point of the next scan line
K_i	performance factor of resulting property *i*
K_{all}	integrated factor
P_{ji}	ability index
V_{ji}	corresponding resulting property value in the case *j*
Set_i	resulting weight factor of resulting property *i*
$R_{i,Best}$, $R_{i,worst}$	best and worst values of resulting properties *i*

[Chapter 6]

T	temperature
T_m	melting temperature of the binder
T_n	process ambient temperature

t_p	time when the laser beam focuses on the sintered point *P*
L	hatch length
σ	ultimate tensile strengths

[Chapter 7]

S	percentage shrinkage
L	nominal length of the test block (hatch line length)
L'	measured length of the test block
a, b and c	coefficients
F	effect of the hatch length on the heterogeneity of each layer
N_{total}	denotes the total number of hatch lines in the layer
α	angle of the hatch direction
x	input variable
y	output variable

[Chapter 8]

β	unknown coefficient
ν	prediction validity
Lc	critical length
$f(.)$	response function
x_1	input variable (scan speed)
x_2	input variable (hatch line length)
y	output (percentage shrinkage)

Chapter 1

Introduction

The manufacturing industry is always looking for ways to improve production while reducing cost. Traditional material subtractive manufacturing technologies such as, milling, tapping, turning, etc. create 3D physical models by removing material using cutting tools. The movement of the cutting tools is manually controlled by the machinist. With the rapid development of CAD/CAE technology since early 70's, automated manufacturing processes with numerical control machine tools have become possible. The emergence of Computerized Numerical Control (CNC) and High Speed (HS) milling technologies reduce the process time and hence significantly increase the productivity. However, as a mature technology, subtractive manufacturing still has some disadvantages due to its working principle. One major disadvantage is the dependence on the geometric complexity. Features such as small holes inside a block are hard to manufacture due to the process constraints, i.e. the interference between the cutting tool and part. Additionally when the sample size is small, the time for process planning and NC programming can constitute a significant portion of the time needed to manufacture the part.

Unlike traditional subtractive machining processes, Rapid Prototyping (RP) (also termed as Layered manufacturing (LM) or Solid Freeform Fabrication (SFF)) is a material additive manufacturing process. It is defined as a group of techniques used to quickly fabricate prototypes or assembly models using 3-D computer aided design (CAD) data. It builds parts using a layer fabrication process, i.e. thin layers of

material are deposited/solidified, intricately, one on top of another. The layer information comes from 2-D cross sections of a 3-D CAD model. The fabrication process repeats, from bottom to top, until the part is completed. This technique permits the construction of literally any shape that can be modeled on a CAD system, including geometric shapes that cannot be formed using conventional techniques. RP technology brought many benefits for the product design and development. It simplified the process greatly compared with the traditional molding method. Parts are being produced with short lead-time and minimal set-up in a wider range of materials. Because of these special advantages, rapid prototyping technologies got a rapid growth since early 90s. Many new RP technologies have been introduced and the application of RP technologies has become wider and wider.

As one of the rapid prototyping processes, the selective laser sintering (SLS) technique builds prototype parts by depositing and melting powder material layer by layer. Although it is a relatively new technology, the RP based SLS process challenges the traditional material removal processes.

1.1 Direct Metal Laser Sintering (DMLS) Process

One ultimate goal in RP technology development is to build 3-D physical models directly from metallic powder. The SLS process is one of the RP methods that have potential to create metallic prototypes. Depending on the application, the metallic powder can be melted directly to build functional prototypes. There are two different metal sintering methods proposed based on SLS technologies: indirect laser sintering and direct laser sintering. Indirect laser sintering does not have wide industrial

applications due to its relatively low-density parts and the necessity of post-processing.

Direct Metal Laser Sintering (DMLS) is a new laser-based Rapid Tooling and Manufacturing (RTM) process developed jointly by the Rapid Product Innovations (formerly Electrolux Rapid Development, Rusko, Finland) and EOS GmbH (Munich, Germany). Besides the ability to sinter plastic or sand materials, DMLS can also process metallic powder directly. The feasibility of producing metallic parts directly by SLS has been demonstrated using various metallic material systems. Similar to SLS, the basic principle of DMLS is to fabricate near net-shape metallic parts directly in a single process, accomplished by using a high-power laser to sinter special non-shrinking steel- or bronze-based metallic powders layer by layer. The DMLS process uses liquid-phase sintering to bind metallic particles together and is a strong contender to SLS to further advance the application of RP in the manufacturing field. Metallic parts serving as a direct function or tooling prototype have wider applications compared with the typical SLS parts made of plastic or sand.

As in the case of a typical RP process, to create a 3-D physical part by the DMLS process, a digital model is first created with the help of a CAD system. After that it can be built automatically from the exported 3-D model file of the CAD system (normally in .STL format). The whole process can be completed in a few days, hence improving the product development time significantly. There are two stages (Figure 1.1) that include the data preparation stage and the part building stage in the whole procedure. The data preparation stage is the digital treatment process that slices the 3-D model into 2-D layer model. The second stage is the actual part fabrication using

the machine. Some process parameters that have close relationship with the final part quality need to be identified.

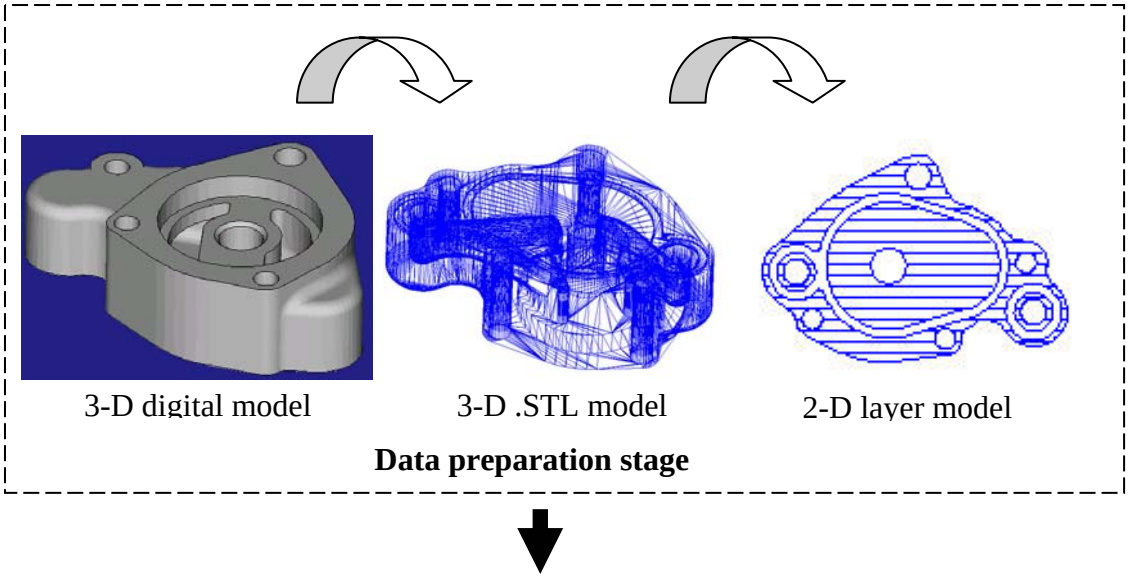

Figure 1.1 Part fabrication stages from 3-D digital model to physical part

1.1.1 Data preparation

In the first stage, the original 3-D CAD model is sliced into a set of parallel layers filled by hatch lines. The layer information is then used to drive the machine directly. There are normally three sub-stages in the data preparation stage, and these are described in the following sub-sections:

1.1.1.1 Build the CAD model

The initial purpose of RP techniques is to rapidly create the concept prototype in the early design stage of the product development. Firstly a 3-D model is designed with a CAD system.

1.1.1.2 Triangulation of the object

The surface of the model is represented by a set of small triangles. To record the information of these triangles, the standard STL file format is adopted. Because STL files use planar elements, they cannot represent curved surfaces exactly. Increasing the number of triangles improves the approximation, but at the cost of larger file size.

1.1.1.3 Transition of 3-D models into 2-D layer models

The STL model is sliced into a series of cross-sectional layers. Each layer is recorded as a machine-readable data file with information on the contour and internal section. The internal section of each layer is filled by a specific scanning pattern.

1.1.2 Part building

In this second stage, a laser is controlled to selectively sinter layers of material continuously to create the 3-D physical model (Figure 1.2). A metallic powder system is equipped with the powder supply cylinder filled up with two kinds of mixed metallic components. The powder is provided to the working cylinder in a thin layer of a fixed thickness. After that the powder surface in the working cylinder will be scanned with a high-energy CO_2 laser system according a definite pattern. The layer sintering process is repeated till the whole part is created.

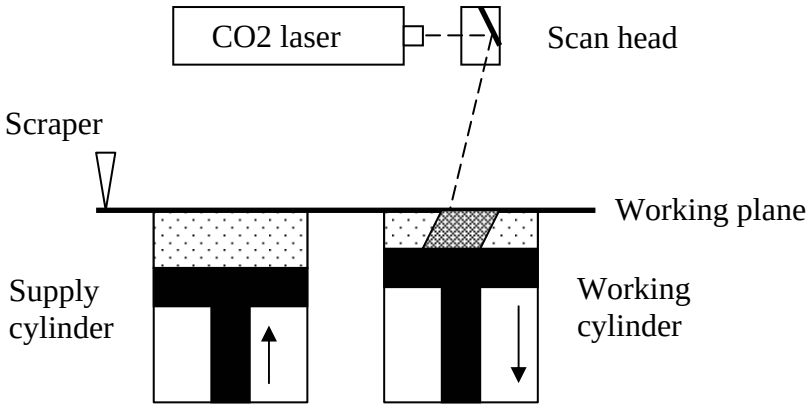

Figure 1.2 Part building of DMLS

1.2 Process Parameters of DMLS

Different process parameters will affect the sintering quality and finally affect the quality of part. Usually, the following properties of the built part are the primary concern to the user:

- Dimensional accuracy
- Mechanical strength
- Processing time
- Surface roughness
- Cost

The DMLS process is characterized by some important process parameters that determine the quality of the sintering part.

- Part orientation

The orientation of 3-D digital model is defined as the normal direction of sliced layers. Part orientation is important because it greatly affects most of the final properties.

- Scan path pattern

The scan paths are important to the final sintering quality. Geometrically, two popular path patterns are widely used in RP (Figure 1.3). One is a contour (spiral) path pattern that comprises of a set of contours parallel to the layer boundary with different offset values. The other is a parallel path pattern that comprises of a series of parallel hatch lines along a fixed direction.

The study in this thesis is derived based on the latter path pattern because the parallel path pattern is simpler to implement hence more popular.

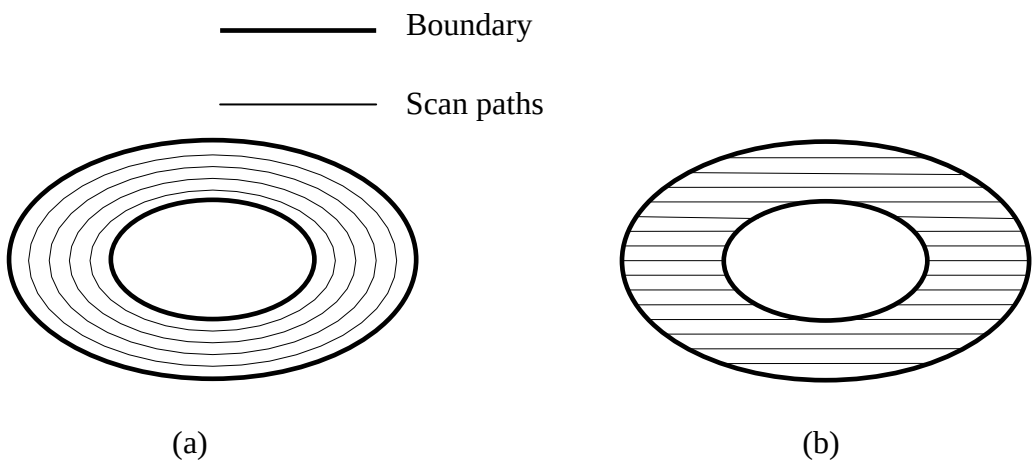

Figure 1.3 (a) Spiral path pattern and (b) parallel path pattern

- Offset and scaling

In the SLS process, a focused laser beam is delivered onto the powder (sand, plastic, metal, etc.), to heat and melt the powder. The material is combined together and the model is built layer by layer. But when the hot part cools down, shrinkage is inevitable. In addition, the finite width of the laser beam causes material to fuse outside the desired part boundaries. In order to build parts with high accuracy, it is necessary to scale the 2D layer files to compensate shrinkage and offset 2D layer file to compensate the beam diameter. So far, some different offset methods have been used such as dihedral offset, normal offset and constant offset. The dihedral offset has been adopted in the system because the dihedral offset method is more accurate than the others (Beaman, 1997).

- Hatch space

Hatch space is the distance between two neighboring hatch lines. It decides the beam overlap area of continually sintering hatch lines that is relevant to the energy distribution.

- Layer thickness

Layer thickness has a close inverse relationship with the total processing time. It is the most important factor when the processing time is concerned more than other resulting properties. The strength of the part, which is primarily a function of fractional density (or porosity) (German, 1994), has a reverse trend with layer thickness. Thickness also has a close relationship with the surface quality. The stair-case error that influences the surface quality is unavoidable when using the finite layer thickness to laminate parts.

- Scan speed and laser power

Before the fabrication, two important process parameters, scan speed and laser power, need to be decided based on the laser system and powder material properties. The presence of the liquid phase results in rapid sintering since mass transport can occur by liquid flow and particle rearrangement (Agarwala et al. 1995). The energy needed to melt the metallic powder is much more than that needed to melt polymer powder, which is often used in the SLS process. Therefore, high laser power and slow scan speed are normally used in the metal sintering. Normally, a higher laser power and slower scan speed also bring higher part strength because more energy is absorbed by the loose metallic powder. It results in a higher density in the built part. But over-sintering will occur when the energy is too high. The resulting properties will then decrease sharply. The higher laser energy will bring a larger fused zone each time but will affect the part accuracy. In general, the sintering layer surface roughness will increase with increasing laser scan speed (Laoui et al. 1998). Therefore, it is important to make a trade-off between the scan speed and laser power setting.

1.3 Research Scope

Currently, rapid prototyping has taken its place alongside CAD software, CNC milling, injection molding and electrical-discharge machining as an indispensable tool in the process of design and manufacturing the world's product (Wohler, 2001). As one of the important technologies that have the potential to build metallic parts directly, direct metal laser sintering technology is an important research field to carry RP technologies forward into the realm of custom manufacturing.

Although DMLS technology can bring about great benefits, the sintered part quality is still not good enough to produce an accurate and dense part. Improvement in the final sintering quality is widely expected in industry. There is still much research work to improve the performance of RP. The research scope proposed in this thesis focuses on the DMLS process parameter issues. Based on the previous work, an experimental DMLS machine was developed for research on the process.

Process parameters are the key factors to control the final properties effectively. As discussed earlier, certain process parameters determine efficiency, economy and quality of the whole sintering process. Therefore, correct setting and control of these parameters is a primary requirement for successful application. Based on this, the research proposed in this thesis is focused on optimizing the key controllable parameters to achieve better performance of the DMLS process. Specifically, this research focuses on the following issues:

1) Analyze the effect of different process parameters on the resulting properties. Several experiments are conducted for this analysis.

2) Develop an intelligent system based on the Feed-forward Neural Network (NN) with backpropagation (BP) learning algorithm to predict the resulting properties of the laser-sintered metallic parts built by different process parameter settings. Compared with traditional approaches, the NN approach can provide a good mapping between inputs and outputs without the aforementioned assumptions and simplifications. Moreover, the NN model is easier to build. These advantages make it a powerful tool to predict complicated process relationships. It is invaluable for users to search for

some specific properties and the system automatically determines the most suitable parameter setting to achieve desired outcome with good accuracy.

3) Measure the quantitative relationship between material heterogeneous and anisotropic properties, and the part quality by designing an experimental method. Material anisotropic and heterogeneous properties cause the sintering quality not uniform and distortion and warpage of the sintered part may occur in such case. In this study, the factors affecting the material heterogeneity and anisotropy are analyzed. With the understanding of the effect of material heterogeneity and anisotropy on the final quality, there can be further control of this effect.

4) Control and minimize the effect due to the heterogeneity caused by the different geometric shapes of each layer. Two methods are presented: i) a hatch direction optimization method based on a proposed genetic algorithm (GA) approach to reduce the short hatch-lines, and hence reducing its negative effect. Because GA does not require derivative information or other auxiliary knowledge and only the objective function and corresponding fitness levels that influence the search (Zalzala and Fleming, 1997), it is suitable for use to solve this optimization problem. ii) a speed compensation (SC) algorithm developed to give more homogeneity properties for sections with hatch lines of different lengths. By changing the sintering speed based on the length of the hatch line, the material property can be more homogeneous. With the optimization methods, the material can be made more homogeneous and the properties become more controllable.

1.4 Thesis Outline

The remaining of this thesis is organized as follows:

Chapter 2 is a literature review on the research work related to sintering quality improvement by optimization of process parameters.

Chapter 3 introduces the developed experimental DMLS system. Important errors caused by the laser system are identified and the methods to calibrate them are given where error effects are serious.

Chapter 4 presents the important resulting properties of DMLS process. The effects of process parameters on them are identified through experimental methods.

Chapter 5 proposes a generic intelligent parameter selection (IPS) system for the DMLS process. The IPS system can capture the causal and inferential knowledge about the relationships between the process parameters and resulting properties to provide expert-level recommendations during the parameter selection process. The purpose of building such a parameter optimization model is to control the quality of the final part and cater to different requirements of the users. By adjusting an identified set of process parameters, the quality of the DMLS part can be appropriately controlled.

Chapter 6 discusses the effect of different geometric shapes on the final quality. The 2-D geometry can be denoted as a batch of hatch lines. Local regions in each 2-D layer with different hatch line lengths have an effect on the material heterogeneity and hence, a negative influence on the sintering performance.

Chapter 7 proposes an optimization procedure based on GA algorithm. The GA-based hatch direction optimisation method can select the hatch direction that reduces the effect of short hatch lines effectively hence improves the homogeneity.

Chapter 8 focuses on a new speed compensation algorithm to improve the part homogeneity. Through controlling the scan speed, the negative neighboring effect can be compensated and consequently control the percent shrinkage to stay at a similar level with the level in the ideal mode.

Chapter 9 concludes and summarizes the contributions of the research presented in this thesis. Some suggestions of future work are also proposed.

Chapter 2

Literature Review

Direct metal laser sintering is designed to manufacture small batches of accurate and structurally sound 3-D metallic parts. Some process parameters have significant influence on the final properties of the part. These are shown in Figure 2.1 where a line with an arrow is used to connect each of these parameters to the property that it has a strong influence.

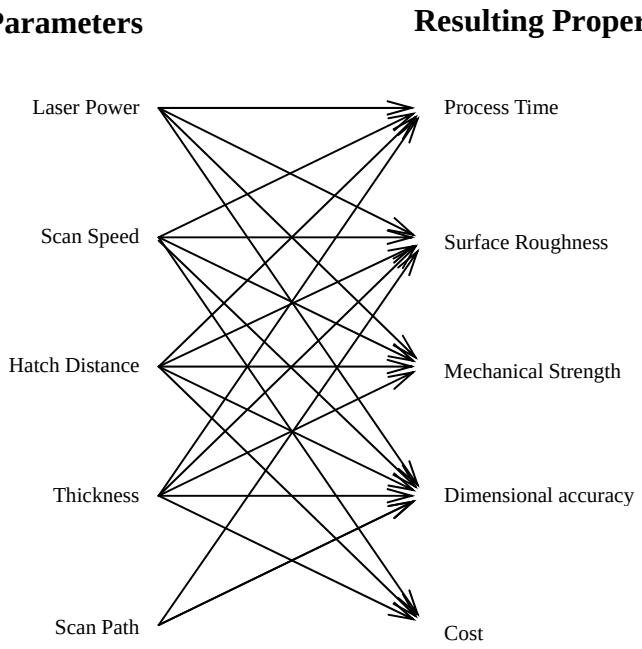

Figure 2.1 Relationship between process parameters and resulting properties in DMLS

To achieve the desired properties of the final part, the appropriate process parameters must be set. For this purpose, many researchers aimed to improve these properties by

studying the effect of process parameters on them. Due to the complicated realtionship, most of the research efforts only focus on one or a few resulting properties. The reported works are highlighted below.

2.1 SLS Process Thermal Modeling

As a rapid liquid sintering process, densification is performed at a high temperature to produce transient liquid sintering of the part to near full density with desired shape and dimensional tolerances. The liquid phase exist time and the wetting ability are critical to the final sintering properties. Temperature is believed the most important factor for the liquid phase exist time and the wetting ability. Increasing the sintering temperature leads to a larger amount of liquid phase formed and with a low viscosity of the liquid flowing. Extending the sintering time will cause more sufficient flow of the liquid. Hence, the history of the sintering temperature is critical for the final sintering quality. When the material system is decided, the sintered powder temperature history and the temperature distribution in the whole powder bed are determined by the energy input and the rate of heat losing. During the sintering process, the powder temperature will increase sharply when the laser scans them by absorbing the energy from laser. Besides the material properties, the laser energy absorbed is controlled by two important process parameters: scan speed and laser power. When the laser beam passes the powder, the temperature will decrease due to the heat loss through the powder bed and atmosphere environment. The heat transfers to the atmosphere mainly by convection and radiation at the surface of the powder bed

as well as conduction into the surrounding powder bed. The loss of the heat is closely related with the whole powder bed temperature distribution decided by hatch space, layer thickness, laser power and scan speed.

To better understand the sintering mechanism with the further effect on the sintering quality, several researchers have attempted to build a reasonable thermal model to denote the heat transfer during the SLS process. Based on that thermal model, numerical modeling can be created to investigate the temperature field of powder bed.

Thermal function is built by considering the energy input from the laser and loss by heat transfer. In the earlier stage, the sintering material is mainly focused on amorphous powders such as polycarbonate bonded by fluid flow that does not incur a phase change hence with a near zero latent heat. Works reported (Nelson 1993, Berzins et al., 1996, Childs et al., 1997, Beaman, 1995; Sun and Beaman, 1995; Williams et al., 1996) analyzed the thermal models with the sintering of amorphous powder. In their models, the heat source input from laser sintering is calculated as a function of the laser position and the power distribution of the laser beam. Heat losses at the surface are considered as results of conduction, radiation and convection.

Later works focus on the crystalline polymer such as nylon are reported (Gibson and Shi, 1997, Tontowi and Childs, 2001, Kandis and Bergman, 1997, Nikolay et al., 2003). Because the crystalline polymer has a low melting temperature, the effect of latent heat is considered in the thermal model.

For the two-phase metallic powder system, only the component with low-melting-point melts to infiltrate and wet the high-melting-point solid powder. Unlike the single-phase sintering, the heat transfer becomes more complicate. In this situation, the melting and resolidification phenomena accompanying with releasing very large latent heat have a significant effect on the thermal distribution of the powder bed. Besides the latent heat, the movement of the two different components during the sintering also has a significant effect on the whole thermal process. Bunnell (1995) and Manzuk et al. (1996) proposed the use of powder mixture containing two powders with significantly different melting point in which only the low melting point powder melts. But the effect of both liquid and solid velocities on the heat transfer is ignored. A more comprehensive model is proposed by Zhang et al. (2000). The liquid flow driven by capillary and gravity forces and the solid particle velocity induced by shrinkage of the powder bed are taken into account in Zhang's model. The predicted results match well with the experimental results obtained with nickel braze and AISI 1018 steel powder.

Based on the developed thermal models, some works were done to predict the part density. Nelson et al. (1993) predicted density of a sintered polycarbonate part, using 1-D finite element and 1-D finite difference methods. Bugeda et al, (1999) reported a 2-D model applied to ABS material. Tontowi and Childs (2001) predicted the part density at various powder bed temperatures applied on nylon 12.

2.2 Part Accuracy

The ability of a Solid Freeform Fabrication (SFF) process to produce accurately shaped geometry is critical to its overall acceptance in the market place (Beaman, 1997). To achieve an accurately built part is a time-consuming and complicated task because many factors can affect the final dimensional accuracy. Some researchers have focused their attentions on one or several of the following factors.

- *Pre-processing error*

Rapid prototyping of 3-D models are performed by generating and stacking in two dimensional (2-D) cross sections of uniform thickness. In rapid prototyping, the fabricated part has a quantification error when the height is not a multiple of the finite layer thickness. Hence, adaptive slicing algorithms (Frank and Fadel 1995; Kamesh et al. 1998) have been developed to reduce these kinds of slicing errors. To process the 2-D layer data, 3-D model is first converted to a faceted model (in STL format). This incurs another pre-processing error during the tessellation of the faceted model when a sufficiently high tessellation resolution is used to meet the accuracy requirement. Some proposals using other data formats such as constructive solid geometry (CSG) and NURBS-based representations instead of the STL representation have been proposed (Rock, and Wozny, 1991; Guduri et al., 1993; Vuyyuru et al., 1994).

- *Machine errors*

Machine errors can be measured, appropriately calibrated and compensated. The effect of the overall system errors can be controlled to a reasonable scale.

- *Random noise*

Besides the error factors mentioned above, the final part dimensions are not uniform in practice even when two processing environments are similar. It occurs due to the small fluctuation of process environment. This error is defined as the random noise and the relevant analysis has been provided by Jacobs (2000).

- *Material processing errors*

The dimensional errors arising from the material processing are the most complicated factors and have attracted much attention in RP research. In the SLS process, the temperature of part or all of the powder is raised above its softening (such as for plastic powder) or melting (such as for metallic powder) temperature to bond and solidify the particles during the laser sintering process. After the process, the sintered part shrinks as it cools. To compensate the effect of material shrinkage, the 2D-layer model needs to be scaled first. Besides these, an offset of the 2D-model is processed to compensate the effect of finite diameter of the laser beam spot. A simple method is to use a constant offset factor and scaling factor during the sintering process. Nelson et al. (1995) described an experimental method to build and measure a part model to confirm the values of scaling and offset compensation factors. Similar work is also reported by Wang (1999). But their models are based on a simple linear relationship between the nominal dimensions and the errors caused after sintering. Percentage shrinkages vary with different geometric shapes causing different accuracy errors in the whole part. But the effect from the different geometric shapes is however not

considered in the linear-fitting model.

It is important to effectively analyze and compensate the effect of different geometric shapes to improve the dimensional accuracy of the entire part. Andre (1997) obtained experimental data for measuring shrinkage values of many different geometric shapes with a fixed parameter setting and then applied different shrinkage compensation factors to the CAD model for each section of a part. It is a tedious task especially for complex geometries that need plenty of experimental data. The results are also difficult to generalize when the process condition changes. The difficulty of using a relatively simplified method to denote the shape character based on the SLS process is another problem. The geometric reasoning becomes a very difficult task in the case of complex geometries.

The final part accuracy is mainly influenced by the shrinkage of sintered material. The difference in the length of hatch lines filled in the different 2-D layered geometry causes uneven shrinkage rate. If the shrinkage rate is not uniform, the compensations become hard to implement. Additionally, the material warpage and distortion related to the inhomogeneous material shrinkage are other serious problems in the laser sintering process. Currently, none of the technologies has the capability to effectively avoid or control the heterogeneous effect caused by the variation of geometry shape.

2.3 Part Mechanical Strength

Part mechanical property is an important resulting property of concern to users especially if they want to build functional prototypes by RP systems. Research works (Subramanian et al., 1994; Badrinarayan and Barlow, 1995; David and Richard, 1995; Gibson and Shi, 1997; Corbel et al., 1999; Ahn et al., 2002; Andrew and David, 2003 etc.) have been done on the effect of different process parameters on part mechanical properties with different RP processes.

For parts built by selective laser sintering (SLS), some models are created based on the understanding of the laser energy delivery system. Nelson (1993) constructs a physical model of the sintering process that relates the sintering depth and laser control parameters. In this model, the Andrew number (An) is proportional to the part strength and is shown to be a combination of the scanner parameter to yield:

$$An = \frac{Laser \quad Power}{Beam \quad Speed \quad \times \quad Hatch \quad Space} \tag{2.1}$$

Nelson (1993) has shown that green strength of composite parts is related to the Andrew number. However, the equation achieved is based on the amount of the energy delivered to the surface where the energy lost though heat transfer is not considered. Williams et al. (1996) and Miller et al. (1997) developed the model by considering the effect of the period of time the powder cools. The change of vector length results in changes in the delay period between successive exposures. Besides

that, the amount of sintering that occurs and the final part strength are expected to be influenced by the number of laser exposures owing to an increase in the amount of overlap. The new model relates the number of exposures and the time of the delay period to the resulting part strength. By using regression models based on a batch or experimental results, the new model is given as:

$$Strength = K1 \times An - K2 \times Scan \quad Rate \tag{2.2}$$

where the coefficient factors *K1* and *K2* can be calculated through statistic method based on the experimental results.Although the model considers the effect of heat transfer between scan lines, it is still hard to predict the strength in the geometry-complicated part because the time period between scan lines varied with the change of geometry shapes in each 2-D layer.

Some works try to understand the relationship between different parameters and the mechanical strength through experimental methods on different material system. Badrinarayan and Barlow (1995) discussed the effect of vector length, bed temperature, polymer melt index and initial binder content on part strength and density by madding some test bars. Gibson and Shi (1997) investigated the influence of scan size, scan spacing, laser power, hatch direction and orientation on the mechanical properties of SLS process.

The length of the hatch line is an important factor found to be significant to affect the quality of the final part according to earlier studies (Richard, 1993; Badrinarayan and Barlow, 1995; Beaman, 1997). As the hatch length increases, the time delay between energy pulses increases thereby lengthening the cooling time and reducing over-sintering (Badrinarayan and Barlow, 1995). However, a short hatch length and its corresponding short scanning time results in heterogeneity in the material properties of the part. This unevenness affects the quality and mechanical strength of the parts built. Although many studies have been reported earlier, little work was done with a systemic research.

Besides the effect of the sintering process in each 2-D layer, the sintering part is not isotropy because of the different build direction (orientation). Subramanian et al. (1994) discussed the anisotropy of green strength due to the selection of different orientations. Then David and Richard (1995) studied the relationship between the strength and part orientation by using the Tasi-Wu interactive tensor polynomial model (Tsai and Wu, 1971).

2.4 Part Surface Roughness

As an important issue affecting the part quality, surface roughness is most important when prototyping is used for casting. Two different types of surfaces are formed when the 3-D physical model is created. The first type of surface is created along the sintering direction by a continued accumulation of the 2-D contour of each layer and defined as contour accumulation surface in this study. Ideally, this type of surface is

smooth when the thickness of each layer is small enough. But because the existence of height of each layer, the surface smoothness when created initially in a CAD system will be broken. On sloping or curved surfaces, a stair-case error will appear. The most popular method to evaluate this stair-case effect is using the cusp height. It is defined as the maximum distance between the CAD model and the built layer measured along the surface normal.

The negative stair-case effect is directly related to the layer thickness. Two methods are widely applied to minimize the stair-case effect in relation to the process parameter. The first one (Suh and Wozny, 1993; Dolenc and Makela, 1994; Kulkarni and Dutta, 1995; Tyberg and Bohn, 1998; Cormier et al. 2000) used the adaptive slicing method to adjust the thickness of each layer based on different geometrical features of the model. To reduce the staircase effect, the layer thickness should be reduced, but this will increase the part building time. The solution of this problem is to adaptively slice the model, so as to achieve a balance between the surface qualities and build efficiency. Another method is the orientation optimization method (Cheng et al. 1995; Frank and Fadel, 1995; McClurkin and Rosen, 1998; Ziemian and Crawn, 2001). By optimizing an appropriate orientation, the specified accuracy can be attained with a minimized processing time. In some studies (Xu et al., 1997), these two methods are combined together.

Another type of surface is the sintering layer surface of vertical with the Z-axis (as the

building direction). The surface roughness is determined by the sintering 2-D layer surface quality. For SLS process, most of the process parameters can affect the second type of surface quality. These process parameters include laser power, hatch spacing, scan pattern, layer thickness, hatch line length and part orientation. Laoui et al. (1998) analyzed the effect of laser scan speed, particle size and the powder content on the 2-D surface roughness. Amol and Richard (2003) analyzed the effect of laser power, powder age, layer thickness, part orientation and the hatch line length on the surface quality based on the SLS process.

2.5 Process Time

Processing time is an important factor affecting the product cost. Several process parameters such as thickness, scanning speed, the orientation and hatch distance can affect the build time of the prototype significantly. Unlike the other properties, for processing time, there is normally a clear quantitative relationship with the parameters, so that a direct mapping function can be deduced based on different processes. There are two methods to estimate the processing time: based on equations derived as a statistic function of the total volume of the parts to be built (Kamash and Flynn, 1995) or a function of the total laser scan distance that the laser travels (Yu and Noble, 1993; Clemson Univ., 1994; Kechagias et al. 1997)

2.6 Multi-objective Parameter Optimization System

The developed thermal model provides a strong theoretical support for understanding of the sintering mechanism. But it is still hard to directly apply to predict the resulting

properties of the sintering part. To build the model, some assumptions are necessary to simplify the model. Many factors including the process parameters and material properties bring different effects on the thermal model and seriously limited the application of these models. In the current research, experimental methods are adopted to build the relationship between the process parameters and resulting properties directly. After the mapping relationship is built with the analysis of experimental result data, the parameter optimization becomes possible.

Many goals such as dimension accuracy, mechanical strength, processing time, and surface roughness are the primary concerns to the users. Some of the important process parameters together could affect the resulting properties significantly. Very often, these goals do not necessarily result in a similar trend as the change in the process parameters. Inevitably, a fixed set of parameter values that can achieve the best outcome even for two of all desired properties inevitably do not exist. Traditionally, the way to solve this is to make a trade-off among these goals.

Ahn et al. (2002) used a DOE approach to optimize some important process parameters with formulated rules. These guidelines are intended in improving the strength and accuracy of the parts made by the FDM machine. Through analysis of the energy delivered to the powder medium, Williams and Deckard (1998), studied the effects of selected parameters on the SLS process response (Williams and Deckard, 1998). A model based on the physical principles involved, including sintering, heat transfer and thermal gradation was presented. McClurkin and Rosen (1998) have

proposed a method based on response surface methodology (RSM) and multi-objective decision support for co-relating the build goals to the build style variables for making build style decisions in stereolithography (SLA) process. RSM is a collection of mathematical and statistical techniques for building empirical models. Amol and Richard (2003) optimized the process parameters that are important in the SLS process with respect to a set of desired quality measures. The basis for the process is D-optimality criterion applied to a series of factorial experiments that capture empirically the relationship between the process parameters and part quality measures. Choi and Samavedam (2001) proposed an integration of the VP and RP techniques to create a modeling that accurately predicts the influence of the process parameters on the part quality.

The way to solve this by making a trade-off among these goals may not be good enough under many different requirements requested by the customers. In fact, in different applications, the users are often more concerned with some of the resulting properties but ignore the rest. For example, if the prototype part is created mainly for design review, processing time and surface roughness will be given more attention; if it is for fit and assembly verification, the dimensional accuracy is more important; and if for limited functional testing, the mechanical strength could be the main property concerned. A good scenario is auto-selecting the process parameter setting to satisfy the various requirements for different users. This could make the RP applications more agile and acceptable.

There are several process parameters that significantly affect the different resulting properties. It is important to build a suitable model by creating a proper mapping between the parameters and properties. However, there still does not exist an intelligent system that can help the user select the correct process parameters for DMLS process based on their applications.

2.7 Summary

The literature review indicates that much research work has been attempted to improve the sintering quality by optimizing one or several important process parameters. However, the relationship between the process parameters and the resulting properties has not been totally understood especially for the metallic materials. To further improve the sintering quality, more research work should be done to satisfy the requirements from users and manufacturers.

Chapter 3

Laser System Calibration

3.1 Introduction

As a promising RP process, DMLS has been investigated by several companies and institutions to further develop high-performance machine and corresponding materials for use. The RP group from the Mechanical Engineering Department of the National University of Singapore, in cooperation with Kinergy Pte. Ltd of Singapore has developed an experimental DMLS system. In order to commercialize the technology, A*STAR (Agent for Science, Technology & Research) in Singapore has provided financial support for the project. During this research, experiments on process parameters of DMLS based on the traditional SLS process were conducted at the developed DMLS machine (Figure 3.1). The corresponding machine structures, such as the motion system and working chamber, were designed to be able to work properly under a high temperature environment. A continuous-wave (CW) 200W SYNRAD (Synrad, 1999) 57-2 "DUO-LASE" CO_2 (λ=10.6μm) laser is employed in this system to supply power to melt metallic powder in the sintering process. The laser features a near diffraction-limited beam of extremely high purity, resulting in a focused spot as small as 0.4mm when used with high quality, low *F0* number focusing optics (SCANLAB, 1998). The optics on the laser assembly is permanently adjusted and the laser requires no field consumables or vacuum equipment. The focus distance of the lens is 375mm and the laser scan speed can be set up to 4000mm/s. A chamber with an atmospheric control, powder delivery system, supply cylinder and working

cylinder is used. To process the 3-D model into a machine-readable layer file hence using to control the system working in a proper sequence to fabricate the part, a software system was developed. Besides the normal function such as the slicing modules, system control module, it also allows the end user to adjust the part size, location and the orientation of the model before it is sliced and hatched. The system is more suitable for directly fabricating small-size metallic parts and can lead to a significant cost saving.

Figure 3.1 The NUS-developed experimental DMLS system

The most important part of the system is the laser system that affects the final part quality significantly. It is because the errors caused due to this system setup mainly come from the laser scanning system. Many important parameters are decided by the laser system such as laser power, scan speed, etc. To achieve good part quality, the laser system must be calibrated first. If the system error cannot be verified and adjusted to be a minimal value, errors will be accumulated and the final parts

accuracy is affect. A systematic method to analysis the effect of machine setup on the sintering accuracy is provided.

3.2 Laser-scanning Path

The laser-scanning path is realized by reflecting a laser beam through two rotating galvano-mirrors in the *X* and *Y* directions. The configuration and mechanism of the two galvano-mirror laser scanning system is shown in Figure 3.2. As a rotating motion system, the two galvano-mirrors scanning system has quite different characteristics from that of a linear-motion system in terms of its effect on the laser scan path. The movement of laser scan spot realized by the two galvano-mirrors can be described as follows:

(1) A point on the surface of the Y mirror is set as the origin and the surface of platform is taken to be at a level where *D* (*z*=*D*) is the focus distance of the lens;

(2) The distance between the centers of X and Y mirrors is taken to be *e*;

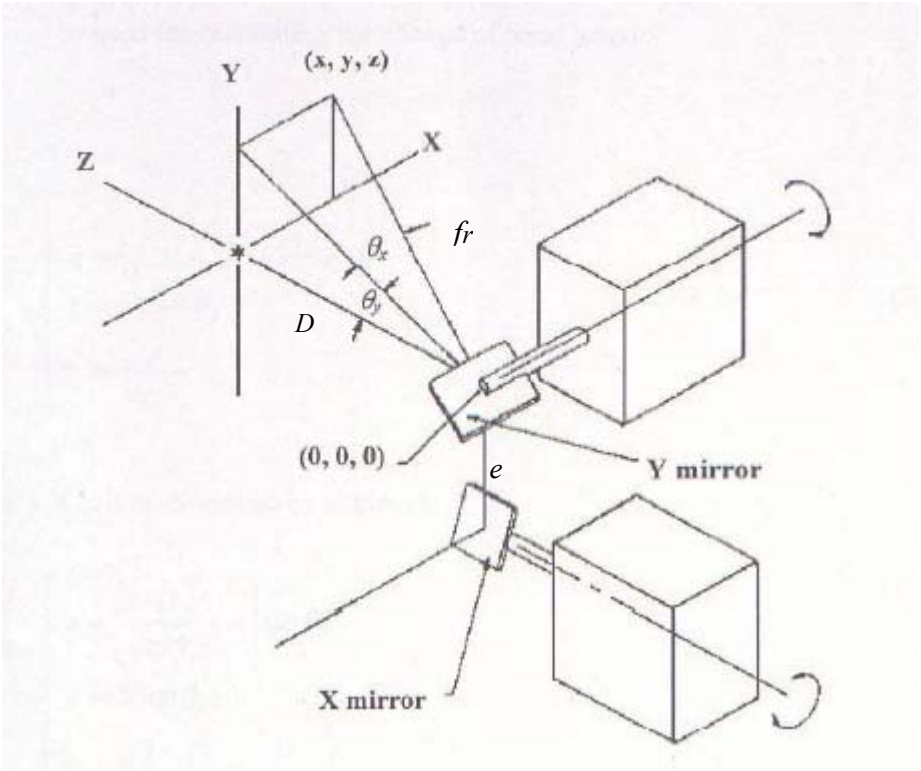

Figure 3.2 Two galvano-mirrors laser scanning system

(3) The projection angles of the beam on the *XZ* and *YZ* planes are θ_x and θ_y respectively;

(4) The travel length of the beam from the center of the X mirror to the focus point in XY plane is f_r which will be used for calculating the change of focal length.

$$\begin{cases} x = (\sqrt{D^2 + y^2} + e) \times \tan\theta_x; \\ y = D \times \tan\theta_y; \\ f_r = \dfrac{x}{\sin\theta_x}; \end{cases} \tag{3.1}$$

Hence all *x, y,* f_r can be described by angles θ_x and θ_y.

$$\begin{cases} x = (\dfrac{D}{\cos\theta_y} + e) \times \tan\theta_x; \\ y = D \times \tan\theta_y; \\ f_r = \dfrac{1}{\cos\theta_x} \times (e + \dfrac{D}{\cos\theta_y}); \end{cases} \tag{3.2}$$

From Equation (3.2), it can be seen that the position of the laser spot is determined by the rotating angles θ_x and θ_y. The focus distance f_r is also changing according to various θ. In order to get the laser beam focused on a horizontal plane that represents the working surface, a *F*-Theta lens has been used in the machine. The *F*-Theta lens has a special optical design that allows different parts of lens to have different focus distance according to the entry angle of the laser beam. This allows the laser beam spot to be focused on a linear plane when the mirror is rotated with a slight error.

3.3 Position Definition

The dimensions of the usable image field are determined by the size of the scan angle and the focal length of the objective. All *x* and *y* coordinates must be specified as signed 16-bit numbers (i.e. as numbers between – 32768 and +32767, Figure 3.3) where the origin of coordinates is in the center of the image field. The ratio of a point coordinate in *bits* and the actual position of the point in millimeters is defined by the calibration factor, *K*. If the length of the vector from the target point to the origin is *s*, a calculated calibration factor $K = 2^{16}/s$ [bit/mm] is used. The maximum working length for the *X* and *Y* coordinate is equal to the division of 2^{16} and the calibration factor *K*.

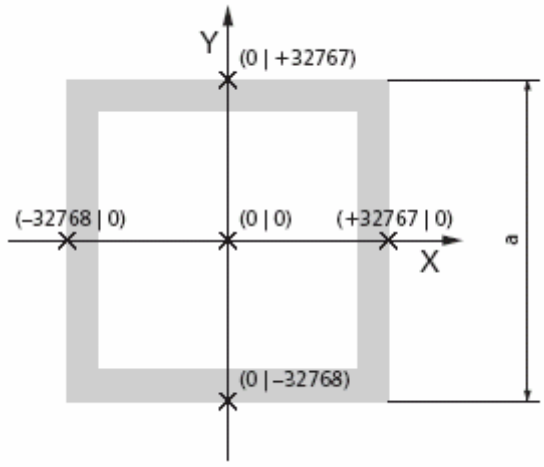

Figure 3.3 Coordinate in the image field

Accordingly, we can see that the Calibration Factor, *K* is a variable that affects the scanning accuracy of the laser system. Thus, to warrant the sintering accuracy, a method to calibrate the *K* value will be provided in section 3.6.

3.4 Control of the Scan Head and Laser

A PC real-time control board was used to control the scan head and laser system. The driver of the board offers a set of commands for the scan head and laser control. These commands mainly include the laser move commands (jump and mark command) and the parameter setting commands (scan speed, scan power and delays). The detailed command format can be found in the manual (SCANLAB, 1998) of the scanning system.

3.5 Working Plane Calibration

In the DMLS process, a laser beam focused by a lens after reflection from the computer-controlled mirror system, sinters the powder material at the processing plane. The sintering effect is ideal only when the process plane is identical with the focal plane. To achieve the minimal size of beam spot located at the focal plane, the working plane should be calibrated to superpose with the focal plane (Figure 3.4). By adjusting the position of the laser system, the focus plane is moved to be identical with the working plane.

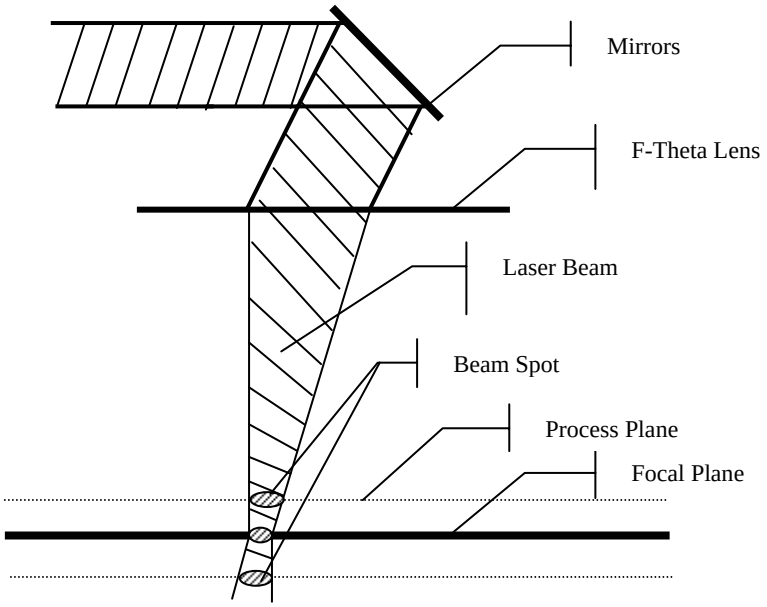

Figure 3.4 Schematic diagram of laser scanning for an incongruent working plane with focal plane

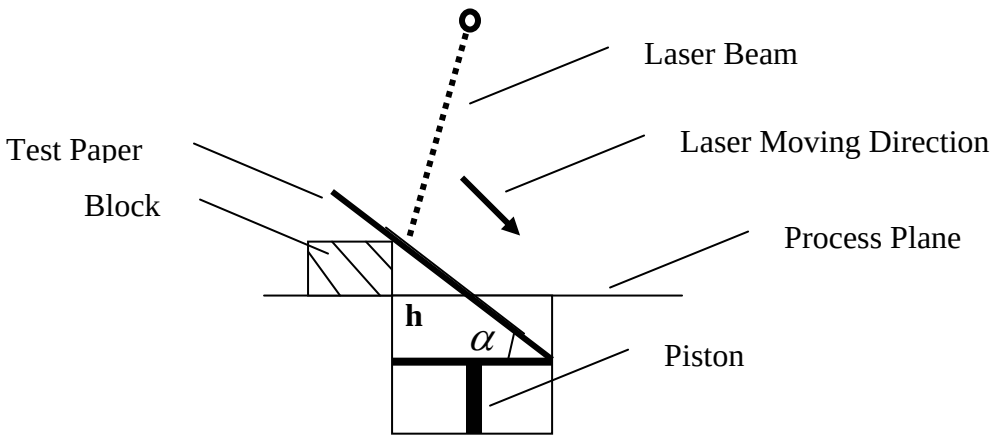

Figure 3.5 Schematic diagram of process plane calibration

To implement calibration, firstly, the working plane is calibrated to the horizon by a gradienter. It guaranties the parallelism of the process plane and the focal plane. Then the focus length should be accurately equal to the distance from the mirror to the working plane. The method to calibrate the process plane is shown in Figure 3.5. This

method uses laser vertically scanning a batch of single lines in a lean test paper. The width of the scan lines will change from broad to narrow and back to broad gradually. The horizontal plane that the narrow points belong to corresponds the focal plane. Adjusting the height of laser equipment can make the focal plane be identical with the process plane.

3.6 Distortion Errors and Calibration

The rotating motion of two mirrors and the *F*-Theta objective causes barrel-shaped distortions of the image field as shown in Figure 3.6 (SCANLAB, 1998). This distortion will obviously affect the shape and accuracy of the built parts and calibration is needed to eliminate this effect. Also when the laser scan angle becomes large, the surface and the laser will not be vertical. It makes the beam not round and the edge enlarged hence brings errors. Furthermore, some distortions are caused by the mirror and lens due to the part fabrication and configuration. All distortions and errors can be corrected and compensated by the software provided by the laser system vender.

The principle of the correction software is based on Equation (3.2). The errors in *x, y* values are corrected by modifying the values of the rotating angles θx and θy. The operation of the correction software is described below:

(1) Put a sheet of white paper on the working surface of the machine, use the laser scanning system and let the laser beam to draw a standard square ($250 \times 250\ mm^2$) on the paper;

(2) The draught square may have a distortion, measure the biggest errors along the central lines of *X, Y* directions, and get the data of Δx and Δy (see Figure 3.7 (a));

(3) Input the Δx and Δy into the software, the software will automatically calculate the modifications for every point of the square, and correct the distorted square into the normal square (see Figure 3.7 (b)).

After the correction, the distortion can be eliminated within the scanning area.

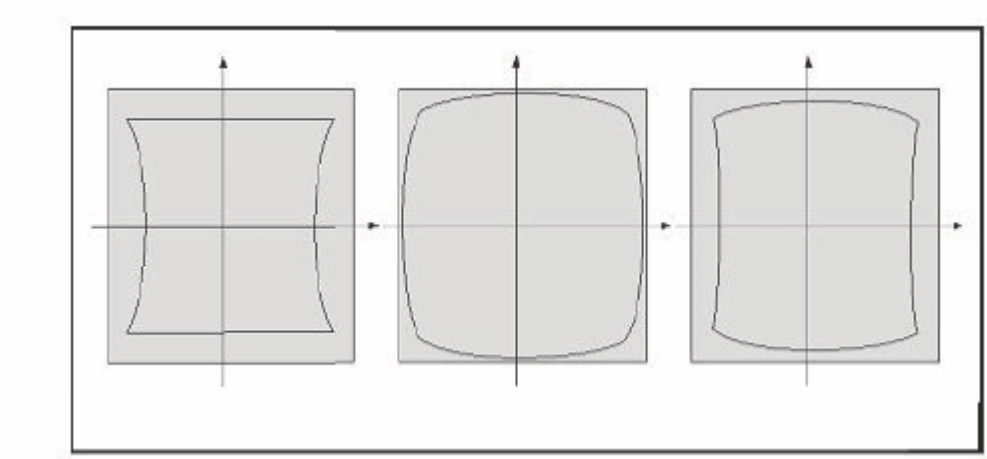

Figure 3.6 Barrel-shaped distortions caused by laser scanning system

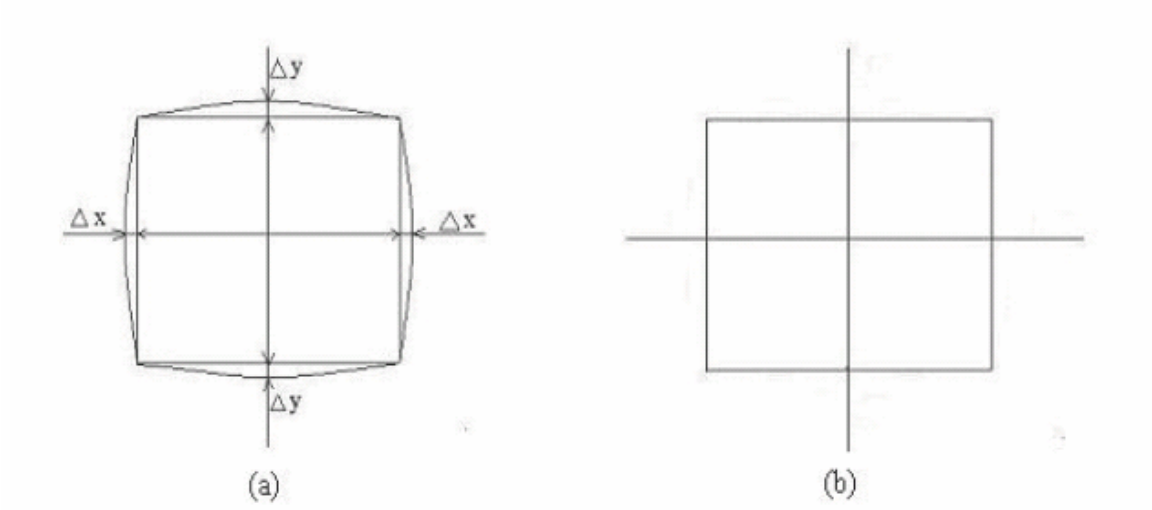

Figure 3.7 Correction of the distortion caused by the laser scanning system

3.7 Calibration of the Field Calibration Factor *K*

Usually the positions have small difference between the specific point and the actual laser scanning point. It is a common practice to recalibrate the field celibration factor *K* manually.

The mirror's tilt that determines the real scan length in the process image is calculated by a computer program. A calibration factor *K* is used to transfer the computer bit signs to the mirror's tilt. The default value is defined as a rounded value, which is smaller but closer to the calculated value. To increase the accuracy, it is necessary to develop a method to calculate the actual *K* value from the experimental data.

For current study, both Calibration Factors, for *X* and *Y* direction are investigated and optimized.

The procedures for optimization of the calibration factor in the *X* direction, K_x are described below:

- The single line scanned pattern is adopted. *L* is the *set length* and is the variable parameter in the experiment where *L*=10, 20, 30, 40, 50, 60, 70 and 80mm. For each value of *L*, the appropriate lines of length *L* are scanned along the *Y*-axis (from –80 to 80mm) at a regular interval of 10mm.

- Using the Deltronic® MPC-5 System (DELTRONIC, 1998) with an accuracy of ±0.001mm, the scanned lines are measured to obtain the *measured length*, L^1 corresponding to their *set length*. Repeat step (a) and (b) for *L*=10, 20, 30, 40, 50, 60, 70 and 80mm.

For optimization of Calibration Factor in the *Y* direction, K_y, the procedure listed above is repeated with the exception that the lines are scanned along the *X-axis*. All measurements were repeated three times to increase reliability of the result.

With the optimized laser scanning parameters, it is possible to improve the laser scanning accuracy of the system through manipulation of the Calibration Factor, *K*. For this experiment, the optimum values of K_x and K_y are determined by using a statistical approach.

The optimum value for K_x and K_y can be derived through the following relationship:

$$L^1_{ave} \times K^1 = L \times K \tag{3.3}$$

where L^1_{ave}: average measured length

L: set length

K: calibration factor that is used before optimizing

K^1: optimized calibration factor to be obtained

The value of K_x and K_y before optimizing were 235 given by (SCANLAB, 1998). Using the formula and the original value of *K*, the individual value of K_x^1 and K_y^1 for each *set length L* and their corresponding average *measured length* L^1_{ave} is calculated.

The obtained values of K_x^1 and K_y^1 by performing similar calculations for all values of *L* and their corresponding L^1_{ave} are given in Appendix. Finally, an average value of K_{xave}^1 and K_{yave}^1 is obtained by taking the average of all the K_x^1 and K_y^1 values (see appendix).

3.8 Identify the Delay Value

When the scan direction or scan speed changes, the mirrors on the galvanometer scanner have to be accelerated up or decelerated down to the defined marking speed and direction. If the laser keeps working at that situation, laser intensity will vary and affect the homogenous sintering results. To make sure that laser scanning is not working under these situations, the delay function will be added automatically. But the value of laser delay time needs to be set carefully and some errors will be brought with the scan delay setting. The negative effects caused by scan delay include:

- Inducing the shape and dimensional error caused by the laser delay
- Increasing the process time

For the DMLS process considered, two kinds of delay formats are important. The first kind is the delay relative to the time of laser on/off: LaserOn and LaserOff delay. Another kind is the delay relative with the command of laser mark/jump: MarkDelay and JumpDelay.

3.8.1 LaserOn/LaserOff delay

When the scan head has to execute a marked command, the mirrors on the galvanometer scanners have to be accelerated up to the defined marking speed. To make sure the laser is not switched on before the mirrors reach a certain angular velocity to guarantee the laser scanning the vectors with constant velocity, a LaserOn delay should be inserted automatically before the scan start. Similarly, a LaserOff delay is needed at the end of the marking. Because the processing time of each marking is the time of the laser moving from the start point to the end point, which has no relationship with the time of laser power on/off; this kind of delays do not affect the whole processing time. But the introduction of these two delays brings a position error such that the sintering of the start point and the end point will be

delayed. The time of the delay cannot be too short because burn-in effect will happen and cause over-sintering at the start point and end point. The rule to set the correct LaserOn/Off delay will be the minimal value that does not cause a burn in effect at the scanning speed. For the metal sintering process, the default sintering speed is 100mm/s, which requires at least 30 μs LaserOn/Off delay by experimental verification. It is the time period that the laser accelerates/decelerates from 0 to 100 mm/s. By simply assuming the laser is accelerated lineally, the dimensional errors brought by the delay can be calculated by the following equations:

$$\text{Start point position error} = \frac{v \times Delay_{on}}{2} = 100(mm/s) \times 30 \times 10^{-6}(s)/2 = 0.0015(mm) \quad (3.4)$$

$$\text{End point position error} = -\frac{v \times Delay_{off}}{2} = 100(mm/s) \times 30 \times 10^{-6}(s)/2 = -0.0015(mm) \quad (3.5)$$

$$\text{The length error} \approx \text{Start point position error+ End point position error} \approx 0 \quad (3.6)$$

The position error with a 0.0015 *mm* is acceptable because the dimensional error caused by the material shrinkage normally is more than 0.1 *mm*.

3.8.2 JumpDelay/MarkDelay

Before the exchange to mark and jump command, the mirrors will be accelerated up to the programmed jumping speed or decelerated down to the programmed decelerated speed. The speed and direction change need a certain setting time to compensate the lag. For this purpose, another group of delays named JumpDelay and MarkDelay is used. A non-sufficient time for the JumpDelay brings an oscillation at

the start field of the sintering vector. An over-short MarkDelay set will make the end of the mark vector turn toward the direction of the following jump direction. When the delay time of the second group is set long enough, there are no visible effects on the scanning quality hence making no difference on the position accuracy. A minimal set of the JumpDelay and MarkDelay is 100 μs for the experimental DMLS machine to achieve a good sintering quality. Unlike the first type, the use of these two delays however increases the whole processing time. The extra time with every mark/jump command can be calculated as:

$$Delaytime = MarkDelay + JumpDelay = 100\mu m + 100\mu m = 200\mu m \qquad (3.7)$$

3.9 Summary

The direct metal laser sintering process is a RP method. Besides plenty of the research works focused on the process itself, the calibration work of the system is also important. The errors caused by the system are often given less attention. But the sintering result will be poor if the system is not calibrated properly. In this chapter, important errors caused by the laser system are identified and the method to calibrate them is presented.

Chapter 4

DMLS Physical Model and Sintering Quality

4.1 Introduction

The mechanism of DMLS process is based on the liquid phase sintering (LPS) principle. But unlike the traditional LPS (German, 1985), the thermal sintering reaction is kinetically fast. A laser system, used as a moving heat source, scans the powder material surface at high speed and the duration for the laser beam to sinter powder particle is quite short.

Early studies on a single-phase metal, such as lead, zinc or tin, were unsuccessful because of the balling phenomenon (Haase, 1989; Manriquez-Frayre and Bourell, 1991). A two-phase powder-mixture material system, which contains a high-melting-point metal (as structural metal) and a low-melting-point metal (as binder), was developed and proven to work effectively to mollify the tendency to form spheres (Beaman, 1997). Direct laser sintering with two-phase metallic powders with different melting points, such as Cu-Sn, Cu-solder, Ni-Sn, Fe-Cu, WC-Co, steel-Phosphor copper, etc, has been investigated (Agarwala et al., 1995a, Schueren and Kruth, 1995, Laoui et al., 1998, Fuwa, 2000). Recently, using super-solidius liquid-phase sintering (SLPS) as bonding mechanism in direct sintering alloy powder has also been reported (Niu and Chang, 1999a, 1999b, Klocke and Wagner, 2002). However, all these researches are still in the stage of laboratorial research.

In the investigation of the DMLS process, a new Cu-based metallic material system was developed (Zhu, 2004). The new metallic powder system is a mixture of 60wt% pure copper powder and 40wt% pre-alloyed metallic powder. The pre-alloyed named SCuP metallic powder, serving as a binder in sintering, is a Cu-based alloy with a melting point of $646°C$. Because of the good thermal properties of the new Cu-based material system, parts fabricated by this metallic powder system have several advantages: high density, suitable mechanical properties, low shrinkage and low cost. Direct laser sintering using this metallic powder system has been carried out in an ambient atmosphere without pre-heating.

4.2 Physical Process

The physical process of direct metallic sintering is different from sintering amorphous polymers such as polycarbonate, which is widely used in the earlier period. Amorphous polymer has a glass transition temperature T_g only and is sintered by viscous flow. For the DMLS process studied, when the laser scans the powder surface, the local temperature increases rapidly and exceeds the melting temperature T_m of the low-melting-point binder but does not reach the melting point of the high-melting-point metallic powder. After rapidly absorbing the laser energy, the binder changes to liquid and the pure Cu powders that have a high-melting-point remain solid as a structural skeleton during the sintering. Under the force of gravity and capillary, the liquid flows infiltrates into the original atmosphere pores in the raw powder bed. The part is densified with the shrinkage of the pores and the porosity decreases. Simultaneously, the solid Cu particles are wetted by the flowing liquid and connected together. In the following cooling stage, the liquid metallic re-solidifies and binds the solid particles effectively. Because the heating and cooling rates are very fast and the

time of sintering is short (~0.1s), it is almost impossible to achieve the full density parts. The sufficiency of the liquid flow for good wetting is critical to the final sintered part quality but the viscosity of the liquid hinders the flowing process. A schematic diagram of process stages is shown in Figure 4.1.

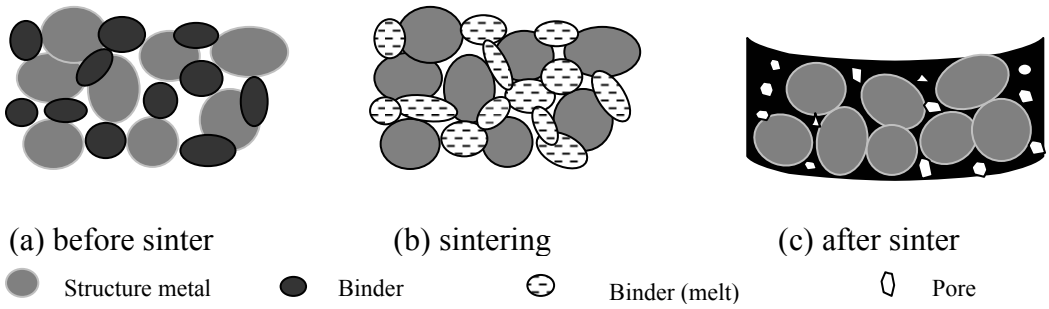

Figure 4.1 Schematic diagram of process stages in DMLS

In the sintering process, there are many parameters influencing the sintering process. All the process parameters set in advance are based on a rule, i.e. to ensure the powder sintering process feasible and the sintering quality acceptable.

4.3 Energy Input by Laser Irradiation

The laser beam, used in the DMLS system, may be approximated by a Gaussian function. For a gaussian laser, the energy intensity (W/m^2) at any point is denoted as (Jacobs, 1992):

$$I(r) = I_0 \exp(-2r^2 / {w_0}^2) \tag{4.1}$$

where I_0 is energy intensity in the center point of the laser beam, r is the distance from the point to the center, w_0 is the distance in which the laser energy equals to 1/e of I_0, and e is the base of natural logarithms. In the study of DMLS system, the standard value of w_0 is 0.4mm (SCANLAB, 1998). I_0 can be calculated based on the laser power *P (W)* by:

$$P = \int_{r=0}^{r=\infty} I(r)dA \tag{4.2}$$

where $dA = 2\pi r dr$

Substituting (4.1) into Equation (4.2),

$$I_0 = 2P / \pi w_0^2 \tag{4.3}$$

Substituting the Equation (4.3) into Equation (4.1).

$$I(r) = [2P / \pi w_0^2] \exp(-2r^2 / {w_0}^2) \tag{4.4}$$

In the operating situation, the moving laser source with a fixed scan value v scans the powder surface according to the defined scan pattern. For the parallel-raster scan pattern, the irradiation E (J / mm^2) at the point K in the surface can be achieved as the integral of the laser irradiance over times. For a limited length of single line, the exposure E at point K (Figure 4.2) can be calculated as:

$$E_K = \int_{r1}^{r2} [2P / \pi w_0^2] \exp(-2r^2 / {w_0}^2) dr \tag{4.5}$$

Where $r = \sqrt{x^2 + y^2}$ and $dr = \dfrac{x}{\sqrt{x^2 + y^2}} dx$

For convenience, Jacobs (1992) set the limits of x as $(-\infty \sim +\infty)$ and got two important conclusions. Firstly, the concept of 'zone of influence' such that within this zone a differential area $dA = dxdy$ that receives 99.99% of its total irradiation is defined. The radius of the zone of influence R is given as:

$$R = 2.146 w_0 \tag{4.6}$$

Secondly, the surface irradiation equation at any point with the y value to the scan line is equal to:

$$E(y,0) = \frac{\sqrt{2}P / w_0 S_{scan}}{\pi} \exp(-2y^2 / w_0^2) \tag{4.7}$$

where S_{scan} is the scan speed. Only part of the laser exposure energy absorbed by the powder system and others are reflected or transmitted by the powder bed. The actual energy absorbed by the powder can be calculated as:

$$E_{absorb} = \alpha_R E \tag{4.8}$$

where the fraction absorbed α_R is called the absorptivity. The absorptivity is dependent on the material characteristic, temperature, etc.Based on Equation (4.8), consider a point located at the m^{th} hatch line of totally *n* lines, the *y* value from the point to the i^{th} hatch line is:

$$y_{i,p} = abs((i-m)HS); \tag{4.9}$$

where function *abs* is the absolution calculation and the *HS* is the hatch space between two continuous hatch lines.

Substituting Equation (4.9) into (4.7), we can obtain the total exposure energy with multiple line scanning as:

$$E = \sum_{i=1}^{n} \frac{\sqrt{2}P / w_0 S_{scan}}{\pi} \exp(-2((i-m)HS)^2 / w_0^2); \tag{4.10}$$

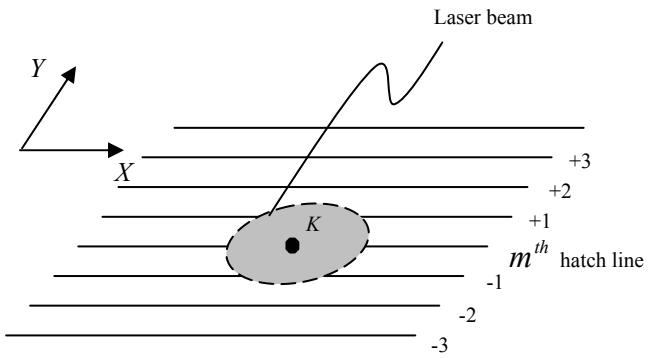

Figure 4.2 Schematic diagram of laser beam sintering of continuous hatch lines

In the current system, the value of w_0 equals to 0.4mm and the default value of *HS* is 0.2 mm. The energy irradiation by the neighboring 6 hatch lines to point *K* located at m^{th} hatch line (Figure 4.2) is listed in Table 4.1:

Table 4.1 Energy irradiation with neighboring hatch lines

Distance ($\times HS$)	Exposure
0 (m^{th} hatch line)	E_0
± 1	E_1=0.607 E_0
± 2	E_2 =0.135 E_0
± 3	E_3=0.011 E_0

Seen from Table 4.1, when the distance from the point *K* to the sintering hatch line is more than three times of the hatch space, the energy achieved can be ignored (<1.1%). The time of the point *K* to absorb effective energy of each line is equal to the time of the laser beam pass the round with radial *R* in the hatch line. The time for the powder to absorb the laser energy (99.99%) can be calculated as:

$$t_{eff} = \sqrt{R^2 - y^2} / S_{scan} \tag{4.11}$$

For default speed value of 100mm/s for S_{scan}, the effective sintering time of each hatch line on point *K* is less than 10ms. The high sintering rate makes the temperature of the sintered powder increase rapidly.

4.4 Sintering Quality

The main properties important to industry include the process time, dimensional accuracy, surface roughness, mechanical properties, etc.

4.4.1 Build time

A reliable and accurate estimation of the build time is necessary to help the user decide the process parameters, cost and product development cycle time. Actual build time depends on the part geometry and the process parameters used. These important controllable process parameters include scan speed, hatch density, layer thickness and laser power. Because each hatch scan can be viewed as a voxel, a 3-D part is accumulated by a series of voxels (Choi and Samavedam, 2001) with a specific height (layer thickness) and width (hatch distance). The built time of the part is equal to the total time to create each of the voxel with respect to the build-time interval between each layer. The total length of all the voxels is equal to $Volume/(hatchspace \times thickness)$. To understand the effect of process parameters on the total build-time, the following equation has been derived based on the volume of the part and the build-time interval between each layer, i.e.

$$t_{Total} = \frac{1}{TH}\left(\frac{V_{Parts}/S_{Scan} + V_{Cavities}/S_{Jump}}{HS} + H_{Height}t_{Layer}\right) \qquad (4.12)$$

where t_{Total}, denotes the total build time, V_{Parts} and $V_{Cavities}$ the total part volume and the cavities volume in the part, H_{Height} the part height, and S_{Jump} the jump-scan speed. t_{Layer} denotes the building time taken from each layer. Some factors were ignored to simplify the function. These factors are mainly related to the time used in the changing of scan state (Chapter 3.8.2). As shown in function (4.12), layer thickness

has a close inverse relationship with the total processing time. It is the most important factor when the processing time is of greater concern than other resulting properties

4.4.2 Material shrinkage

The dimensional error inherent by the sintering process is mainly due to the material shrinkage of the solid-liquid-solid phase changes. During the sintering process, two different kinds of material shrinkage occur i.e. sintering shrinkage and thermal shrinkage.

4.4.2.1 Sintering shrinkage

The sintering shrinkage is mainly caused by the change of pore size and the porosity. During the sintering process, the molten binder flows to wet the surface of the structure powder and fill the pores by capillary and gravity forces. The sintered material is densified due to the shrinkage of pores and causes the final part volumetric shrinkage. Although the volumetric shrinkage occurred along the *X, Y* and *Z* directions simultaneously for a single scan line, the shrinkage along the *Z* (orientation) direction will be compensated by the deposited metallic powder from later sintering layers except the last layer and thus the effect of material shrinkage on the dimensional errors in the *z* direction can be neglected. Hence only the shrinkage along the laser sintering direction in plane is considered. Besides the shrinkage of pores, the grain growth of the binder and the rearrangement of the Cu powder have also some effects on the final shrinkage.

4.4.2.2 Thermal shrinkage

For metals, usually the yield stress decreases to a very low level if the temperature exceeds a definite value (Willems et al. 1981). Thus the thermal shrinkage ΔL can be simply regarded as elastic compressive shortening.

$$\Delta L = \mu \times \Delta T \times L \tag{4.16}$$

where μ is a linear thermal expansion coefficient of the material, and ΔT is the temperature gradient of the sintered powder due to the absorbed energy and the material thermal properties of the materials.

Both the sintering shrinkage and thermal shrinkage work together for the final parts volume change and it is hard to separate them strictly by experiments.

4.4.3 Surface roughness

Two kinds of surfaces are formed at the built part. One is defined as the sintering layer α-surface that is the side faces accumulated by the outside surfaces of layers. The other kind is not the layer surface but an accumulation of the contour of each layer defined as contour accumulation β-surface (Figure 4.3).

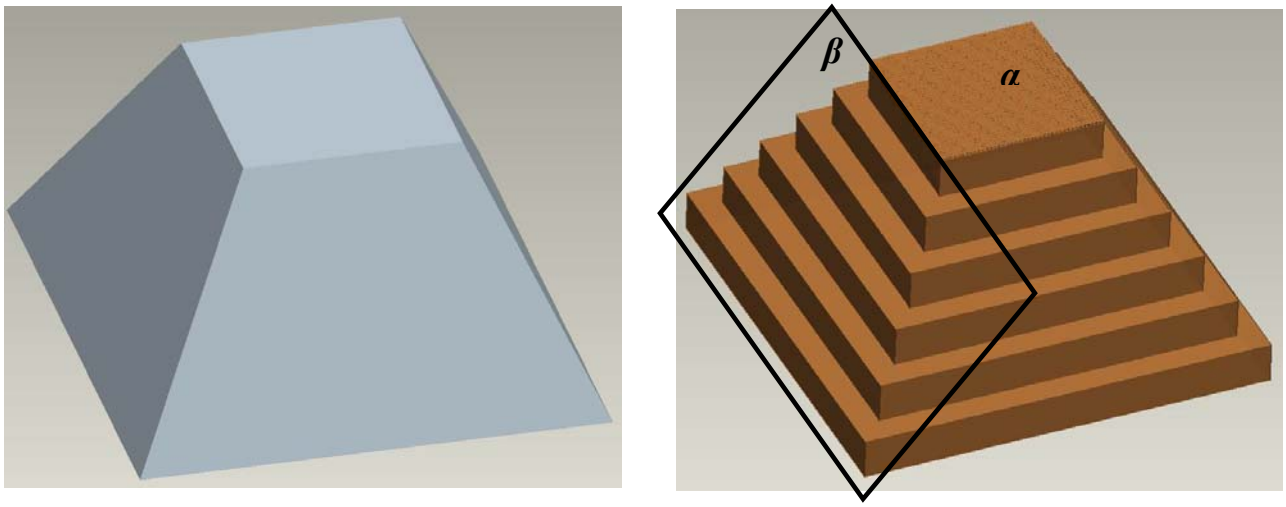

(a) Digital model (b) Two kinds of surfaces in the physical part

Figure 4.3 Sintering layer surface (α) and contour accumulation surface (β)

4.4.3.1 Sintering layer surface quality

Some part of layer surfaces without covered by others are exposed outside. The quality of these surfaces is mainly determined by the sintering process. During the process, the melted powder will flow to the pores and connect the structure powder. After cooling down, the residual pores remain at the surface. The shape of the structure powder and the re-solidification fluid with the impurity dust will also destroy the flatness of each layer.

R_a known as the arithmetic mean deviation of the measured surface profile is the most commonly used parameter to describe the average surface roughness and is defined as an integral of the absolute value of the roughness profile measured over an evaluation length (Whitehouse, 1994):

$$R_a = \frac{1}{l}\int_0^l |y(x)|dx \tag{4.17}$$

The average roughness is the total distance of the peaks and valleys divided by the evaluation length and is expressed in μm.

4.4.3.2 Contour accumulation surface quality

Because this kind of surfaces is an accumulation of the layer contour with a fixed thickness, the sintering quality is not the main factor to influence the roughness of the final part. An error known as stair-case error is the main factor to affect the surface quality. The stair-case error that strongly influences the surface quality seriously is unavoidable when using the finite layer thickness to laminate parts. The value of the stair-case error is mainly effected by the geometry shape of the build part, the part orientation and the thickness. Three different methods were used to quantifiy the error.

- Cusp Height

Using cusp height is the most popular way to evaluate the effect of staircase. Cusp height is defined as the maximum distance between the sliced layer and the desired surface measured along the direction of the surface normal. As shown in Figure 4.4, the Cusp hight can be calculated as:

$$Cusp = T \times \sin\theta \tag{4.18}$$

Where T is the layer thickness and θ is the angle between the digital model surface and the building direction.

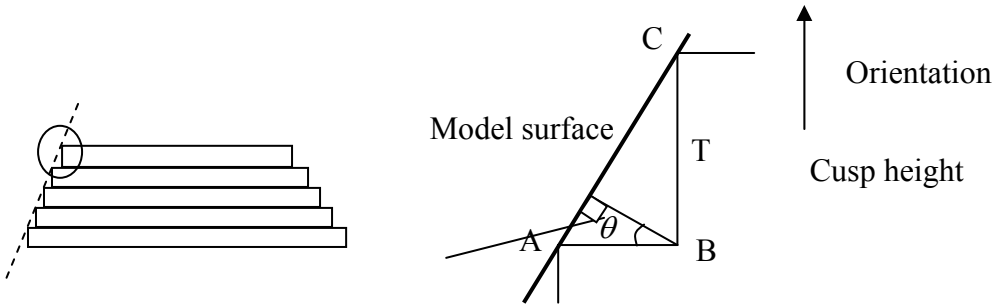

Figure 4.4 Cusp height

- Sectional area: the sectional area is the area of ΔABC and equal to:

$$S_{\Delta ABC} = \frac{h^2 \cdot tg\theta}{2} \tag{4.19}$$

- Volumetric error:

Volumetric error is defined as the volumetric difference between the 3-D digital model and the actual sintered part. The error of layer *i* is equal to (Lin, 2001):

$$e_i = \oint de_i \cdot dl \tag{4.20}$$

where *dl* is the differential length along the layer contour and de_i is the sectional area of ΔABC. The volumetric error of the entire part will be denoted as the sum of each layer:

$$E = \sum_i e_i \tag{4.21}$$

The quality of contour accumulation surface can be quantitatively achieved for each 3-D digital model. The relationship between the surface quality and process parameters (part orientation and layer thickness) exists. Some proposed methods by optimizating these two parameters can control and improve the surface quality effectively (Suh and Wozny, 1993; Dolenc and Makela, 1994; Cheng et al. 1995; Frank and Fadel, 1995; Kulkarni and Dutta, 1995; Xu et al., 1997; McClurkin and Rosen, 1998; Tyberg and Bohn, 1998; Cormier et al. 2000; Ziemian and Crawn, 2001; etc.).

4.4.4 Mechanical strength

The tensile strength can be often interpolated linearly with the part density, while the elongation at fracture and impact strength exhibit a stronger dependence on porosity (Thümmler and Oberacke, 1993). When the air in the powder bed cannot be released resulting in the residual pores in the part, and the density of the part will be low. The residual pores left inside the part is believed as the main reason for low strength, as the crack will first occur there under an applied load. The previous research shows the relationship between the density and strength by the following equation (Zeng, 1989):

$$\sigma = C\sigma_0 p^m \tag{4.22}$$

where σ_0 is the strength of fully dense material, C and m are empirical material constants, and p is the fractional density. Also, the strength depends on the inter-particle connect level. When the wetting between the liquid and the structure metal is poor, the strength will be low. The connection is mainly decided by the material properties and the sintering condition provided.

Because of material accumulation in the process, the strength of the sintered part is not isotropic. The mechanical properties of the final part are also dependent on its orientation in the process. Previous studies (Subramanian, 1994; Ahn et al., 2002 etc.) have proven the strength along the orientation (the *Z*-direction of the building process) is weaker than the strength at in-plate directions. The connection between the two layers is not as good as the connection between two continuous hatch lines because the sintering in-plate is more sufficient. Also the time interval between two layers is much longer than that of between the hatch lines hence reducing the energy strength.

4.5 Research on the Influence of Single Process Parameter on Resulting Properties

To understand the effect of process parameters

1) laser scan speed

2) laser power

3) hatch density

4) layer thickness

on the following resulting properties

a) part accuracy

b) strength

c) roughness

was experimental determined.

4.5.1 Experimental setup

4.5.1.1 Scan path

A cross zig-zag scan path (Figure 4.5) was chosen during all the experiments. Unlike the single zig-zag scan path, the scan paths are made in directions that are alternatively vertical and horizontal for consecutive layers. This type of scan mode aims to reduce the performance difference in the X and Y directions and bring about more homogeneous properties to the final parts.

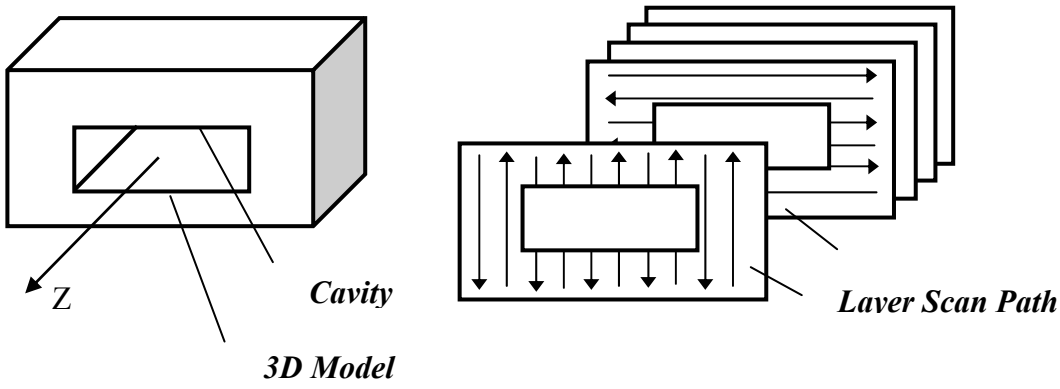

Figure 4.5 Cross Zig-zag scan path

4.5.1.2 Test parts

According to the ASTM standard E8 (ASTM, 1999) for the tensile testing of metallic materials, specimens were built with a 0.235mm offset (Tang el al., 2004) for the laser beam set by the machine to evaluate the resulting properties. The thickness and reduced section width at the specimen are both 6.35mm. The overall length *L* is 92mm (Figure 4.6). All the size values are set following the ASTM standard. The developed system software can perform functions such as transferring the CAD

models in STL format to the layer data required by the machine. Besides, it could combine several parts to be built on one base and select the drive data according to different process requirements of each part. Five test specimens that have the same layer thickness were built on one base each time (Figure 4.7). Because the geometric shapes and the process parameters for all these samples are the same, the effect of other factors, such as temperature, that are decided by the process parameters and layer geometric shape, can be ignored. After the specimens were built, the surface roughness (*Ra*) and the tensile strength of each one were tested.

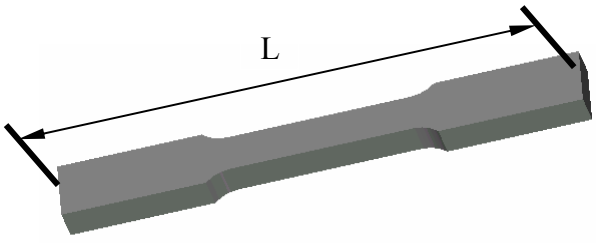

Figure 4.6 CAD part model of specimens **Figure 4.7** Five parts built in one base

The value of the length *L* was measured accurately to determine the dimensional accuracy. In fact, many factors have an effect on the dimensional accuracy, such as the material, powder size, machine position error and process parameter values. Since part distortion often happens, one part size is not enough to fully evaluate the dimension accuracy. But if one size is very close to the design size, most of the other sizes of these parts will show a consistent result to the design sizes. When the part is built, all parts show similar distortion trend most of the time. The parameter settings for the experiment are listed in Table 4.2.

Table 4.2 Parameter settings for experiments

	Variable parameter settings *	Other parameter settings
Group #1	P =70; 90; 110; 130; 150; 170; 190	S_{Scan} =180; HS=0.2; TH=0.1
Group #2	S_{Scan} =85; 115; 145; 175; 205; 235	P=120; HS=0.2; TH=0.1
Group #3	HS=0.13; 0.15; 0.17; 0.19; 0.21; 0.23	P=120; S_{Scan} =180; TH=0.1
Group #4	TH=0.03; 0.05; 0.07; 0.09; 0.11; 0.13; 0.15	P=120; S_{Scan} =180; HS=0.2

** P: Laser Power (W); S_{Scan} : Scan Speed (mm/s); HS: Hatch Space (mm); TH: Thickness (mm).*

4.5.2 Results and discussions

4.5.2.1 Effect on the material shrinkage

When increasing the laser power or decreasing the scan speed, the shrinkage along the sintering (length) direction of the part is more serious because both sintering shrinkage and thermal shrinkage will be larger when more energy is absorbed by the powder. (Figure 4.8) Because the main concern is focused on the in-plane shrinkage, the effect of thickness is not significant. But when we increase the layer thickness, the in-plane shrinkage will be larger because more powders need to be sintered each time hence increase the porosity when other parameters keep unchanged.

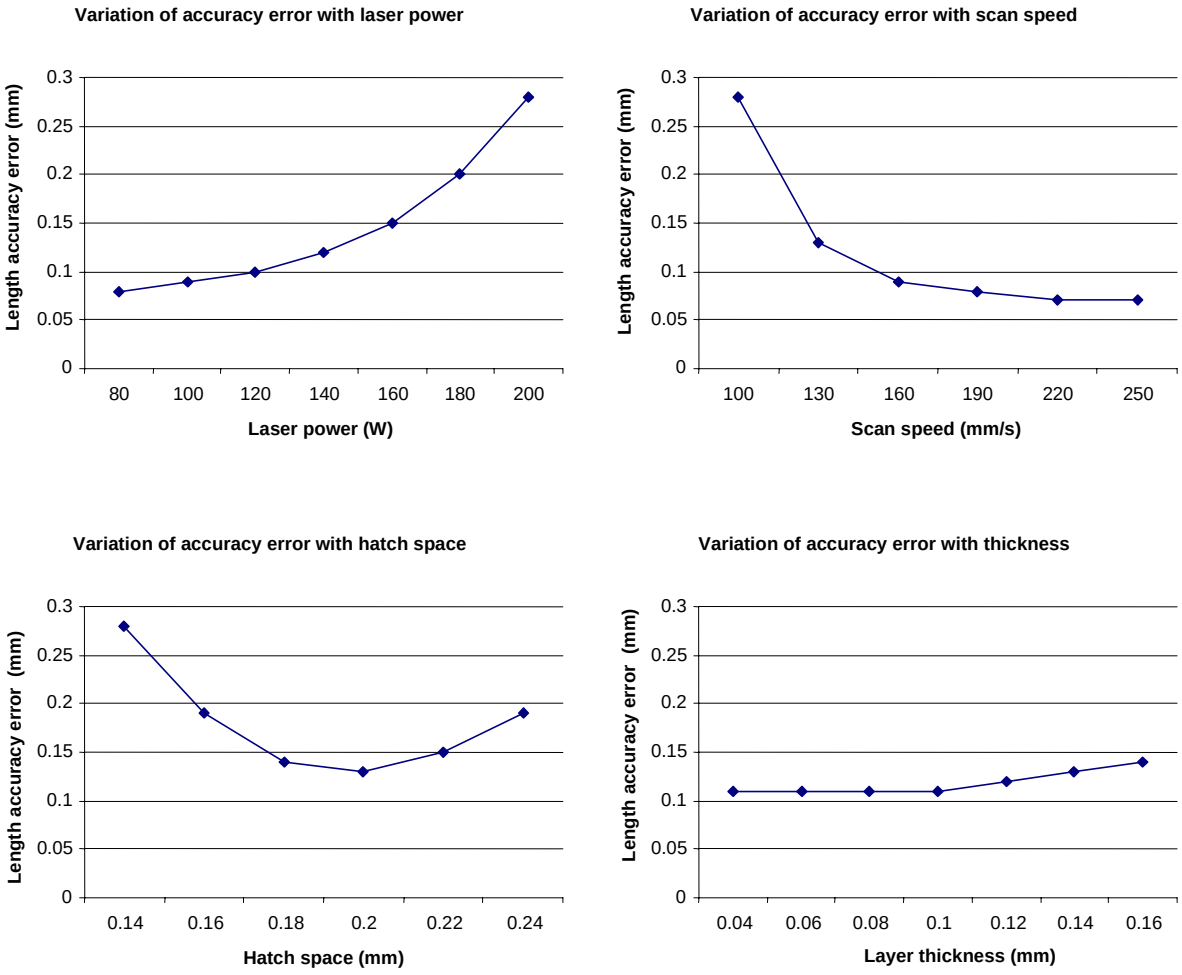

Figure 4.8 Parameters effect on part length accuracy error

4.5.2.2 Parameter effect on the sintering layer surface roughness

Surface roughness was measured using a Surfcom 120A surface measuring instrument. The experimental results (Figure 4.9) show that the surface roughness deteriorates with an increasing laser scan speed or decreasing laser power. Under the processing conditions, it seems that the amount of porosity decreases in the thin layer after sintering affects the surface roughness directly. When more laser energy is provided by adjusting the scan speed or laser power, more binder powder will be melted to fill the pores. The reduction of porosity and shrinkage of pores make the surface smoother. A denser hatch lines and thinner layer also improve the surface quality

because the volume of each sintering hatch line is reduced hence reducing the pores with a fixed amount of fluid provided.

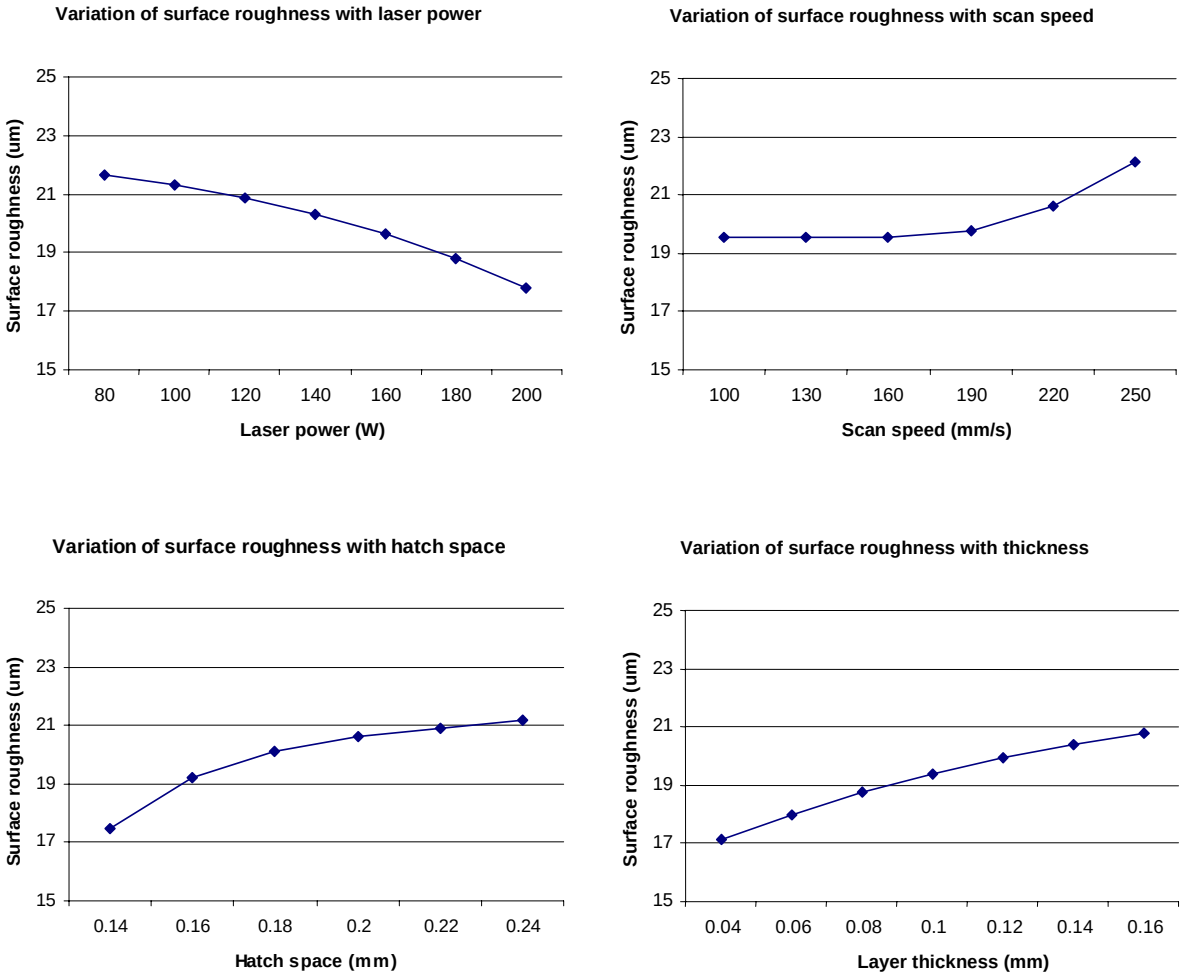

Figure 4.9 Parameter effect on the sintering layer surface roughness

4.5.2.3 Parameter effect on the tensile strength

The strength of the sintered part increases with its density. More energy absorbed by the metallic powder with a high temperature achieved increases the sintering time. The higher temperature of the sintered powder facilitates the flow of the metal. It results in a higher density and mechanical strength. The strength and porosity of the material can be controlled by adjusting various process parameters, such as laser scanning speed and power. Higher laser power, slower scan speed, high hatch density

or smaller thickness (Figure 4.10) could bring about high mechanical strength because more energy is absorbed by the metallic powder.

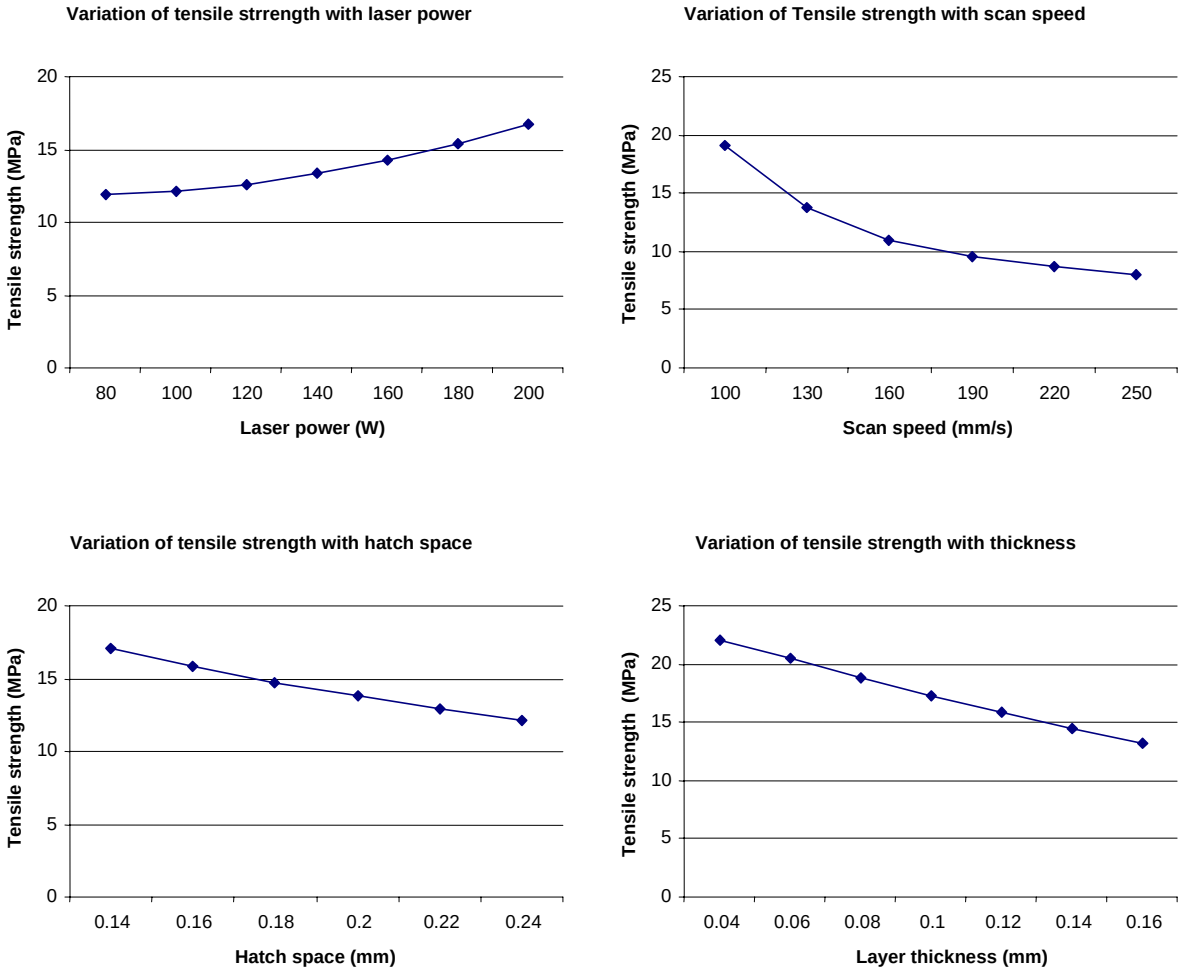

Figure 4.10 Parameter effect on the tensile strength

4.6 Summary

The experimental results show that the effect of different process parameters on the target goals can be quite different and sometime contradict to each other. To optimize the parameters to cater for these target goals, it becomes a multi-objective optimization problem. To solve the problem, an intelligent parameter optimization software system has been developed based on the neural network technology, which is described in the next chapter.

Chapter 5

An Intelligent Parameter Selection (IPS) Methodology for DMLS

In the RP process, the process parameters can greatly affect the final part quality. But some of the relationships between these parameters and their resulting properties are quite complicated. In many cases, the effects of different parameters on the resulting properties contradict one another. For example, to take less time to finish the process, a thicker layer and faster scan speed are needed; but normally higher mechanical properties cannot be achieved in such a case. A fixed set of parameter values that can achieve the best outcome even for two of all desired properties typically do not exist. Very often, these goals do not necessarily result in a similar trend as the change in the process parameters. The way to solve this is to make a trade-off among these goals. But it may still not be good enough when many different requirements from the customers arise. In fact, in different applications, the user is usually more concerned with some of the resulting properties but ignore the rest. For example, if the prototype part is created mainly for design review, processing time and surface roughness will be given more attention; if it is for fit and assembly verification, the dimensional accuracy is more important than the others; and if the part is for limited functional testing, the mechanical strength could be the main (resulting) property concerned. A good scenario is to auto-select the process parameter setting to satisfy the various requirements for different users. This could make the RP applications more agile and acceptable.

To implement the parameter auto-selection system, a generic intelligent parameter selection (IPS) software system is proposed for the DMLS process. The IPS system can capture the causal and inferential knowledge about the relationships between the process parameters and resulting properties to provide expert-level recommendations during the parameter selection process. The purpose of building such a parameter optimization model is to control the quality of the final part and cater to different requirements of the users. In the current stage, the research focused on the developed Cu-based material system needed in the Direct Metal Laser Sintering (DMLS) process. Several important process parameters including scan speed, laser power, hatch space and layer thickness are considered. The resulting properties are mainly focused on the processing time, sintering layer surface roughness, tensile strength and dimensional accuracy.

5.1 Overall IPS System Architecture

The overall architecture for IPS system is shown in Figure 5.1. According to the

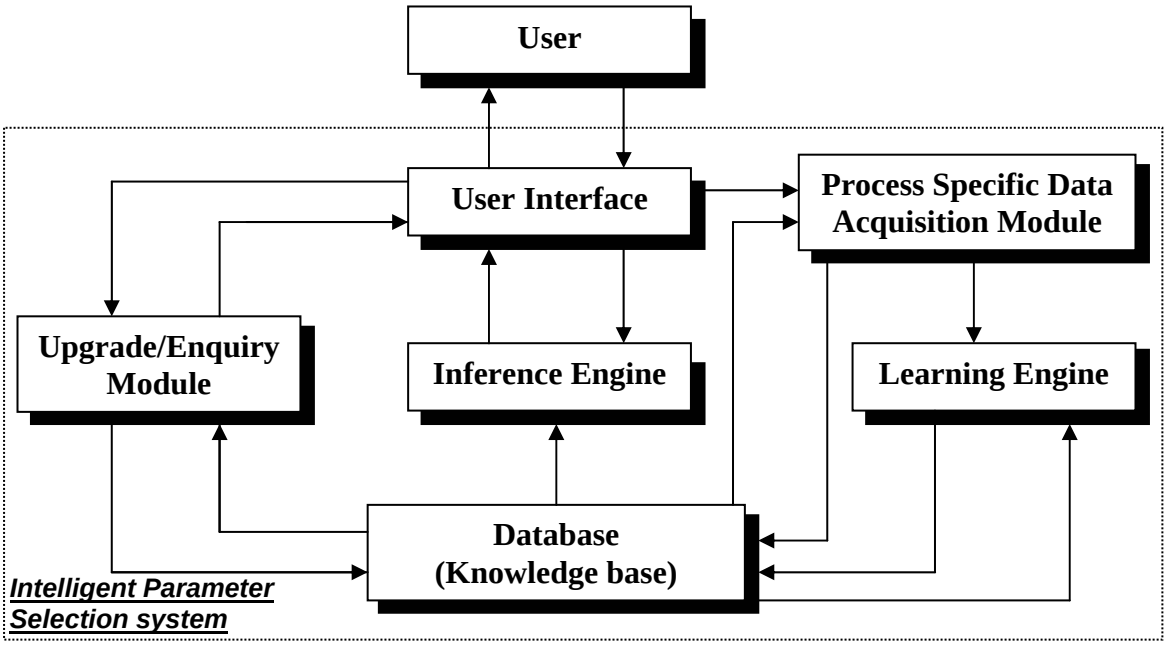

Figure 5.1 Intelligent Parameter Selection (IPS) system architecture

difference in functionality, the system is divided into 6 major subsystems, namely, user interface, process-specific data acquisition module, learning engine, inference engine, upgrade/enquiry module and a global database.

To select a correct parameter setting, the necessary knowledge to build the corresponding database is necessary. Some experimental case results at different parametric values are initially used to help the IPS system create the knowledge base. The IPS system acquires the experimental data through the process-specific data acquisition module and then transfers the data to the learning engine. A neural network (NN) is used to extract rules for system learning. After that, the knowledge base will be built automatically by the learning engine and then stored in the global database.

After the knowledge base is built, the IPS system can help the user select the process parameters automatically to satisfy the different requirements of the resulting properties. Through an effective reasoning mechanism in the inference engine, the IPS will select the most suitable parameter setting and return the optimal result to the user.

In addition, an new upgrade module is to be developed with the purposes for future research given below:

- **Add new material system:** Help the user to implement these methods on other future-developed material systems;
- **Update the knowledge:** some errors or outdated system information needs to be corrected;

- **Update the experimental results to the learning engine:** the user wants to increase the model accuracy by providing more experimental data.

In the following sections, the implementation of each subsystem is described in detail.

5.2 User Interface Module

The primary function of the user interface is to:

- Collect data from user;
- Feedback useful information and help the user make decisions;
- Distribute/gather relevant information to/from the corresponding function modules in the software system.

In the IPS system, a Graphical User-Interface (GUI) module was developed (Figure 5.2) using “Microsoft Windows” as a platform, so to allow the user to interact with the IPS software by means of a graphical display. This allows the user to input data to set up modeling cases, acquire suggestions, access database, and update the IPS system with new knowledge. Some dialog boxes are used to realize the communication between the user and the system.

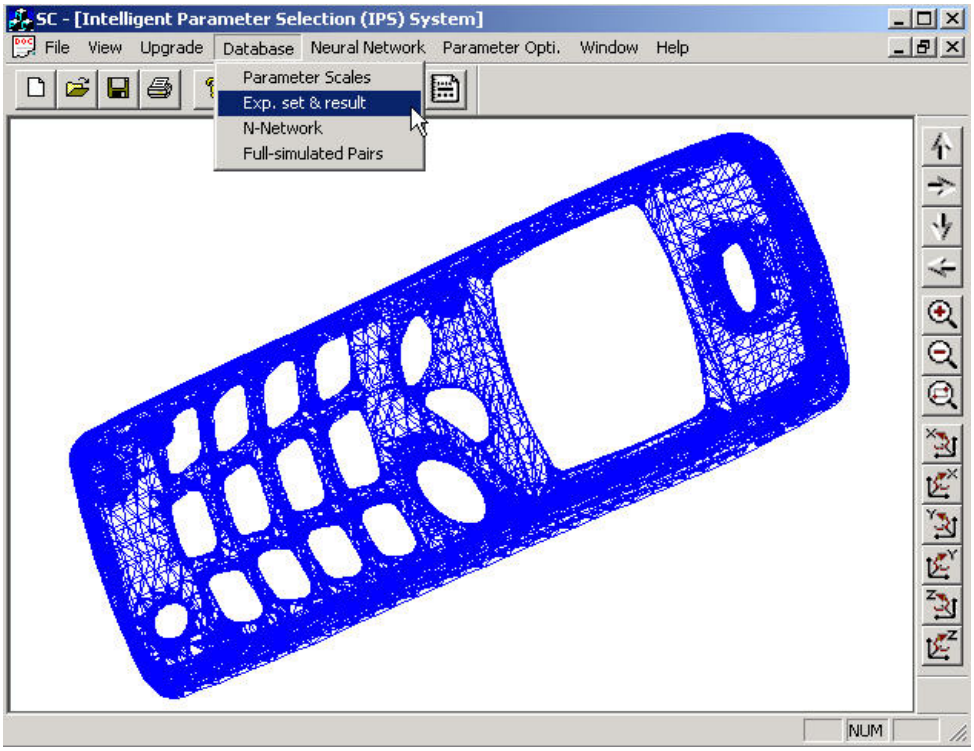

Figure 5.2 GUI of the IPS software system

5.3 Process-Specific Data Acquisition Module

One very important component in this IPS system is its process-specific data acquisition module. Based on the user interface, the process-specific data acquisition module will receive the knowledge that is requested by the system.

5.3.1 Function of the process-specific data acquisition module

To build the mapping relationship between the process parameters and the resulting properties, the process-specific data acquisition module will search the knowledge base and return the necessary information to instruct the user to provide the knowledge for the system. The main process includes the following steps:

- Indicate the process parameter's operating range

For the Cu-based material system used in the current study, the corresponding process parameters were identified. Based on the experiment study, an approximate operating

range of each parameter has been identified and saved in the database (knowledge base). If the user has expert knowledge on the material system that he wants to optimize, he can adjust the operating range of the parameters through the dialog box of the GUI.

- Determine the experimental quantity and parameter setting

The knowledge needed by the IPS system is the factual experimental results with different parameter values. They are the essential data for the IPS system to derive the relationship between the process parameters and resulting properties. Using too few experiment case data impairs the neural network and prevents the accuracy mapping of input and output. Using too many experimental case data increases the experimental time. A common strategy to solve it is to provide the experimental scenarios with a trade-off between the two factors. To ensure reliable NN training results, the process parameter (level) settings should cover the whole working range. The interval between each pair of parameter (level) settings, which can be specified by the application users, will determine the number of experimental cases.

- Import the experimental results

After the user has completed the experiment and gathered the case results, the process-specific data acquisition module will provide a standard format to record the data from user and pass it to the next subsystem, the knowledge learning module.

5.3.1.1 Operating range setting in DMLS process

The maximum and minimum working values of each parameter for the Cu-based material system's used in the DMLS are shown below:

Table 5.1 A sample of the table structure

Sub-table 1 (RP System-DMLS)		
Parameter	Minimum Value	Maximum Value
Scan Power (W)	80	200
Scan Speed (mm/s)	100	250
Hatch Space (mm)	0.14	0.24
Slicing Thickness (mm)	0.04	0.17

5.3.1.2 Parameter level setting

To research the relationship between the concerned parameters and the resulting properties, experiments were conducted. The design of the test part is given in Chapter 4.5.1. Because the operating range of each parameter is large, 2 levels are not enough to cover the whole scale. All these considered parameters were then set in three levels. If using the full factorial designs (Frigon and Mathews, 1997), total of 81 test parts need to be built. To reduce the experimental trials, one of the fractional factorial design methods, called orthogonal arrays experimental design method was adopted. To further reduce the experimental time, a module in the system software was developed to combine several parts to be built onto one platform and based on different process requirements of each part to set the scan speed and laser power. Because layer thickness cannot be changed in one processing time, we set the other three parameters level according to orthogonal arrays with a fixed layer thickness level. The layer thickness also set to 6 levels and totally 54 test parts were built in this work. The setting of the parameter levels is shown in Table 5.2.

Table 5.2 Parameter setting for the experiments

Test No.	**SS* Value**	**LP Value**	**HS Value**	**LT Value**	**Test No.**	**SS Value**	**LP Value**	**HS Value**	**LT Value**
For training samples									
#01	100	100	0.25	0.05	#28	120	80	0.25	0.075
#02	150	100	0.20	0.05	#29	120	120	0.20	0.075
#03	200	100	0.15	0.05	#30	120	160	0.15	0.075
#04	150	150	0.25	0.05	#31	180	80	0.20	0.075
#05	200	150	0.20	0.05	#32	180	120	0.15	0.075

#6	100	150	0.15	0.05	#33	180	160	0.25	0.075
#07	200	200	0.25	0.05	#34	240	80	0.15	0.075
#08	100	200	0.20	0.05	#35	240	120	0.25	0.075
#09	150	200	0.15	0.05	#36	240	160	0.20	0.075
#10	100	100	0.25	0.10	#37	120	80	0.25	0.125
#11	100	150	0.20	0.10	#38	180	80	0.20	0.125
#12	100	200	0.15	0.10	#39	240	80	0.15	0.125
#13	150	100	0.20	0.10	#40	180	120	0.25	0.125
#14	150	150	0.15	0.10	#41	240	120	0.20	0.125
#15	150	200	0.25	0.10	#42	120	120	0.15	0.125
#16	200	100	0.15	0.10	#43	240	160	0.25	0.125
#17	200	150	0.25	0.10	#44	120	160	0.20	0.125
#18	200	200	0.20	0.10	#45	180	160	0.15	0.125
#19	100	100	0.25	0.15	#46	120	80	0.25	0.175
#20	150	150	0.25	0.15	#47	180	120	0.25	0.175
#21	200	200	0.25	0.15	#48	240	160	0.25	0.175
#22	100	150	0.20	0.15	#49	120	120	0.20	0.175
#23	150	200	0.20	0.15	#50	180	160	0.20	0.175
#24	200	100	0.20	0.15	#51	240	80	0.20	0.175
#25	100	200	0.15	0.15	#52	120	160	0.15	0.175
#26	150	100	0.15	0.15	#53	180	80	0.15	0.175
#27	200	150	0.15	0.15	#54	240	120	0.15	0.175

*SS, *Scan Speed* (mm/s)*;* LP, *Laser Power* (W)*; HS, Hatch Space* (mm)*;* LT, Layer t*hickness (mm).*

5.4 Knowledge Learning Module

In the RP field, several important process parameters could determine the final properties effectively. But the relationship between them is complicated and has not been precisely known thus far. The knowledge extraction from the experimental data to derive these relationships is a formidable task that requires sophisticated modeling techniques. A neural network (NN) that adopts the backpropagation (BP) learning algorithm (Fu, 1994) is used as the learning model to solve this problem. The widespread applications of the NN are attributed to its excellent performance in the modeling of nonlinear relationships involving multiple variables, in place of conventional techniques.

5.5.1 Multilayer feed-forward network

An NN is a massively parallel-distributed processor made up of simple processing units (neurons) (Haykin, 1999). Simulating interconnected neurons working in parallel, NN is a simplified mathematical model to simulate the neural behavior. Following the fast development of computer technology, intensive calculations are no longer the bottleneck to NN. Since the mid-80's, many novel NN models, for examples back-propagation (BP) network, radial-basis function (RBF) network, adaptive resonance theory (ART) network and Hopfield network, have been widely applied to optimization problems, pattern classification, image processing, regression problems, simulation and so on. NN applications have gotten a much success in many fields now.

The multilayer feed-forward network is now the most popular NN structure. The network consists of three parts: the input layer that receives the training sample data; the output layer that gives the training results; and one or more hidden layers that connect the input and output layer. The connection between the two units in consecutive layers is weight. Normally, one hidden layer can solve most non-liner approximation problems. In this study, a 3-layer NN model, including one hidden layer, is employed. To simulate the network, a NN software called SNNS (Stuttgart Neural Network Simulator) (1995) was used for this purpose in the study.

During the training process, each non-input unit *k*'s value is described by:

$$\hat{y}_k = \varphi(\sum_{j=1}^{m} \omega_{kj} x_j) \tag{5.1}$$

where $x_1, x_2, ..., x_m$ are the input values of unit *k*; $\omega_{k1}, \omega_{k2}, ..., \omega_{km}$ are the weights

between inputs and unit *k*, $\varphi(\cdot)$ denotes the activation function. The most common activation function, the sigmoid function, used in approximation problems is adopted as:

$$\varphi(v) = \frac{1}{1+\exp(-v+\theta_j)}; \tag{5.2}$$

$$v = \sum_{j=1}^{m} \omega_{kj} x_j; \tag{5.3}$$

where θ_j is the bias of unit j.

Comparing the network output with the target output, the error is computed by:

$$e_j(n) = y_j(n) - \hat{y}_j(n), \tag{5.4}$$

Neuron j is an output unit and $y_j(n)$ is the corresponding target output (given by experimental data). n, is the nth number of the test sample. The backforward errors are used to adjust the weights according to the learning rule. The adjustment gradually brings the output closer to the target output. Till now the BP algorithm is still the most common and powerful learning method.

5.4.2 BP algorithm

The BP network is a multilayer feed-forward network with a different transfer function based on the artificial neuron and powerful learning rules (Haykin, 1999). It was discovered by Parker (1974) and Werbos (1985) independently. Many books (Fu, 1994; Haykin, 1999, etc.) give detailed descriptions about the multi-feedforward network and BP algorithm.

Using the standard BP algorithm, the n^{th} training inputs first propagate forward by a fixed weight until the network's output $\hat{y}_j(n)$ is obtained. Then the errors between the training outputs and target outputs are used to backforward layer-by-layer until it reaches the input layer. During this backforward process, the weights will be corrected according to the delta rule (Haykin, 1999), i.e.,

$$\Delta w_{ij} = \eta \delta_j o_i$$
$$\delta_j = \begin{cases} \varphi_j'(v)(y_j - \hat{y}_j) & \text{if unit } j \text{ is an output-unit} \\ \varphi_j'(v)\sum_k \delta_k w_{jk} & \text{if unit } j \text{ is a hidden-unit} \end{cases} \quad (5.5)$$

where: η denotes the learning factor; o_i the output of the preceding unit *i* (if unit *j* is an output unit, o_i equals to $\hat{y}_j$.); *i* the index of the units with link w_{ij} from *i* to *j*; *j* the index of the current unit; and *k* the index of the units with link w_{jk} from *j* to *k*. During the next training process, the corrected weights will be kept unchanged again at the forward pass. Each sample data pair is used to train the network in the two-pass circulation. The NN is trained by all training samples iteratively until the error can be accepted.

5.4.3 Realization of the DMLS process learning

To develop a backpropagation NN model as the knowledge learning module of the IPS, several stages are necessary:

- Determining the input and output of the NN

At first, the process parameters and resulting properties interested to the user are identified in the process-specific data acquisition module. Their roles in the NN are for determining the input and output parameters.

- Gathering the experiment data for training and testing of the NN

The experiment results of the resulting properties at different parameter level settings contribute to the necessary knowledge that can be used by the NN-based knowledge learning module to derive the relationship between the parameters and result properties.

- Preprocessing the data

After the data are imported to the process-specific data acquisition module, preprocessing of the data is usually required before it is passed to the NN. This is necessary because the sigmoid transfer function in BP algorithm modulates each output to a value between 0 and 1. And the input is also required to have a value in the scale from 0 to 1. Therefore for an input V with maximum and minimum values of $V_{\max}$ and $V_{\min}$ respectively, each value V is scaled to its normalized value A by:

$$A = (V - V_{\min}) / (V_{\max} - V_{\min}) \tag{5.6}$$

- Training the network

In the NN, the process parameters are the input units and the resulting properties are the output units. The data are then randomly separated into a training set and a testing set. A 3-layer NN model with one hidden layer is employed to train the data. The number of hidden layer has a key effect on the training results and should be optimized. The structure that can achieve the best training results would be recorded and used. The network structure and the connected weight values are recorded in the knowledge base after the learing/training is completed.

5.4.4 Training results

Of the 54 sample data pairs, 48 were randomly chosen to train the network. In addition to the 48 samples, 6 other samples were used to validate the training results.

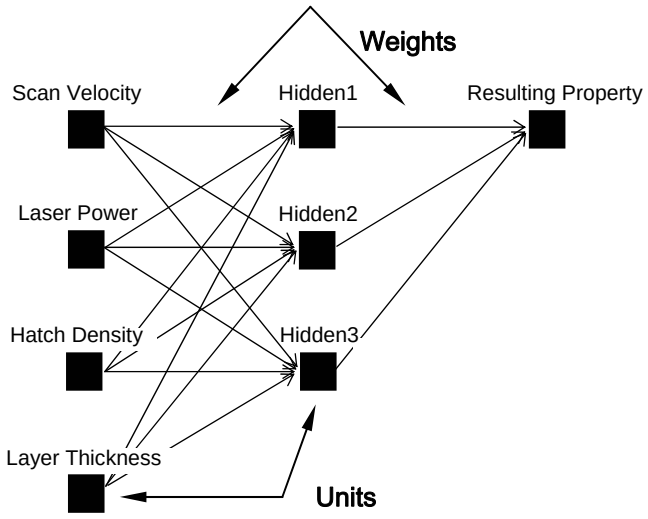

Figure 5.3 Multi-feedforward networks used in the study

Note that the size of the input and output layers are defined by the number of inputs and outputs of the network and, therefore, only the number of hidden neurons has to be specified when the network is defined. The unit number in the hidden layer plays a major role in the network's prediction and generalization capability. In order to avoid over-fitting, the number of hidden layer neurons should not be too large. Unfortunately till now, no effective methods can help decide the network structure accurately. In practice, the training results are fed back to determine the hidden layer and the correlated unit number chosen. A multi-layer feed-forward NN with one hidden layer of three units as shown in Figure 5.3 is selected based on the best training result. Three neural networks with the same structure (Figure 5.3) for different resulting properties: strength, accuracy and surface roughness are built in the SNNS software environment (Stuttgart Neural Network Simulator, 1995). The training session is stopped when the training error is less than or equal to the 0.001 specified. If the training error does not reach the specified minimum error, the session will stop when the number of training cycles exceed 10000.

After training the matrices of the final computed weights and biases of the NN are:

$$\omega_{Strength} = \begin{bmatrix} -0.20529 & -5.20048 & 0.63824 & 0.60013 \\ 0.38141 & -1.34075 & -1.85845 & 4.00797 \\ -0.38032 & -1.23551 & 0.33572 & -2.68487 \\ 0.20270 & -0.52230 & 1.36313 & - \end{bmatrix}; \quad (5.7)$$

$$\theta_{Strength} = \begin{bmatrix} -0.64422 & 0.63439 & -0.04947 & -0.6889 \\ -0.12887 & 1.00304 & 0.08811 & - \\ -0.11929 & - & - & - \end{bmatrix}; \quad (5.8)$$

$$\omega_{Accuracy} = \begin{bmatrix} -0.26094 & -2.37844 & 2.92112 & 0.60013 \\ 7.10154 & 1.08031 & 4.48401 & 4.00797 \\ -3.01699 & 4.21532 & 3.09381 & -3.82447 \\ 7.26316 & -0.81073 & -7.71918 & - \end{bmatrix}; \quad (5.9)$$

$$\theta_{Accuracy} = \begin{bmatrix} 0.21256 & -0.20963 & -0.98822 & 0.41575 \\ -0.91542 & -4.68116 & -6.64827 & - \\ 1.95385 & - & - & - \end{bmatrix}; \quad (5.10)$$

$$\omega_{Roughness} = \begin{bmatrix} 2.26406 & -0.85549 & -0.51144 & -4.24662 \\ -0.02887 & -7.32855 & -1.24812 & -4.32365 \\ 2.73133 & 1.20549 & -1.19670 & 3.17141 \\ 1.66786 & 0.58890 & 6.72328 & - \end{bmatrix}; \quad (5.11)$$

$$\theta_{Roughness} = \begin{bmatrix} 0.92608 & 0.39152 & 0.84960 & -0.62011 \\ -1.57323 & -0.66284 & 2.00800 & - \\ 1.86685 & - & - & - \end{bmatrix}. \quad (5.12)$$

The model performance can be evaluated by the Root-Mean-Square Error (RMSE),

$$RMSE = \frac{\sqrt{\sum_{i=1}^{N} (y_i - \hat{y}_i)^2 / N}}{\bar{y}} \times 100\% \quad (5.13)$$

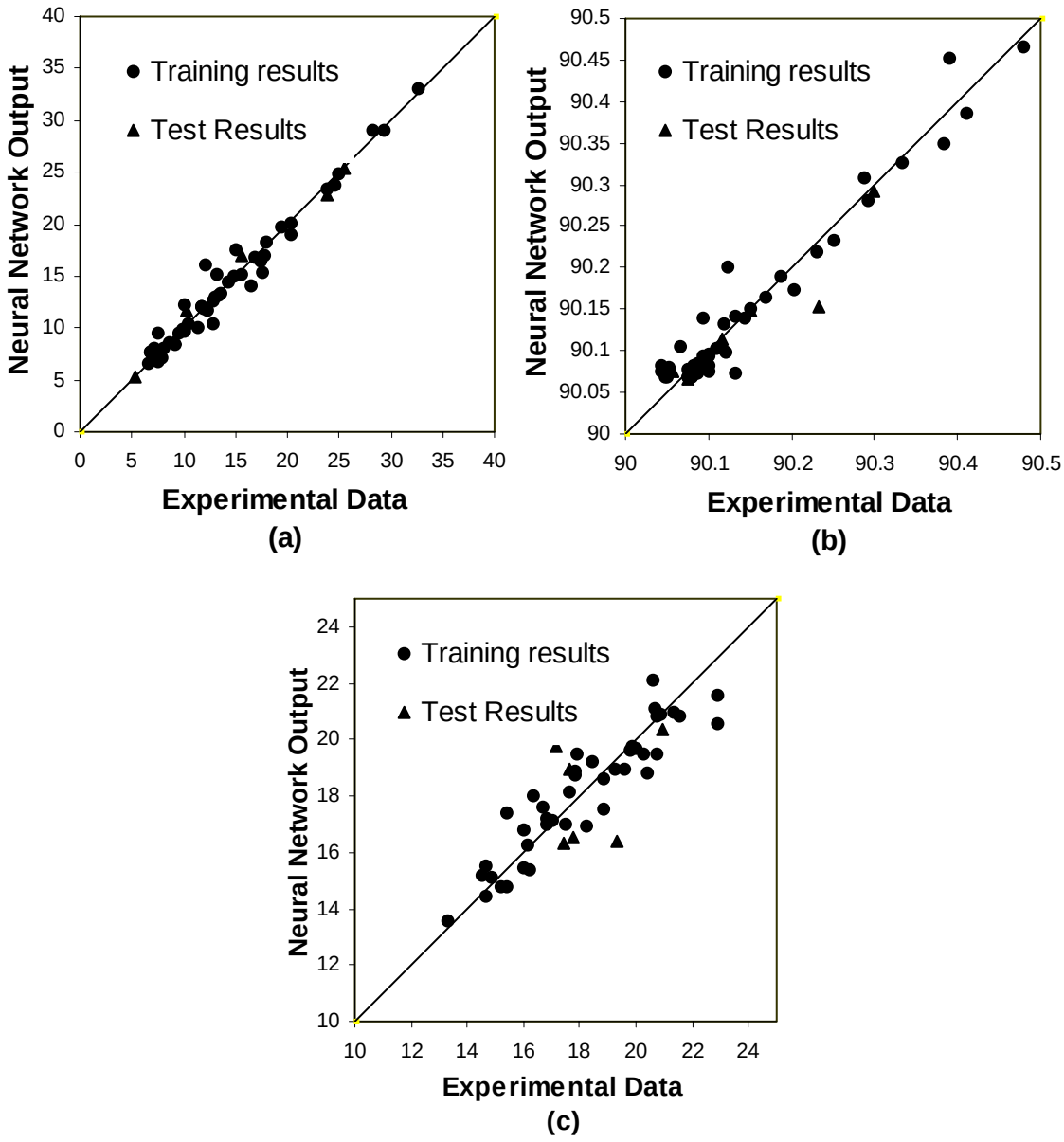

Figure 5.4 Comparisons of experimental vs. predicted **(a)** tensile strength (MPa), **(b)** dimension accuracy (mm), **(c)** surface roughness (μm).

where N, denotes the total number of sample pairs, $\bar{y}$ the average value of the corresponding target outputs. The strength, roughness and accuracy of the prediction RMSE errors for training samples are 8.7%, 15.7% and 10.1% respectively. The RMSE errors for the testing samples are 7.9%, 17.8% and 12.5% respectively which

are at the same level of the corresponding training error. The comparison between the training results and desired results is shown in Figure 5.4 respectively. The training outputs are well matched with the target values.

5.4.5 Full-scale data pairs based on the trained NN

To respond to different users' requirements, only building an inverse mapping between the resulting properties and process parameters is not enough. Most of time, the user's requirement is not specific. In that case, more than one parameter setting scheme may satisfy the demand. So the best one among all the satisfied settings should be selected and fed back to the user. On the contrary, if the requirement is so rigorous and no suitable process parameter setting scheme agrees with it, a corresponding "better" answer will be fed back to user. To realize such function, different parameter settings with the interrelated resulting properties are saved in a case-based database system in advance. To create the database, all the four process parameters were set into different levels according to a fixed interval in the accepted setting range (Table 5.3). Corresponding properties were calculated by the clear mapping relationship built by the NN model according to Equation (5.1). Total of 22022 (13x11x11x14) case settings were achieved.

Table 5.3 Process parameter settings for simulation

Process Parameter	work scale	setting interval	Level number
Scan Power (W)	80--200	10	13
Scan Speed (mm/s)	100--250	15	11
Hatch Space (mm)	0.14--0.24	0.01	11
Slicing Thickness (mm)	0.04--0.17	0.01	14

By embedding the neural network models into the program according to Equations (5.3) and (5.4) and with the weight and biases shown in Equations (5.7) ~ (5.12), the

corresponding results in the surface roughness, dimensional accuracy and strength to the 22022 parameter settings were calculated and saved into the database file automatically. For the processing time, it is not only influenced by the four process parameters, but also related to the processed part volume. So an initial database system, which keep all the processing time units blank, was created includes the process parameter setting values and their corresponding results.

The estimation of processing time can be achieved according to the Equation (5.6). When an STL file of a part's CAD model is read by the slicing software, the part volume and the cavity volume of the part could be calculated according to the following equations:

$$V_{Parts} = \sum L_{Scanlines} \times D_{Hatch} \times D_{Thickness}; \tag{5.14}$$

$$V_{cavity} = \sum L_{Jumplines} \times D_{Hatch} \times D_{Thickness}; \tag{5.15}$$

where: D_{Hatch} denotes default hatch value; $D_{Thickness}$ default thickness value; $L_{Scanlines}$ the distance of each produced scan line and $L_{Jumplines}$ the distance between the endpoint of the first scan line, with the start point of the next scan line. When volumes need to be calculated, a pre-slicing function is run with the default hatch and thickness setting in 0.1 mm.

After computing the part volume and cavity volume, different sample processing times were estimated according to Equation (5.6). The initial database file was updated and all the units in the "processing time" field were filled by the correlative values. Then, the whole database architecture toward the part was dynamically completed. The best value and the worst value of different resulting properties, *i*, were

recorded in the two array variables $R_{i.Best}$ and $R_{i.Worst}$. For the processing time, surface accuracy and dimensional accuracy, the best values should be the minimum one and the worst is the maximum one. But for the strength, it is just the reverse.

5.5 Global Database

To manage the knowledge in the IPS system systemically, a global database was developed. The knowledge is stored according to different RP technologies. At first, a trunk data structure is used to save the different RP system lists. All the useful information for each RP technology is stored in four sub-tables separately. The overall architecture is shown in Figure 5.5.

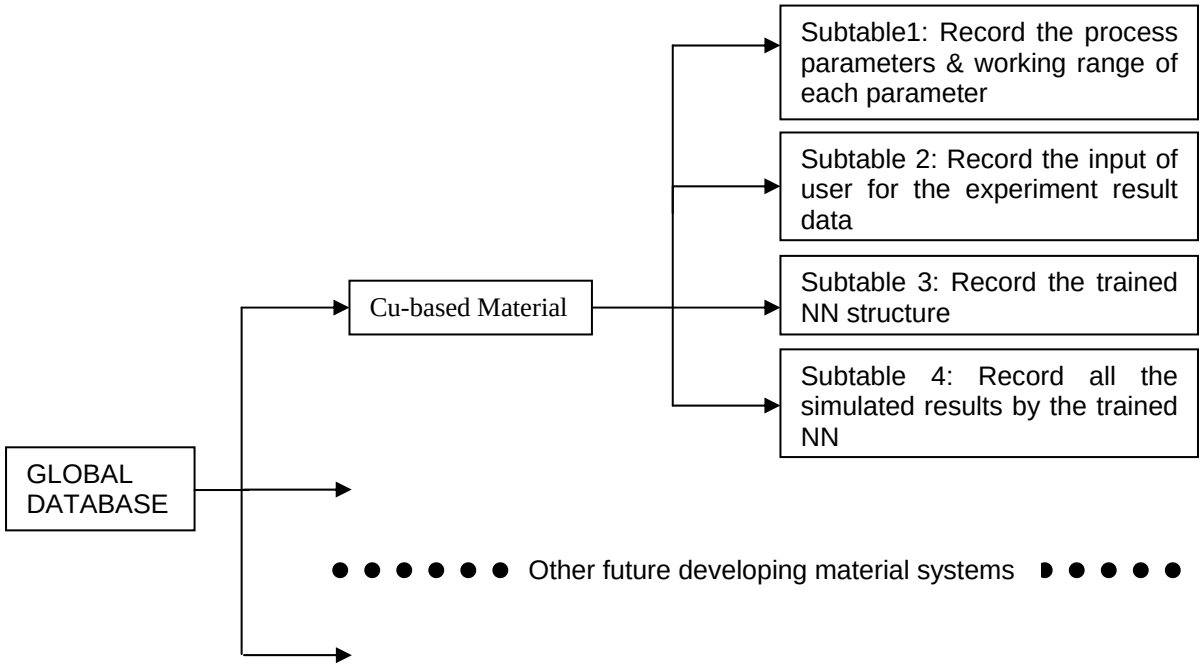

Figure 5.5 Global database architecture

A Microsoft ACCESS® database software was used to manage these data. Microsoft Access allows the user to program the Jet database engine directly through its programming interface known as Data Access Objects (DAO) (Roman, 1999.) The Microsoft Foundation Class Library (MFC) supplies classes for programming with

DAO. A functional program in Visual C++ (VC) embedded in the slicing software was developed to connect the database and user. By calling these DAO classes, a programmer could create and control a database system under the VC program environment securely. Some further programming details for the DAO can be found in (Kruglinski, 1997).

5.5.1 Database for process parameters and working range

The first sub-table records the important process parameters of the corresponding material system. The maximum and minimum working values of each parameter are also saved in this table. The Cu-based material system's sub-table1 database structure is given in Table 5.1 previously.

5.5.2 Database for experiment result data

The second sub-table is used to record experimental data obtained from users. When a user input the experimental case results, the data will be transferred to the learning engine and the mapping between parameters and properties will then be built. At the same time, all these case data make a copy in the sub-table2. The data is useful for further development of the optimization model when some new experiment data are obtained. For data storage in the database system, a blank table with 8 fields was created first. The first four fields correspond to the four process parameters and the second four fields correspond to the four resulting properties. An extra 'ID' field was added to record the setting case number automatically. A sample is shown in the following table:

Table 5.4 A sample of the sub-table 2 structure

Sub-table 2 (DMLS -Cu-based material system)								
ID	Accuracy	Protime	Strength	SurFin	Power	Speed	Hatch	Thickness
1	0.35	36608	33.06	15.54	150	100	0.15	0.05
2	0.1	26733	17.6	13.7	120	160	0.15	0.05
3	0.09	23120	15.85	14.63	160	205	0.15	0.05
. . .	. . .	. . .	. . .	. . .	. . .	. . .	. . .	. . .
54	0.16	9361	17.62	20.83	110	100	0.2	0.16

5.5.3 Database for trained NN structure

All the data in the sub-table2 are transferred to the learning engine to train the NN. After training, the NN structure and weights are saved in sub-table3. A sample of the sub-table 3 that records the NN structure with 4 input units, three hidden units and one output unit is shown below:

Table 5.5 A sample of the sub-table 3 structure

Sub-table 3 (RP Syste-DMLS)							
No.	UnitName	Bias	Layer	Weight1	Weight2	Weight3	Weight4
1	Velocity	-0.64422	Input	0	0	0	0
2	LaserPower	0.63439	Input	0	0	0	0
3	HatchDistance	-0.04947	Input	0	0	0	0
4	Thickness	-0.68889	Input	0	0	0	0
5	Hidden1	-0.12887	Hidden	0.43576	0.38141	-0.38032	0.20270
6	Hidden2	1.00304	Hidden	-0.52230	-1.23551	-1.34075	-5.20048
7	Hidden3	0.08811	Hidden	0.63824	-1.85845	0.33572	1.36313
8	Strength	-0.11929	Output	0.60013	4.00797	-2.68487	0

5.5.4 Database for NN-simulated results

All these data pairs simulated by the trained NN (Chapter 5.4.5) are saved in the sub-table4 (Figure 5.5). This table has the same data storage structure as sub-table 2. The difference between the two tables is: sub-table2 is used to store the actual

experimental results for training the NN, but sub-table4 stores the simulated results by the trained NN. The data saved in sub-table4 are used by the inference engine to search for the most suitable parametric setting for the user.

5.6 Upgrade/Enquiry Module

The upgrade module provides a connection between the users and the database. When a new material system is developed in future, the new experimental data with the NN optimization results can be saved into the database and make the parameter selection function more comprehensive. Besides that, the data saved in the four databases can also be revised based on the future work. The main task is to insert, delete or create data in the database.

5.7 Inference Engine

For a new user's requirement, the system uses a reasoning mechanism to give a recommended parameter setting from the large number of cases that are available in the database. A user interface was built to help the user choose the resulting weight factors for all the four resulting properties. The inference engine is the center of the IPS system. The IPS provides a mechanism that can control the consultation process, and combine rules in the knowledge base with input requirements to give the recommendations. After the trained NN model has been built and thousands of the simulated resulting properties with different parametric value levels have been saved in knowledge base, the system can search for the most suitable parametric setting in the knowledge base according to the different requirements from the user. When the user selects the expected resulting properties and submits the requirements to the IPS, the inference engine will retrieve all the cases stored in the knowledge base and return

the results to the user. During the database retrieval, one of the following three situations will happen:

- Only one case saved in the knowledge base satisfies the user's requirement
- More than one case in the knowledge base satisfy the user's requirement
- All the cases saved in the knowledge base cannot satisfy the user's requirement

In the first situation, the sole result will be returned to the user without any judgments. But in practical applications, often the second or third situation will be encountered. For example, if the user does not input any requirements, all the 22022 cases are selected as candidates to determine the best trade-off parameter setting for all the four resulting properties. In these situations, it is necessary to develop a strategy to help the system select the case that best caters to the demand of the user. The method that will be employed to solve this problem is to use an integrated factor K_{all}. Users can decide the resulting weight factors from 0 to 100(%). Maximum 300 points can be distributed randomly toward the four resulting properties. For example, if the user wants to build a part in the least time and ignore all the other three, he should set the 'track bar control' button into 100(%) and keep the others zeros. If he wants to use the trade-off setting to get the 'best' setting for all four results, he should set the all four 'track bar control' button in the same value. For each case in the knowledge base, half of part that exceeds the user requirement is a bonus and will be added to an integrated factor K_{all}. But if the resulting properties in the case do not satisfy the requirement, the difference will be subtracted from K_{all}. In all the saved cases, the one that has the highest K_{all} value will be returned to the user.

5.7.1 Standard of judgment

It is important for the system to identify the requirement efficiently and find out the most suitable parameter settings from the case database. To compare all the available cases with the new requirement, the system will read the four resulting properties for each case *j* in the database and calculate the ability index (P_{ji}) of the resulting property *i* for the sample *j* as:

$$P_{ji} = (V_{ji} - R_{i,Worst}) / (R_{i.Best} - R_{i,Worst}) \tag{5.16}$$

where V_{ji} denotes the corresponding resulting property value in the case *j*. $R_{i,Best}$ and $R_{i,worst}$, the best and worst values of different resulting properties *i*. The system will then query all the cases in the database and record the one with the maximum integrated factor K_{all}. Based on the condition given by the user, the rule of K_{all} is defined by:

$$K_{all} = \sum_{i=1}^{4} K_i; \tag{5.17}$$

where

$$K_i = \begin{cases} P_{ji} & \text{if} \quad P_{ji} < Set_i \\ Set_i + (P_{ji} - Set_i)/2 & \text{if} \quad P_{ji} > Set_i \end{cases} \tag{5.18}$$

Set_i is defined as the resulting weight factor of different resulting property *i* set by the user.In case *j*, resulting property *i*'s performance factor K_i is determined by the user's requirement (Set_i) and the ability index (P_{ji}).

When more than one case (or no case) meet the user's requirements, a case-based database can help system choose the best answer effectively. After the best-matched

settings is found from the database, the data is selected from the database, and a user interface is displayed to feed-back the 'optimal' answer. The detailed algorithms of the whole process are given in Figure 5.6.

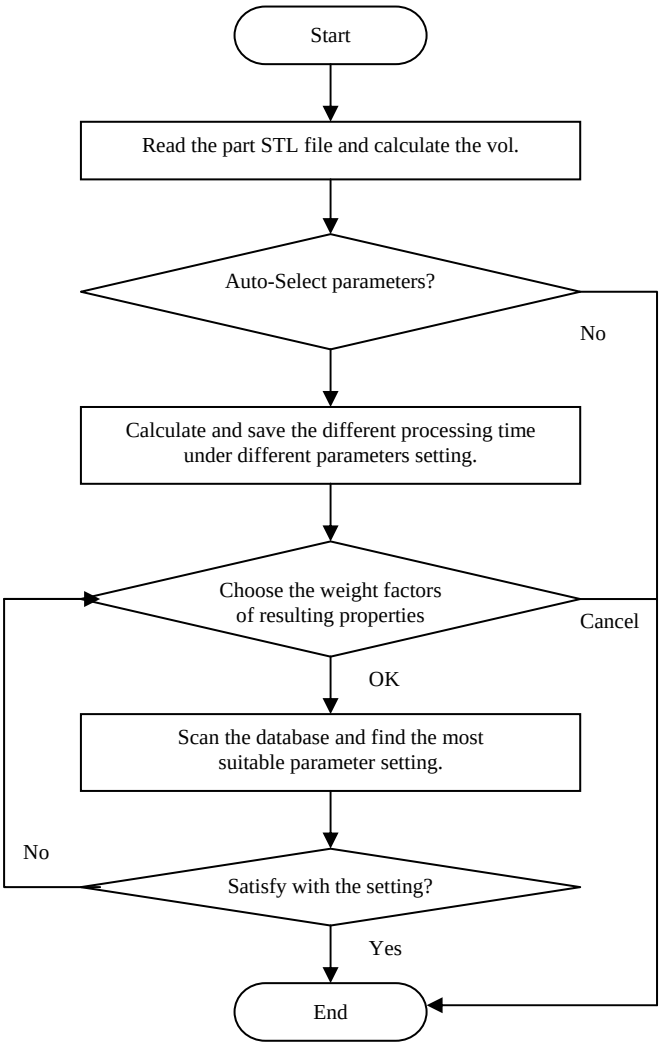

Figure 5.6 The algorithms of the selection process

5.8 Case Study

Two cases (Part I and Part II) of test parts (Figure 5.7) under different property requirements were built to evaluate the methodology and the system. More priority was given to the processing time and dimensional accuracy for the first part. The

second part was given priority on the other two resulting properties. After the user inputs the weights correctly, the system feedback the relative process parameter setting and gives the expected result values. The requirement setting and corresponding outputs for the two parts are shown in Figure 5.8 and Figure 5.9

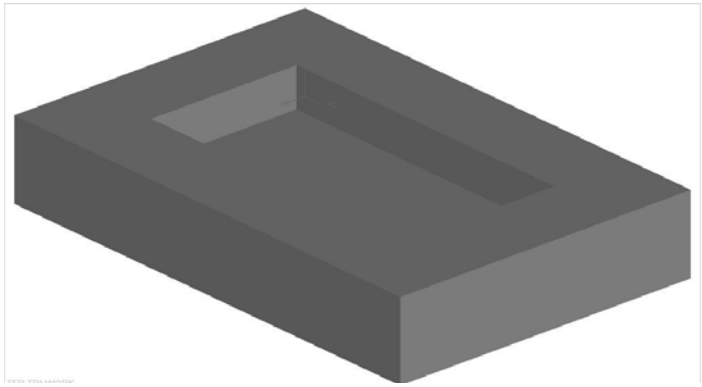

respectively. The figures show the best process parameter setting scheme for each one.

Figure 5.7 3D test part model

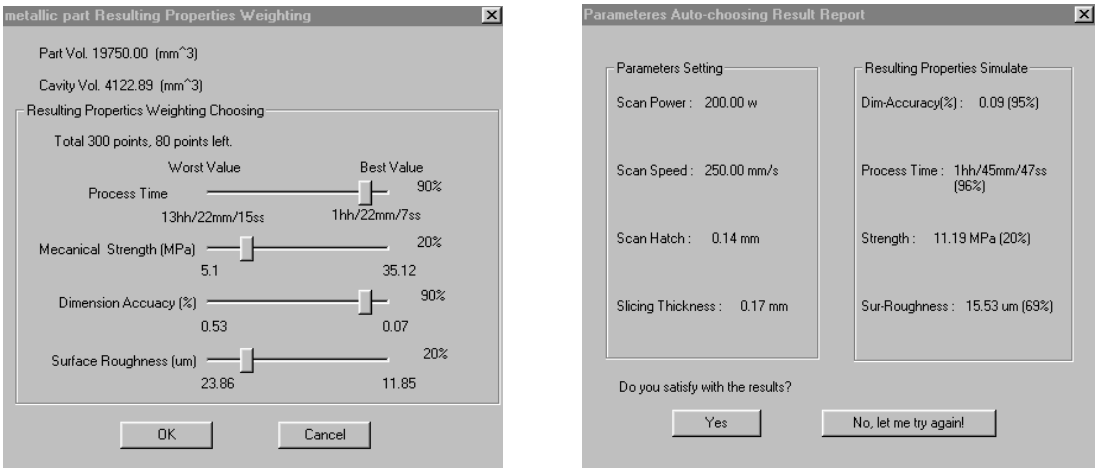

Figure 5.8 User interfaces for user's requirement set-up and corresponding result output (Part I)

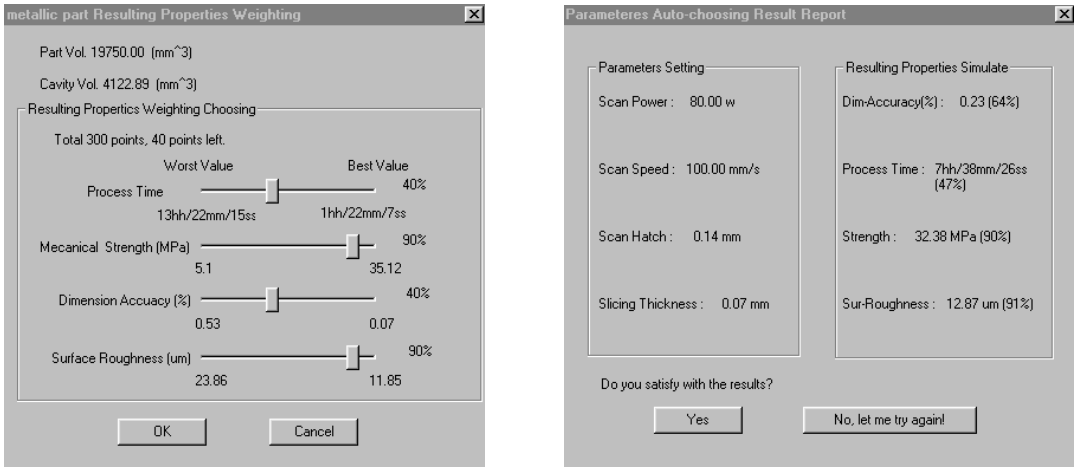

Figure 5.9 User interfaces for user's requirement set-up and corresponding result output (Part II)

Because the strength is linearly related to fractional density (Equation 3.22), the fractional density of the parts was tested as a criterion for the mechanical strength. The comparison between the predicted property values and measured property values on each part is shown in Table 5.6. As can be seen, the actual values show a good correlation with the estimated one. It shows that the software system can generate the correct parameter setting for different property requirements. It also can be used as a tool to predict the final part's process attribute effectively.

Table 5.6 Experimental results for Part I & II

Resulting properties	Changing scale	**Part I** ***LP:200W SS:250mm/s HS: 0.14mm TH: 0.17mm**			**Part II** **LP:80W SS:100mm/s HS: 0.14mm TH: 0.07mm**		
		Pre-Requirement	Predicted Values	Measured Values	Requirement	Predicted Values	Measured Values
Build Time	From 13h22min 15s to 1h22min7s	90%	1h45min47s (96%)	1h45min20s (96%)	40%	7h38min26s (47%)	7h37min21s (47%)
Strength (MPa)	From 5.1 to 35.12	20%	11.19 (20%)	11.44 (21%)	90%	32.38 (90%)	33.2 (92%)
Average Dimensional Accuracy (%)	From 0.53 to 0.07	90%	0.09 (95%)	0.11% (91%)	40%	0.23 (64%)	0.21% (70%)
Surface Roughness (μm)	From 23.86 to 11.85	20%	15.53 (69%)	16.44 (62%)	90%	12.87 (91%)	13.25 (88%)

**: LP: Laser Power; SS: Scan Speed; HS: Hatch Space; TH: Thickness.*

Note: The percentage value denotes the worst to the best performance; 0%~~ the worst performance; 100%~~ the best performance

5.9 Summary and future work

By adjusting an identified set of process parameters, the quality of the DMLS part can be appropriately controlled. For accurate prediction of the resulting properties of the laser-sintered metallic parts, a software system to generate the correct parameter settings for different weight requirements leading to the important resulting properties has been developed. In the first stage, the focus is mainly on the developed Cu-based material Direct used in the Metal Laser Sintering (DMLS) technology. A feed-forward NN is introduced to build a mapping between the goals in relation to the process parameters through experiments, some input-output data pairs have been identified. After continuous training by using the data pairs, this NN constructs a good mapping relationship between the process parameters and the resulting properties.

After the trained NN model was built, each of the parameter was set by using several levels. By combining these levels, 22022 different cases in total were generated and the relative resulting properties were simulated by the mapping model. Users can adjust the value of resulting weight factor for different application requirements. The system will then scan the database and display the most suitable parameter setting. It gives the user a proper guidance and helps the user to quickly determine what they want for a particular application.

Traditional approaches are typically based on mathematical models that need some assumptions and simplifications on their mapping relationships. These assumptions tend to limit the practical applications. Compared with traditional approaches, the NN approach can provide a good mapping between inputs and outputs without the aforementioned assumptions and simplifications. Moreover, the NN model is easier to be built. These advantages make it a powerful tool to predict complicated process relationships. The proposed NN approach is able to predict the properties of the parts built by the DMLS based on the experimental data training. But just 48 training samples are too few for the NN to be sufficiently robust. More experimental data should be provided for the NN training to improving the accuracy of the predicted results in future work.

The software system described in this thesis realizes the multiple process parameter decision support for the DMLS process.

Chapter 6

Material Heterogeneity and Anisotropy of DMLS Process

6.1 Introduction

Unlike the traditional material removal process, rapid prototyping is based on the layered manufacturing principle and is a material additive process. Lin et al. (2001) defined the principle of layered manufacturing fabrication as a decomposition-accumulation process. A 3-D CAD model is first created using a CAD software, such as *AutoCAD, ProEngineer,* etc. Then the model is decomposed with a series of parallel layers with a specific thickness along a predefined part orientation. After that, for most of RP processes such as SLS, SLA, FDM etc, each layer is filled with a series of discrete lines. The building of each 2-D layer can be regarded as the accumulation of parallel hatch vectors. In the SLS process, the laser continuously sinters along the defined hatch vectors to build the layer. Each thin layer of sintered material is successively added over a previous layer. As the laser scans over the material, it melts and sticks together to form the 2-D layer. The sintered material is anisotropic because of the directional nature in the hatching and the part orientation.

Besides direction dependency, the material property of each layer is also not homogenous. The varying lengths of the hatch lines cause local process variations, resulting in heterogeneous material properties. Small variations of process environment, such as the fluctuation of ambient temperature, laser power, etc, can also affect the homogeneity of material.

The length of hatch line has been found to be one significant factor that affects the quality of the final part according to earlier studies (Richard, 1993; Badrinarayan and Barlow, 1995; Beaman 1997). As the hatch length increases, the time delay between energy pulses increases thereby lengthening the cooling time and reducing over-sintering (Badrinarayan and Barlow, 1995). However, a short hatch length and its corresponding short scanning time results in heterogeneity in the material properties of the part. But the effect of material heterogeneity on part quality has not been studied by the former researchers systemically.

6.2 Heterogeneity and Anisotropy

6.2.1 Material anisotropy

Two critical factors determine the material anisotropy. The first is part orientation. Because the part is accumulated layer-by-layer along the orientation direction, material properties are very different in the orientation (build) direction from those directions perpendicular to the orientation. The material properties in these sliced layers are also different in different directions because of the influence of another factor, which is the hatch direction. Unlike the effect of heterogeneity, the effect of the anisotropy on the part quality is comparatively simple because the difference is direction-dependent.

6.2.2 Material heterogeneity

Besides the influence on the material properties due to hatch direction and orientation, the microscopic structure of each layer is uneven. The properties in the local fields filled with different lengths of hatch lines are not uniform. These differences affect the heterogeneity of the material property. The effect of small fluctuation of the

process environment can be neglected because low variability at a macroscopic scale is referred to as quasi-homogeneous (Isaac and Ori, 1994).

Effective control of material anisotropy can be achieved by adjusting orientation and hatch direction. If the built part needs to be on operation under a load, the direction with a higher strength should be in the load direction to prolong the life cycle of the built part. However, it will be difficult to control material heterogeneity because the hatch lengths vary greatly for different geometric shapes. The resulting microscopic material structure varies according to the location on a layer. This property is undesirable because it disrupts the homogeneity in each sintered line and is difficult to control.

6.3 Material Heterogeneity for Different 2-D Layer Geometries

During sintering, the structure powder is wetted and bonded together by the flowing of the liquid binder. The capillary and gravity are the main driving forces for flowing liquid binder to reduce free energy of the system. By the flowing of the liquid metal, the structure powders are wetted and bound together when the binder re-solidification. Sufficiency of the liquid flow is critical to the sintered part density and further affect the sintering quality. Being primarily thermal in nature, the sintering process strongly depends on the temperature variation with time. For a selected material, the physical properties of prototype parts resulting from the DMLS processing are strongly influenced by the temperature history during the laser-material interaction period (Williams and Deckard, 1998). If the time of the liquid-phase is prolonged, the flow of the liquid-phase metal will improve filling up the pores and thereby increasing the densification. Besides the time of the liquid-phase, the highest temperature achieved

at the powder surface is another important factor because it brings about higher temperature gradient to give more surface activation energy for improved liquid-phase flow.

Generally, the distribution of powder temperature vs. time is one of the key factors to affect the final sintered part quality. The sintering process is a dynamic progress and the temperature change of the powder can be divided into two stages. The first stage is the very short time interval in which the laser sintering creates the heat effect zone of the powder material. At this stage, the temperature of the sintering material will increase quickly to achieve the melting point of the binder. The main temperature increase is by absorbing the laser energy (the effect of laser sintering). The remaining time is mainly a heat transfer process decided by the physical properties of the powder on the heat flow and the surrounding temperature. By neglecting the start and end regions of each layer, the temperature variation can be controlled in a similar situation for homogeneity.

6.3.1 Dexel (hatch) model

Based on the RP process, the 2-D layer is filled by parallel hatch vectors. The laser continuously sinters along the hatch vectors to build the 2-D layer. Each hatch vector can be considered as a dexel (Chiu and Tan 1998; Choi and Samavedam, 2001). During processing, the laser sinters along the trajectory guided by the hatch vectors. A voxel with the specific height and width can be built around each hatch vector (Choi and Samavedam, 2001). Each 2-D layer of a specific thickness can be represented as the accumulation of a list of voxels inside as illustrated in Figure 6.1. The change in the sintering quality of the 2-D layer is regarded as a composite effect of the voxels.

To simplify the model, the hatch line vector (i.e. dexel) is used to denote the corresponding voxel. Based on the model, diverse shapes can be regarded as different combinations of hatch lines with different lengths. Analyzing the accuracy due to the effect of geometric shapes can be considered to be similar to analyzing the effect by the hatch lines and their interaction. This method is more direct and easy.

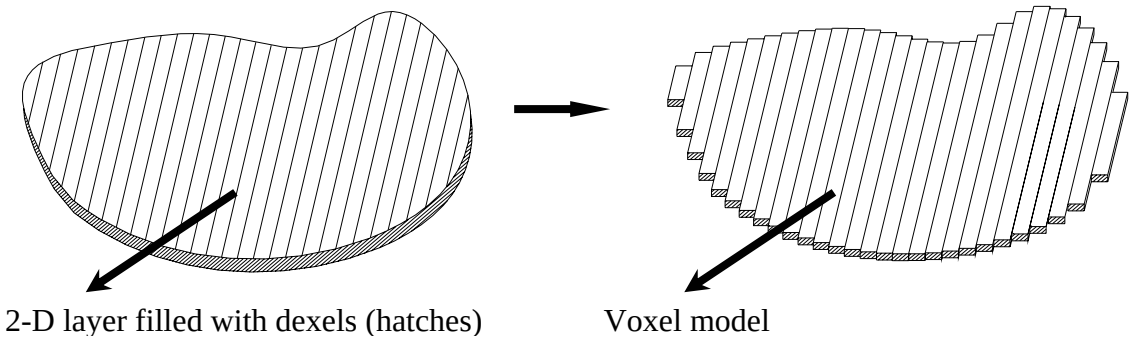

Figure 6.1 Translation from a layer to voxel combination

6.3.2 Neighboring effect brought by the change of hatch length

During the laser sintering process, each sintered point on the surface of the powder bed receives multiple energy pulses of varying intensity (Beaman, 1997). Consider a model in an ideal situation where the length of each hatch is long enough for the temperature to decrease near to the surrounding temperature before receiving next energy pulse. The temperature vs. time curve of a point *P* in hatch *C* is illustrated in Figure 6.2. *T* denotes temperature and *t* denotes time. T_m is the melting temperature of the binder, T_n the process ambient temperature, and t_p is the time when the laser beam focuses on the sintered point *P*. The neighboring second and third energy pulses are due to the effect of sintering the neighboring hatch (A, B, D, E). This effect is defined as neighboring effect.

In this situation and neglecting the hatch lines at the edges, the shrinkage of each hatch line is similar because the temperature variation with time is similar in each hatch line. The integrated 2-D layer shows similar percentage shrinkage along the sintering direction in different geometric regions of the layer.

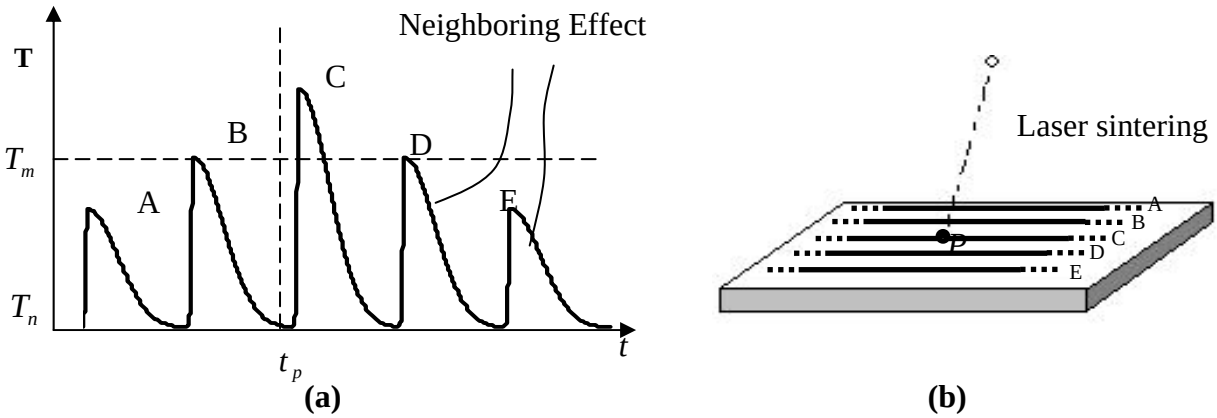

Figure 6.2 Temperature vs. Time curve of point P in 2-D infinite lines sintering

But in practice, the hatch line lengths will be much different for different geometric shapes. In the regions with short hatch lines, the interval between successive irradiations is relatively short. When the interval is not sufficiently long for the surface to cool down, the temperature in the region will be gradually built up, resulting in higher temperature and longer existing time of the liquid-phase. The variation in the temperature history when sintering hatch lines of different length causes differential shrinkage in the 2-D layer and thereby reduces the sintering accuracy. The negative effect of the short hatch line sintering on accuracy is referred herein as the negative neighboring effect. In this situation, the curve of temperature vs. time will change to the situation as shown in Figure 6.3. Tontowi and Childs (2001) studied the effect of different pre-heating temperatures of the powder bed on the part density and energy density. The effect brought by the neighboring hatch lines can be

regarded as pre-heating and post-heating that could change the pattern of powder bed temperature distribution dynamically. When the temperature and time feature in different regions are not similar, the sintering quality would most likely to be different.

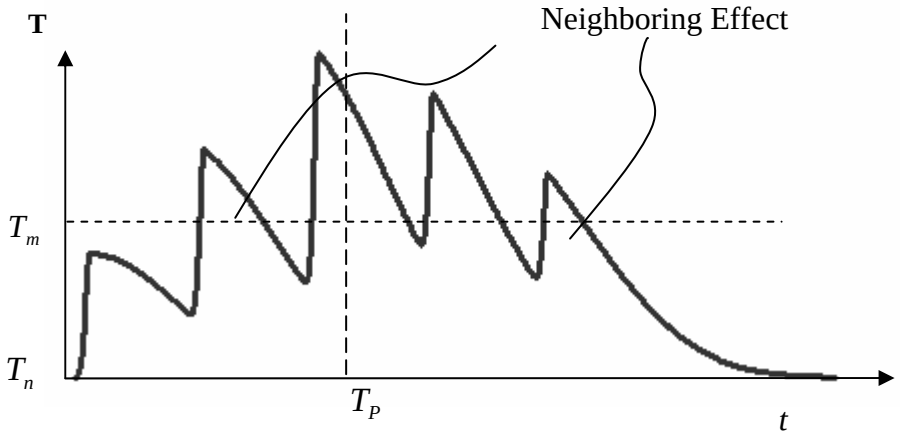

Figure 6.3 The negative neighboring effect on the Temperature vs. Time curve

Williams and Deckard (1998) have tested the effect on the density and strength of variable delay periods between successive irradiation exposures during the laser-material interaction period due to change in geometry using bisphenol-A polycarbonate material. The results show an obvious change on the density with the variation of delay period. Similarly, the other properties such as the percentage shrinkage around the region of shorter dimension are expected be different and affect shrinkage uniformity of the layer. More seriously, distortion and warpage of the sintered layers may occur with such differential shrinkage in the part. Besides the neighboring effect causing uneven shrinkage, the heat-affected zones arising from the finite diameter of the laser beam are also different when sintering regions of short hatch lines due to the variation in the temperature profile. To solve these problems, the temperature profile of the sintered powder should be maintained as uniform as possible.

6.3.3 Experimental validation

6.3.3.1 Apparatus setup

To verify the aforementioned analysis of the temperature variation on regions with different hatch line lengths, several experiments have been conducted using a RAYTEK® MXCF modal non-contact infrared thermometer (Figure 6.4). The distance between the measured object and the sensor of the infrared thermometer was set to be around 500mm and the measured spot size was around 6mm. The temperature in the measured spot was measured continuously and the average temperature was recorded at an interval of 300ms. Three parts of lengths (l) (Figure 6.4) of 40mm, 15mm and 5mm were sintered respectively. The scan speed was set at 100mm/s, with hatch line distance of 0.2 mm and layer thickness of 0.1mm. The laser power was reduced to 10W and the measured temperature was located at the measuring range of the infrared thermometer from –50°C to 900°C.

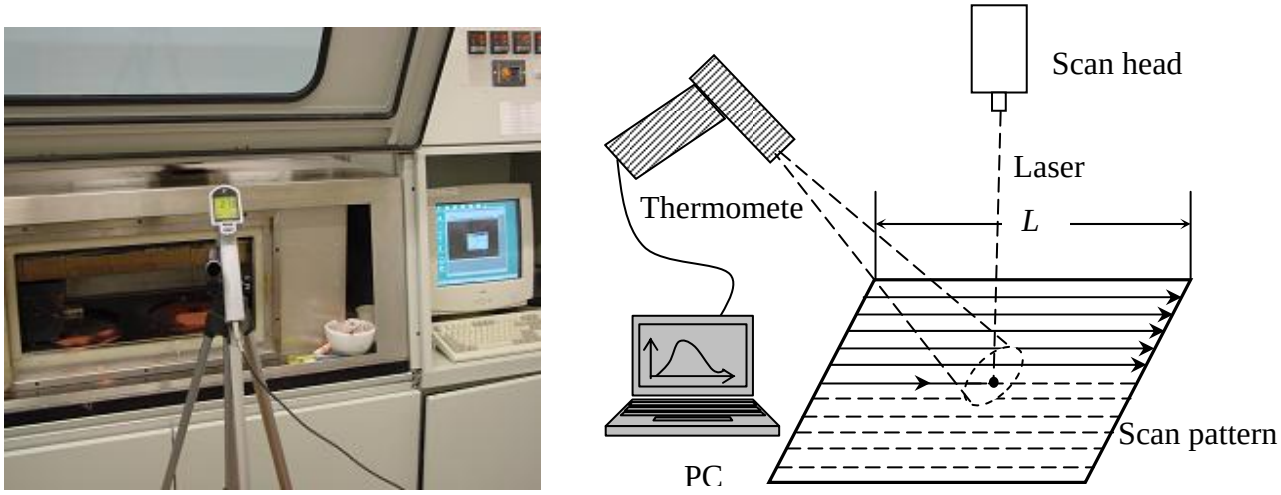

Figure 6.4 Experimental setup for continuous temperature measurements

6.3.3.2 Experimental results

The curve of the average temperature against time in the measured area during the sintering process was obtained. Figure 6.5 shows the measured results of the three parts with different hatch lengths. As shown in Figure 6.5 (a)~(c), the temperature accumulation by the pre-heating and post-heating of the neighboring effect is more serious when the hatch line is shorter. The highest temperature shown in (a) is greater than 900°*C*, which is much higher then the ~700°*C* shown in (c). It provides evidence of the difference in the temperature history obtained in the regions with different hatch line lengths. The flat region in (a) is due to the actual temperature exceeding working- range limit of 900 °*C* of the thermometer device.

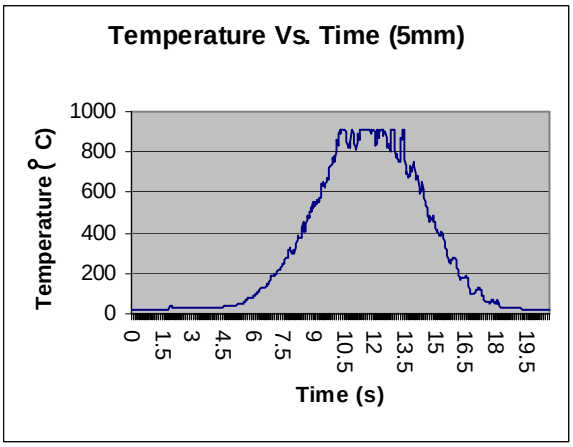

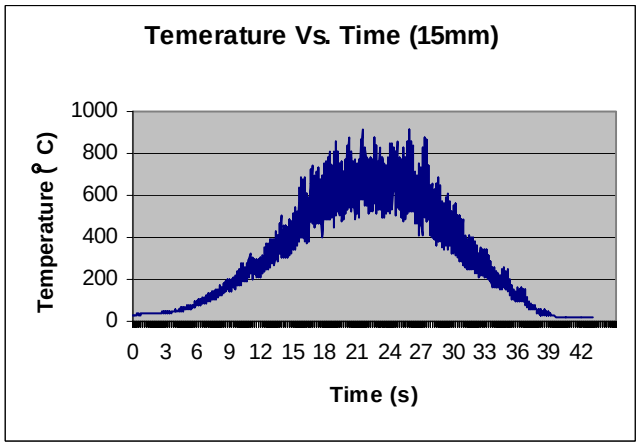

(a) (b)

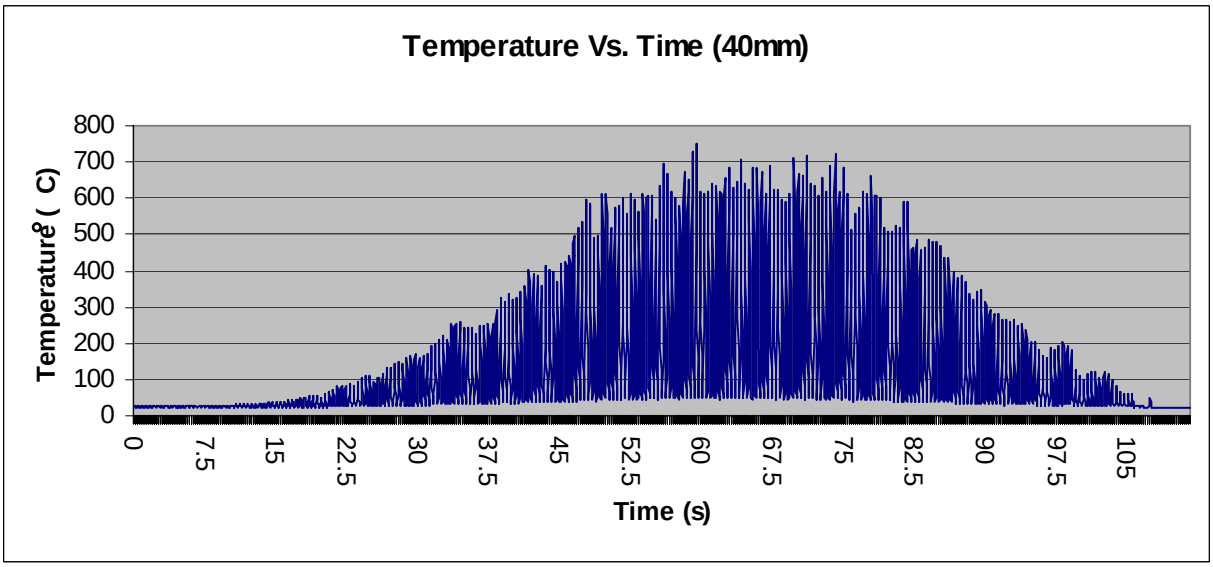

(c)

Figure 6.5 Temperature variation at the measured spot during the sintering process

6.4 The Effect of Material Heterogeneity and Anisotropy on the Part Quality

6.4.1 Microstructure of the part built with different hatch length

The morphologies of the sintered parts built with different *L* were observed using the scanning electron microscopy (SEM) JESL® JSM-5500 System (JESL, 1999) and are shown in Figure 6.6. In Figure 6.6 (a), *L* is the smallest and it can be seen that the inter-connected pores are small. With increased *L*, the inter-connected pores become bigger. But when *L* is sufficiently long, there is little change in inter-connected pore

size, as can be seen in Figures 6-(d), (e) and (f). These indicate that the sintered material becomes denser with shorter hatch lines (Table 6.1). Under that circumstance, the sintered powder does not have sufficient time to cool down as it absorbs energy transferred from the neighboring hatch during the sintering process. The absorbed energy adds to the density of the energy, resulting in a denser structure.

Table 6.1 Fractional density of sintered sample using different length of hatch lines

	Packed powder	*L*=3mm	*L*=10mm	*L*=30mm	*L*=50mm	*L*=70mm
Fractional Density	60.5%	79.6%	75.2%	70.3%	69.1%	68.6%

6.4.2 The effect of material anisotropy and heterogeneity on part strength

To investigate the effect of material anisotropy and heterogeneity together on the tensile strength of the part, a set of experiments was designed and implemented.

6.4.2.1 Experimental study on tensile strength

The specimens were designed according to the ASTM Standard E8 (ASTM, 1999) for the tensile testing of metallic materials with a 0.235mm offset (Tang et al., 2004) for the laser beam compensation. The thickness and reduced sectional width of the specimen are both 6.35mm. The over-all length *L* is 92mm. All the dimensions follow the ASTM Standard E8.

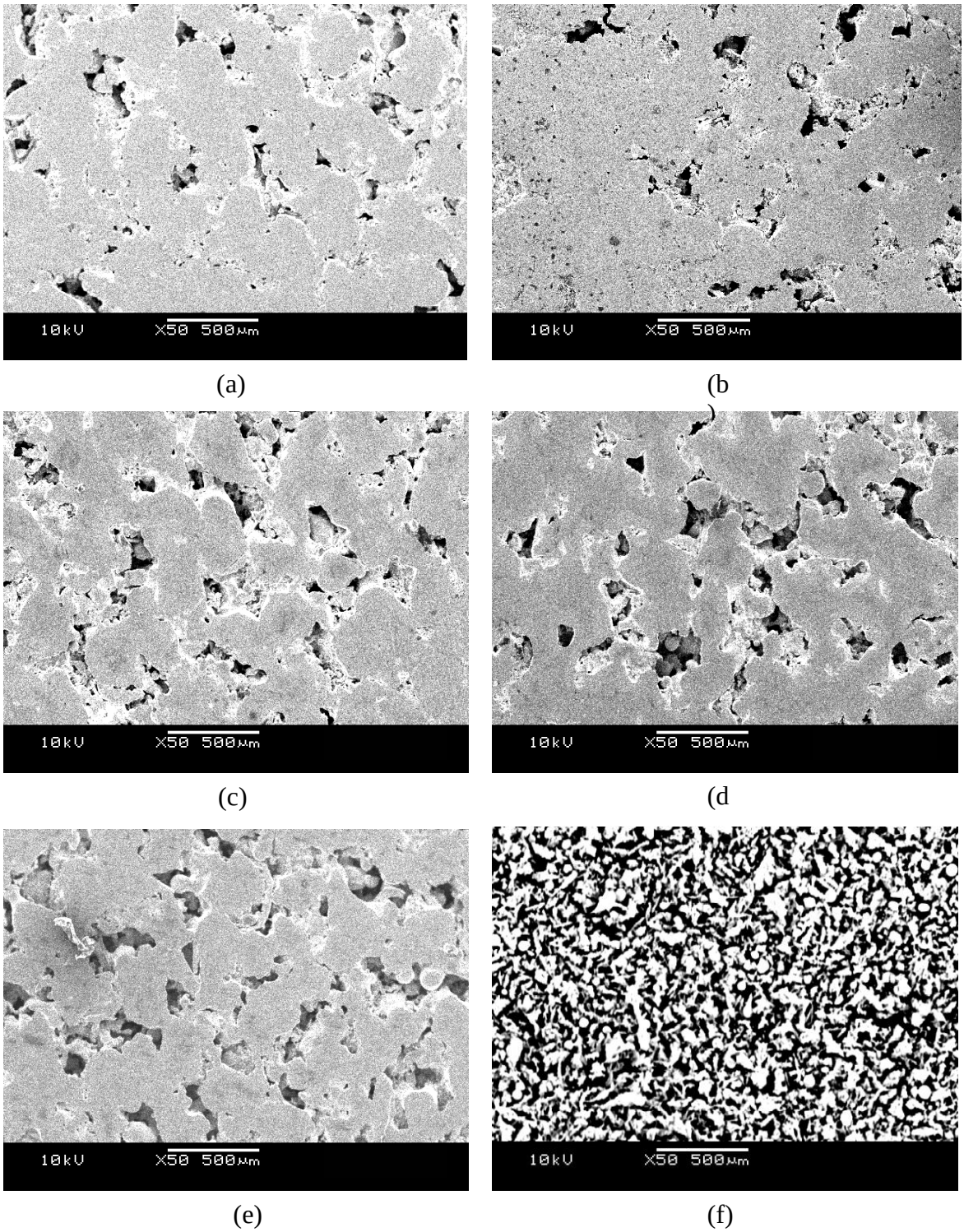

Figure 6.6 SEM image of sintered samples using different length of hatch lines: (a) *L*=3mm; (b) *L*=10mm; (c) *L*=30mm; (d) *L*=50mm; (e) *L*=70mm; (f) Packed powder

To study the influence of material anisotropy and heterogeneity on the part strength, two groups of experiments were designed. Except for the hatch direction and part orientation, all the other process parameters are set as follow:

Laser scan speed: 100mm/s; laser power: 100W; hatch space: 0.2mm; and layer thickness: 0.2mm.

In the earlier research (Gibson and Shi, 1997; Ahn et al., 2002), different hatch directions usually result in different hatch line lengths that consequently cause significant difference of mechanical strength. But the direct relationship between the hatch direction variation and the mechanical strength when hatch line kept unchanged was not investigated. In these experiments, the first Group A (Table 6.2) includes three cases with different orientations and hatch directions. In Group A, the specimens were built by the DMLS machine directly and the length of hatch lines were different. These were designed to test the different mechanical properties in different orientations and hatch directions with the effect of hatch line lengths (short: A1 and A3, long: A2). The other group, Group B, was designed to remove the influence of material heterogeneity (caused by short hatch lines) on the mechanical properties. In Group B, a cuboid was built first. After the cuboid was built, it was cut to the standard specimen by using the wire cut Electrode Discharge Machine (EDM). A subgroup (B1) in Group B has the same orientation and hatch direction as another subgroup A1 in Group A. The only difference between these two parts is the hatch length in each layer. Unlike the short hatch lines sintered in A1, the hatch line that makes up the layers of B1 is part of a long hatch line. This difference in hatch length is similarly applied to B2 and A3.

Table 6.2 The design of experimental specimens for Group A & B

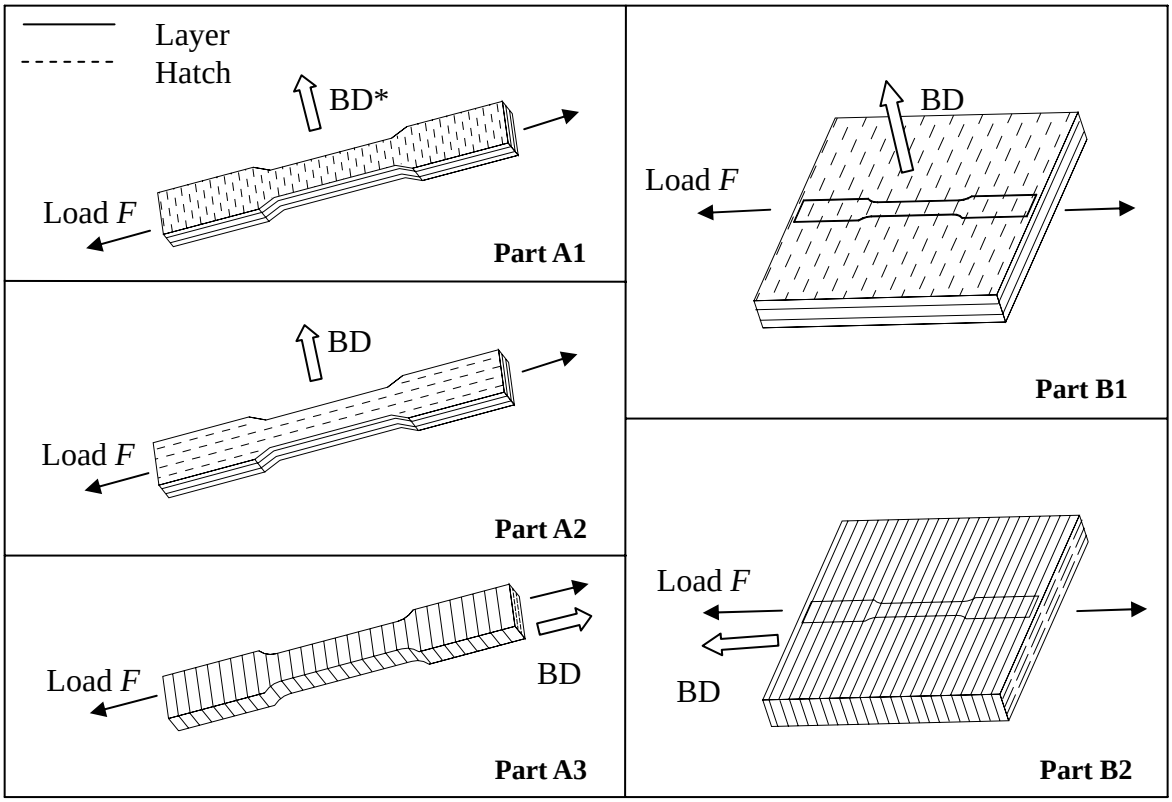

*BD: build direction.

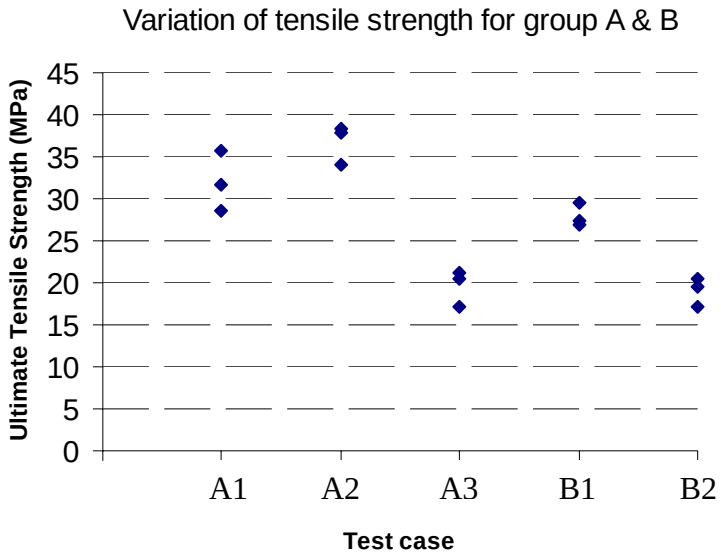

Figure 6.7 Variations of ultimate tensile strength for groups A & B

6.4.2.2 Results and Discussions

Each of the subgroup sets was built three times by the DMLS system. Using the Instron® model 8501 dynamic testing system (Instron, 1990), the ultimate tensile strengths σ of the test parts are obtained and shown in Figure 6.7. When the part orientation is perpendicular to the load direction, the average part strength is higher than the parallel ones (i.e. >25 MPa, Subgroups A1, A2 & B1). In these three parts with a build orientation perpendicular to the load direction, the average strength of subgroup A2 is 36.78 MPa. In this case their hatch directions are parallel to the load direction. The other two in Subgroups A1 and B1 have a lower average strength of 32.01 MPa and 27.90 Mpa ($\sigma_{A2} > \sigma_{A1}$, $\sigma_{A2} > \sigma_{B1}$) when the hatch direction is perpendicular to the load direction. The average strength of those in Subgroups A3 & B2 with the part orientation parallel to the load direction was lower (i.e. 19.61 MPa and 19.03 MPa, respectively). The part that uses a longer hatch line has reduced part strength when other process parameters are kept unchanged ($\sigma_{A1} > \sigma_{B1}$, $\sigma_{A3} > \sigma_{B2}$ respectively). This is because a higher density brought by the short hatch lines improves the part strength.

Two findings can be summarized from the above results are: first, although both the orientation and hatch direction affect the anisotropy, orientation has greater influence on the part strength; second, the length of the hatch line also affects the part strength. The strength of the built part using short lines is bigger than that using long hatch lines.

From the study of the strength variation with different hatch directions and orientations, the effect of the length of hatch line on the part strength has been identified.

6.4.3 The effect of the 2-D layer geometric shape on the material shrinkage

The infiltration of the liquid binder into pores causes significant volume shrinkage due to the reduction of the amount and volume of the porosity in the sintered layer. Besides these, some other factors also affect the final volume shrinkage result. These include the grain growth of the binder and the thermal shrinkage due to the elastic compressive shortening in the cooling stage.

The shrinkage along the orientation direction could be compensated by the deposited metallic powder from the next sintering layer except the top layer. Because the thickness of each layer is quite small (0.1mm), the effect of material shrinkage on the dimensional errors in the build orientation can be neglected. For the parallel scan pattern, the in-plane shrinkage is mainly along the sintering direction. From a previous research (Jacobs, 1992), the material shrinkage is determined by the energy (temperature) change of the sintered powder and the material properties. When the history of the amount of energy transferred to powder material with time is changed by the effect of negative neighboring effect, the uniform shrinkage in different regions in the same layer would be broken. In this situation, it will be hard to use a fixed scaling factor to compensate the shrinkage effectively. The effect deteriorates the dimensional accuracy of the final parts. A more serious distortion and warpage problem would occur due to different percentage shrinkage changed with different geometry shapes.

From the analysis above, it is feasible to control the shrinkage by adjusting the energy density of the laser. If the temperature variation at each hatch line is properly controlled, the composite 2-D layer would show more consistent behavior in shrinkage. Two developed methods were given in the next chapters to reduce the negative effect of heterogeneity on the material accuracy.

6.5 Summary

In DMLS, the sintered material is anisotropic and heterogeneous, affecting the quality and performance of the built parts. This chapter presents a study that focuses on these two material properties and based on the experimental results, presents the causes of these two properties and the effects of the properties on the part quality, including tensile strength, microstructure, and material shrinkage.

Chapter 7

A GA-based intelligent hatching method for improving the material homogeneity of DMLS process

7.1 Introduction

As discussed in the previous chapter, material properties in each layer are heterogeneous because of different lengths of hatch lines in sintering. By applying a proper hatch direction, the variation of the lengths of hatch lines can be controlled effectively. But thus far, other hatch direction search methods only aim to reduce the number of hatch vectors. Rajan et al. (2001) proposed an algorithm to select the scan hatch direction by minimizing the hatch vector segments. Qiu et al. (2001) chose the path direction with two intelligent features: "least number of paths" and "closest next starting point". No implemented method is available to effectively reduce the negative effect brought by the length of hatch line by optimizing the hatch direction. Therefore, the relationship between the hatch direction and length of hatch line should be studied. This chapter presents a method to reduce the effect of short hatch lines by optimizing the hatch direction.

7.2 Quantitative Relationship between the Hatch Length and the Material Heterogeneity

7.2.1 Experimental setup

In order to study the relationship between the hatch length and the material heterogeneity, a series of blocks (Figure 7.1) of different length L have been built. L has seven values, with greater length towards shorter one. These are listed in Table

7.1. The height of every block is 10mm.Three of each block (illustrated by *A, B, C* in figure 7.1) were built and the average of the measured values from the three parts were taken. The process parameters were laser power of 100W, hatch space of 0.2mm and layer thickness of 0.1mm. In each layer, the laser sintered the block at a turn; i.e. started sintering block A1 and after sintering A1, moved the beam to the top-left corner of A2 and sintered the block, until finally, C7 was sintered.

Table 7.1 Lengths setting

	1	2	3	4	5	6	7
Size(LxW)mm	3x20	6x20	10x20	18x20	30x20	50x20	70x20

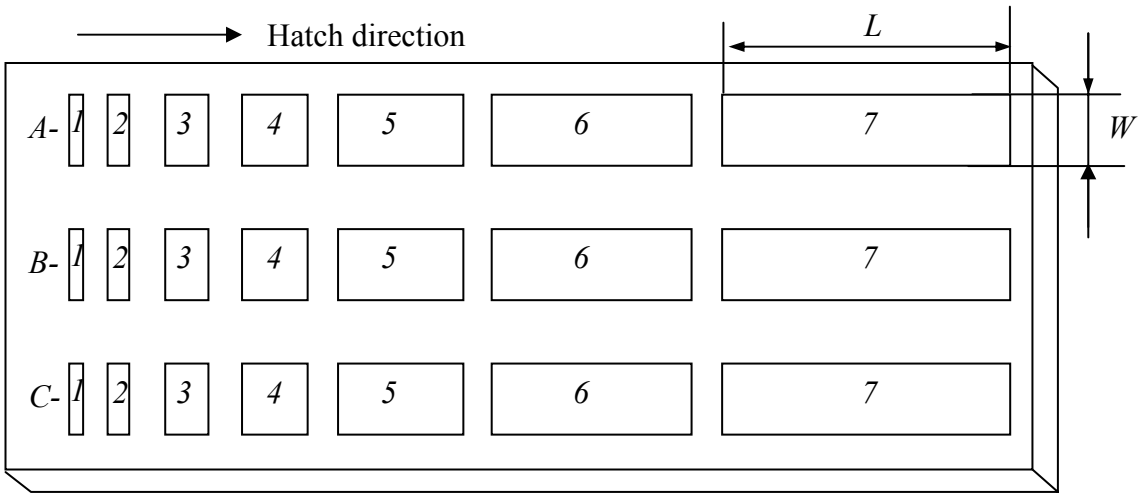

Figure 7.1 Sintered blocks with different lengths

7.2.2 Variation of percentage shrinkage with hatch length

Results of SEM experiments (Chapter 5.4.1) indicate shorter hatch lines will have more serious effect on the homogeneity of the part. As a denser part will result in higher percentage shrinkage, this can be used as a measure of the effect of hatch length on the part property. The percentage shrinkage *S* of each block can be calculated as:

$$S = (L - L')/L \tag{7.1}$$

The actual length *L'* of the block was measured using the Deltronic® MPC-5 System (DELTRONIC, 1998) with an accuracy on 0.001mm. The percentage shrinkage obtained for each case of nominal length *L* is based on the mean value calculated from the three built parts and is shown in Table 7.2.

Table 7.2 The change of percentage shrinkage with varied *L*

L	Percentage shrinkage
L=3mm	9.8%
L=6mm	5.2%
L=10mm	2.9%
L=18mm	1.6%
L=30mm	1.1%
L=50mm	0.8%
L=70mm	0.8%

Table 7.2 shows that shorter *L* results in a greater shrinkage. With increased *L*, shrinkage tends towards a steady value (0.8%).

7.2.3 Data fitting

As shown in Figure 7.4, the shorter hatch lines make the part denser and bring more serious shrinkage. With greater difference between the actual percentage shrinkage with the steady percentage shrinkage, the material caused by the shorter hatch lines becomes less homogeneous. To reduce this negative effect, short hatch lines should be avoided. Because the length of the hatch line affects the material homogeneity, the relationship between the hatch length and the material properties is first established by a suitable curve fitting. Several different curve models were considered. The inverse model curve with the best fitting result was finally adopted. The general equation of the inverse model is:

$$S = a + b / L + c / L^2 \tag{7.2}$$

where *a, b and c* denotes the unknown coefficients to be estimated. The fitted result has been found to be:

$$\boldsymbol{S} = 0.20496 + 28.40192/\boldsymbol{L} + 1.46881/\boldsymbol{L}^2 \tag{7.3}$$

where *S* denotes the percentage shrinkage and *L* denotes the length of the hatch line. The fitted curve is shown in Figure 7.2.

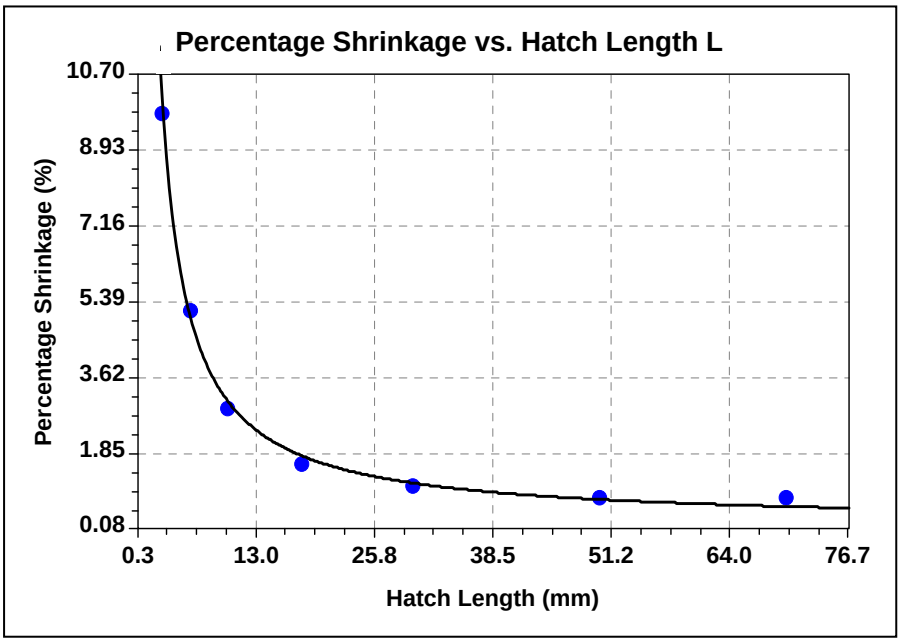

Figure 7.2 Inverse model relating percentage shrinkage and hatch length

Based on the achieved fitting function, the relevant effect *F* of the hatch length on the heterogeneity of each layer can be defined and estimated as follows:

$$\boldsymbol{F} = \frac{\sum_{\boldsymbol{i}=1}^{\boldsymbol{N}_{total}} ((0.20496 + 28.40192/\boldsymbol{L}_i + 1.46881/\boldsymbol{L}_i^2) - 0.8)}{\boldsymbol{N}_{total}} \tag{7.4}$$

where the value 0.8 denotes the steady percentage shrinkage. $\boldsymbol{N}_{total}$ denotes the total number of hatch lines in the layer.

7.3 Minimization of the Effect of Shorter Hatch Lines on Material Properties by GA Optimization

By optimizing the hatch direction for each sliced layer, the number of short hatch lines can be controlled.

For a given section of a layer, the hatch length can be significantly different with respect to the different hatching direction. As it is too complex to mathematically identify the hatch direction because of the variation in the layer geometry, an approach based on genetic algorithm (GA) is used. GA is a stochastic searching and optimization method based on the metaphors of natural biological evolution (Zalzala and Fleming, 1997). Because GA does not require derivative information or other auxiliary knowledge and only the objective function and corresponding fitness levels that influence the search (Zalzala and Fleming, 1997), it is suitable for use to solve this optimization problem.

The developed method was implemented using a C++ programming software package called GAlib from MIT (Matthew, 1999). GAlib is a set of genetic algorithm objects and includes tools for searching optimisation routines written in any C++ program.

7.3.1 Optimization procedure

The slicing software has been programmed in Visual C++(VC). The developed software can transfer the CAD models in STL format to the layer data required by the RP machine. To implement the optimization procedure, the system software calls the functions in GAlib.

A 3-D model is first pre-sliced and translated to 2-D layers with their contours recorded. GA is then applied to optimize the angle of the hatch direction, α, for each layer.

A real number genome, which is based on the hatch direction angle α, is used. Initially, the value of the genome α is randomly set to a value in the scale of (0, π). The objective function is defined by Equation (7.4) and used to evaluate the genome. The optimization is to find the hatch direction α that gives minimum F value. The value of F determines the fitness of individual value α for evolving. The smaller value of F represents a better result. A mutations factor is created by introducing random changes from a Gaussian distribution to the parent. New generations of hatch direction α are derived using the mutation operator based on the fitness value F. A stopping criterion is used to stop the run after the GA converges to within a specified tolerance of 0.01 for F value in 3 continuous generations, which means there is no further or only very little improvement. The procedure is depicted in Figure 7.3.

7.3.2 Case study

In this case, two rotor blades were built to study the effect of different hatch directions on the final part quality. The geometric shape of the blade is shown in Figure 7.4. Two parts were sliced with the same orientation in the *Y*-direction. But different hatch directions were applied to them. The hatch direction used in the first part was in the *X*-direction; the second one adopts the optimized direction that is in the *Z*-direction (vertical to the hatch direction of the first part). Both the rotor blades were built with identical process parameter settings. The two built parts are shown in Figure 7.5.

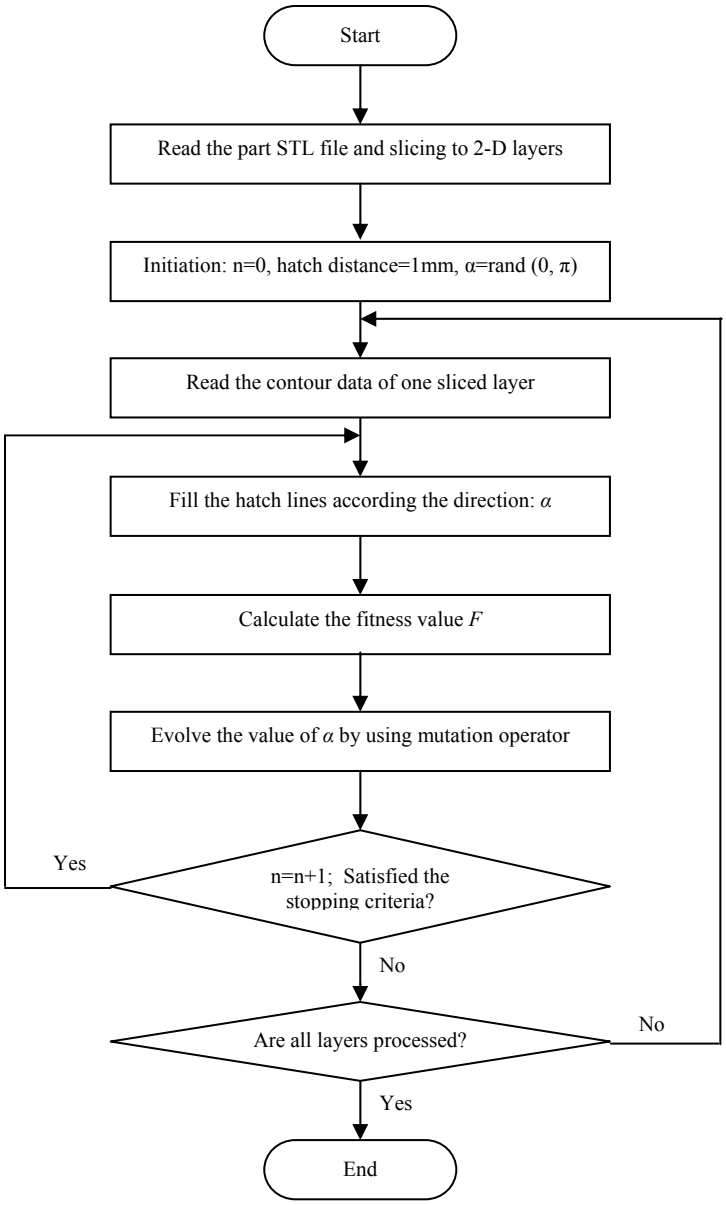

Figure 7.3 The process flow of the hatch direction optimization with GA

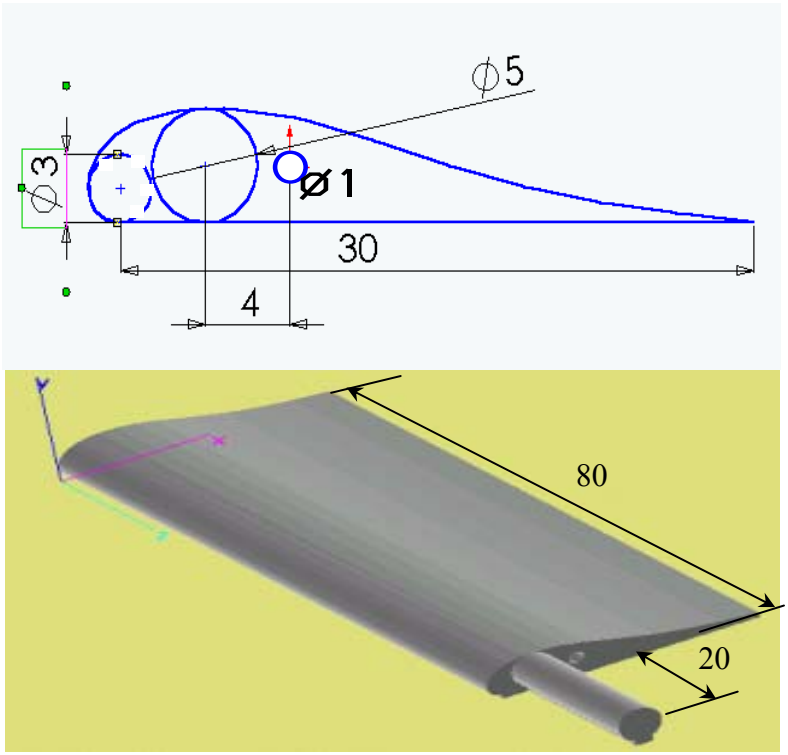

Figure 7.4 The geometric shape of the rotor blade

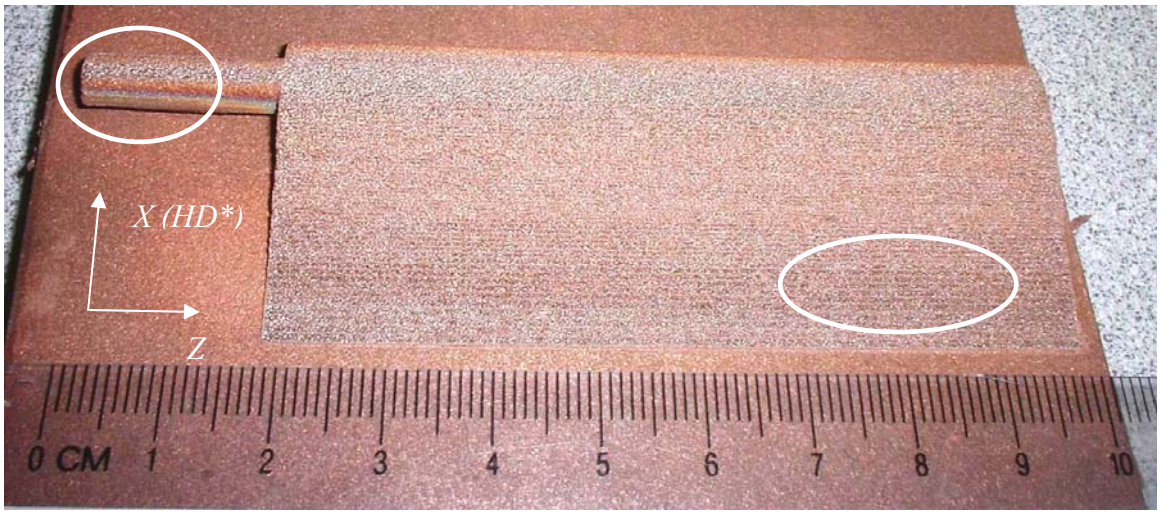

*HD: hatch direction.

(a)

(b)

Figure 7.5 Two blades built with different hatch directions (a) *X*-direction (without optimization). (b) *Z*-direction (with optimization)

The results show that the part (Figure 7.5 (b)) using the optimised hatch direction that can achieve long hatch lines and better surface quality without warpage phenomenon (Figure 7.5 (a)). In the first part (Figure 7.5 (a)), the handle of the rotor blade is warped around 1mm due to the occurrence of over-heating. This is due to the small diameter of the handle (only 5 mm) such that at each layer. The adjacent short hatch lines were sintered quickly, resulting in fast build-up of heat, and hence over-heating the small region. In addition, the surface roughness of the first case was worse than the second case (Ra=29.46μm vs. 21.71μm) since the material of the second part was more heterogeneous.

7.3.3 Case study 2 (by simulation)

To demonstrate the effectiveness of the aforementioned GA approach, a case based on an engine carburetor cover model with the size of 159.72 (width) x 130 (length) x 114.18 (height) mm was investigated. To limit the number of layers for illustration, the thickness of each layer was set at 5mm giving totally 23 layers. The 2-D contours

filled with hatch lines along the optimized directions are shown in figure 7.6. The top left one is the 3-D model of the engine carburetor cover. As the figure shows, the hatch directions were significantly different when the 2-D geometric shapes varied. To validate the optimization result of the GA algorithm, the F values based on the optimized direction α and those with a fixed direction (α=0) are compared and listed in Table 7.3. It can be seen that the effect factor F due to the short hatch of each layer can be reduced significantly. Therefore the effect of the short hatch lines on the quality of final parts can be reduced by minimizing the number of short hatch lines.

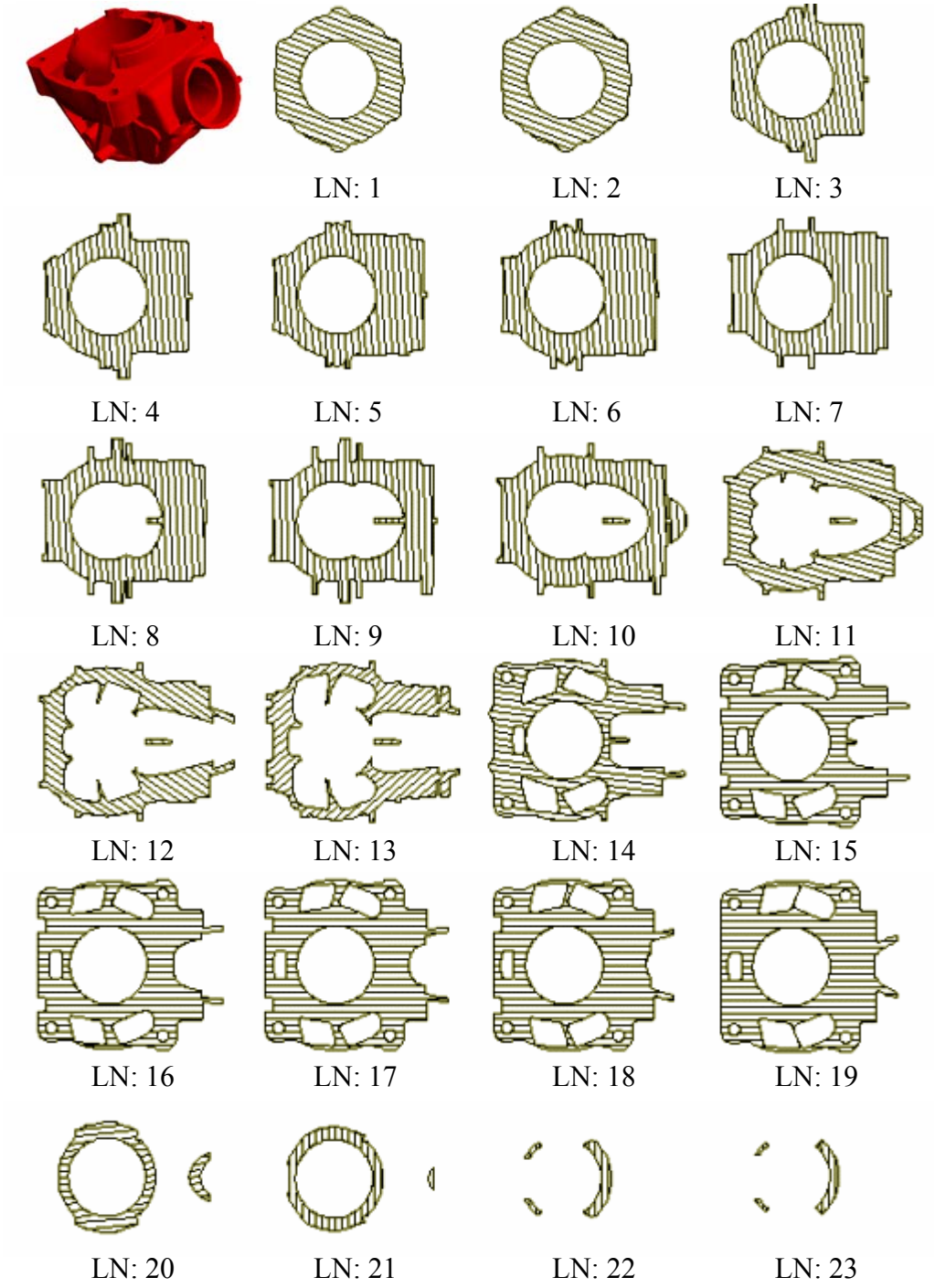

(*LN: Layer Number)

Figure 7.6 Case study: Optimised hatch direction for an engine carburettor cover

Table 7.3 Comparison of traditional method and the proposed optimisation method

Layer No.	$\alpha_{optimized}$	F Value	$\alpha_{traditional}$	F Value	Layer No.	$\alpha_{optimized}$	F Value	$\alpha_{traditional}$	F Value
#01	160	0.028	0	0.313	#13	41	0.508	0	0.547
#02	160	0.028	0	0.314	#14	173	0.166	0	0.206
#03	99	0.121	0	0.451	#15	180	0.125	0	0.125
#04	94	0.096	0	0.349	#16	180	0.066	0	0.066
#05	94	0.079	0	0.323	#17	180	0.050	0	0.050
#06	94	0.135	0	0.400	#18	180	0.036	0	0.036
#07	91	0.134	0	0.590	#19	180	0.030	0	0.030
#08	93	0.154	0	0.391	#20	6	0.438	0	0.528
#09	91	0.184	0	0.373	#21	90	0.467	0	0.788
#10	93	0.254	0	0.516	#22	89	1.152	0	5.743
#11	164	0.240	0	0.528	#23	91	1.321	0	6.543
#12	146	0.494	0	0.641					

7.4 Summary

In DMLS, varying lengths of the hatch line cause the built layer to be inhomogeneous. The quantitative relationship between the final quality of the part and its hatch lengths has been experimentally determined by measuring the different percentage shrinkage with the different hatch line lengths. The experimental results show that shorter hatch lines can affect the homogeneity of the properties to a great extent. To reduce this negative effect, a GA-based approach has been proposed to optimize the hatch direction based on different 2-D layer geometric shapes.

The GA based hatch optimisation method can select the hatch direction that reduces the negative effect of the short hatch lines effectively. The part homogeneity can be improved effectively based on different geometry shapes. However, it still cannot completely prevent short hatch lines, especially when the 2-D layer geometry has small independent features.

Chapter 8

Speed Compensation (SC) Method to Minimize the 2D Geometric Shape Effect on the Part Accuracy

8.1 Introduction

The effect of short hatch lines, which essentially causes short scanning intervals between each scan, results in higher and faster heat buildup in such a region. Hence, the energy absorbed in the short hatch lines should be reduced by setting different process parameters. As Equation (3.10) shows, the energy absorbed by the powder bed from laser radiation is determined by the process parameters of laser power, scan speed and beam diameter. To reduce the neighboring effect between hatch lines and attain more uniform temperature profile for the sintered powder, higher scan speed or lower laser power should have the same effect. Through controlling the scan speed and laser power separately or together, the negative neighboring effect can be compensated and consequently, the percentage shrinkage can be controlled to stay at similar level. In this stage of the work, the effect of scan speed is investigated. The optimization method of using different scan speed based on different hatch line lengths is proposed. Zhang *et al.* (2000) has quantified the variance of heat-affected zone (HAZ) at the cross-sectional area with two different scanning velocities by numerical and experimental methods. It provides a powerful support for the feasibility of using the scan speed to compensate the error caused by the geometric shape. The relationship between the scan speed and the percentage shrinkage is difficult to deduce directly because an accurate temperature vs. time curve is difficult to obtain. Many factors such as the environment, material, process parameters, etc. can affect

the temperature history. Some research works have been done on it (Zhang and Faghri, 1998; Kandis et al., 1999; Aditad and Jack, 1999) to build the mathematic model based on some assumptions. However, a generalized curve that can be well adopted according to the actually process situation for the adopted Cu-based material system has not been obtained so far. A more effective method to achieve the relationship is to use the experimental method combined with the statistical analysis.

8.2 Experimental Design and Analysis of Results

In order to build the relationship for different scan speeds with the hatch line length to the final accuracy, a series of cuboids with different length *L* have been built under different scan speed for the necessary data. The scan speed was set at 6 levels, according to a fixed interval in the accepted setting scale. The length of the cuboids was set at 7 levels that pay more attention on the short length not considered in the earlier researches. The value of each level is listed in Table 8.1. By a full combination of these different levels, totally 42 cuboids were built to help decide the relationship between the length *L* with the scan speed and the percentage shrinkage. All the other process parameters, including the laser power of 100W, hatch line distance of 0.2mm, and layer thickness of 0.1mm were kept unchanged.

Table 8.1 The parameter setting for the experiments

Level	1	2	3	4	5	6	7
ScanSpeed (mm/s)	100	124	148	172	196	220	N.A
Size (mm)	3x10	6x10	10x10	18x10	30x10	50x10	70x10

All of the 42 test cases were built thrice by the DMLS system. The length of the built part was measured using the Deltronic® MPC-5 System (Deltronic, 1998). The error

obtained for each case of nominal length *L* is based on the mean of the errors determined from the three built parts. The experimental results are shown in Table 8.2.

Table 8.2 The percentage shrinkage of the experiment parts

	SS*=100mm/s	SS=124mm/s	SS=148mm/s	SS=172mm/s	SS=196mm/s	SS=220mm/s
L=3mm	9.8%	7.5%	6.3%	5.0%	3.2%	1.9%
L=6mm	5.2%	3.3%	2.0%	2.0%	1.4%	1.0%
L=10mm	2.9%	1.9%	1.3%	1.2%	0.8%	0.5%
L=18mm	1.6%	1.2%	0.9%	1.0%	0.5%	0.4%
L=30mm	1.1%	0.8%	0.7%	0.6%	0.4%	0.3%
L=50mm	0.8%	0.7%	0.5%	0.5%	0.4%	0.3%
L=70mm	0.7%	0.7%	0.5%	0.5%	0.4%	0.3%

SS: Scan speed

The experimental results on the corresponding set of speed and length are shown in Figure 8.1. It can be seen that the percentage shrinkage of the materials under a fixed process parameter setting is different with the variance of hatch line length. As shown in the experimental results, when the length of hatch line is shorter, the percentage shrinkage is larger because of a higher sintering temperature attained. When the length of the hatch line exceeds a critical value, the percentage shrinkage tends to a stable value. This is due to the sufficiently long time for sintering the hatch line to allow the powder to cool down before it receives the succeeding energy as the laser scans the next hatch line. Hence the strategy to achieve the uniform percentage shrinkage is based on two principles:

- Using faster scan speed for the shorter hatch line region to reduce the energy buildup by reducing the duration of exposure to the laser energy.
- Using a fixed scan speed for the region where the lengths of the hatch lines inside it exceed the critical value.

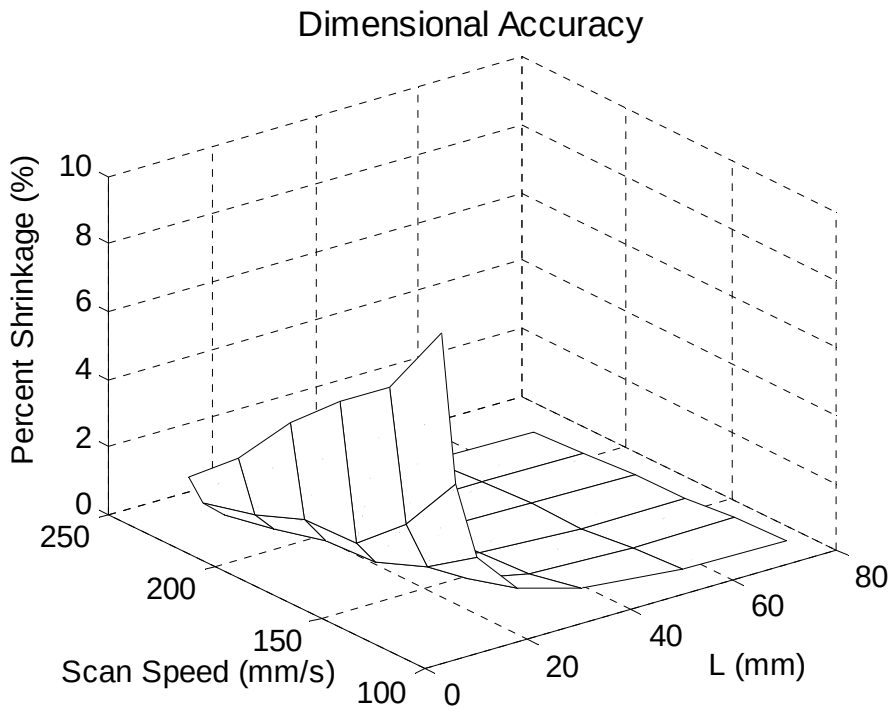

Figure 8.1 Percentage shrinkage with the change of scan speed and hatch line length *L*

8.3 Building the Relationship with the Response Surface Method (RSM)

To achieve the quantitative relationship between the two input variables: the scan speed and the hatch line length and the output variable: percentage shrinkage, the response surface methodology (RSM) was used. Response surface methodology is a collection of statistical and mathematical techniques useful for developing, improving, and optimizing processes (Box and Draper, 1987; Myers et al., 1995). The RSM can simulate the relationship between the input variable x and the response (output variable) y with a response function f.

$$y = f(x_1, x_2, ..., x_k) \tag{8.1}$$

where k denotes the total number of input variables.

In this research, the input variables are the scanning speed and hatch line length. The response is the percentage shrinkage. A second-order polynomial model is used,

which has been widely used in RSM for its flexibility in applications. The general equation (Myers et al., 1995) of the second-order model is:

$$y = \beta_0 + \sum_{j=1}^{k} \beta_j x_j + \sum_{j=1}^{k} \beta_{jj} x_j^2 + \sum_{i<j} \sum \beta_{ij} x_i x_j \tag{8.2}$$

where β denotes the unknown coefficient to be estimated.

The model performance can be evaluated by the Root-Mean-Square Error (RMSE) (see Equation 4.13). The prediction validity ν is denoted as:

$$\nu = (1 - RMSE) \times 100\% \tag{8.3}$$

The estimated result of the coefficient (the β 's) is achieved using the Matlab (Shapour et al., 2000) software tools. But the fitting result of directly using the second-order regressor is not good enough, as the RMSE error is 0.010879 and the prediction validity ν is 68.7%.

As shown in Figure 8.1, the response (percentage shrinkage) turns to a stable value following the increase of input variables. By a direct second-order polynomial model, the final fitting surface cannot achieve a stable value, so that a transformation is necessary. Because the reciprocal function has this property, we will take the reciprocals of the two input variables first. The transformation of the design variables from x to x^{-1} leads to a fairly good prediction, with an estimation error RMSE of 0.0024228 and the prediction validity ν 93.0%. The model with the transformed input variables has a significant improvement over the original model. The final response surface equation is shown below:

$$\begin{aligned} PS = & -0.003309 + 1.9275 \times \bar{x}_1 - 0.18679 \times \bar{x}_2 + 41.963 \times \bar{x}_1 \times \bar{x}_2 \\ & -129.29 \times \bar{x}_1^2 + 0.19092 \times \bar{x}_2^2 \end{aligned} \tag{8.4}$$

where $\bar{x}_1 = x_1^{-1}$; $\bar{x}_2 = x_2^{-1}$;

where PS is the percentage shrinkage with different values of the scan speed and the lengths of hatch lines.

From Equation (8.4), the critical length *Lc* can be determined. When *L>Lc*, the percentage shrinkage of the cuboids along the scan direction will be identical as the stable percentage shrinkage. Equation (8.4) can be used to derive the relationship between the length *L* and the scan speed for the stable percentage shrinkage. A speed compensation factor will be added to every hatch line with different lengths. When processing, the laser scan speed will be adjusted based on the hatch line length. It is easy to implement this technique because the laser system used for DMLS can set the scan speed directly.

8.4 Speed Compensation (SC) Algorithm

For the computation of the compensated scan speed value based on different hatch line length, the speed compensation (SC) algorithm involves:

Step 1. Decide the working scale of scan speed. For the Cu-based metal powder sintering used in this study, the laser scan speed can be set from 100mm/s to 250mm/s.

Step 2. Set the default scan speed. The default scan speed is the set value of the initial speed. It is the used speed value given by the system operator and is the same as the fixed speed without speed compensation.

Step 3. Calculate the stable percentage shrinkage in the default speed. To calculate the stable percentage shrinkage, the default value of speed setting will substitute the x_1 into Equation (8.4). By increasing x_2 (hatch line length), *y* (percentage shrinkage) will run to a stable value. This value is defined as the stable percentage shrinkage. For example, if the default scan speed is set to 220, the stable percentage shrinkage can be read from table 8.2 directly and is equal to 0.3%. The stable percentage shrinkage should be the same with the one achieved by the traditional method described in (Nelson et al., 1995) and used as the scaling factor to compensate the material shrinkage error during the whole process.

Step 4. Calculate the effective length of hatch lines on the same line in the scanning direction. The hatch line data will be read from sliced layer files. If there is only one hatch line on a line in the scanning direction, the effective length of the hatch line is just the distance between the start point and the end point of it. If there are more than one hatch vector on the same line in the scanning direction, the effective length of these hatch vectors is defined as the sum of all of their lengths. This is because there is no neighboring effect between these continuous hatch lines.

Step 5. Calculate the scan speed based on the effective length of hatch lines. To achieve the scan speed value of each hatch line, the stable percentage shrinkage is used as the *y* value in the Equation (8.4). The solution of scan speed (x_1) with different hatch line lengths can be achieved by solving the quadratic equation. If the solution is under the working range of scan speed, the solution will be set as the corrected speed value of the corresponding hatch line. If the solution is out of the range, the maximum speed allowed in the working range will be used. This is because

when the effective length of hatch lines is small enough, only by increasing the scan speed cannot make its macroscopical shrinkage reach the stable shrinkage value. In this situation, the relatively 'best' solution is to use the 'maximum' speed value for achieving the 'minimal' percentage shrinkage.

Step 6. End the process until all the hatch lines have their own corresponding speed value .The new hatch line data with the corresponding speed value will be saved and used to drive the laser system to build parts.

8.5 Case Study

As a metal prototyping part, the final part strength is concerned most by the customers. Normally, a slower scan speed results in a higher strength because more energy is absorbed by the loose metal powder. It leads to a higher density in the built part. Therefore the default speed value is set to 100mm/s for this study case. Other parameters are set as laser power 100W, hatch line distance 0.2mm, layer thickness 0.1mm, offset factor 0.235mm and scaling factor 0.8% (stable percentage shrinkage).

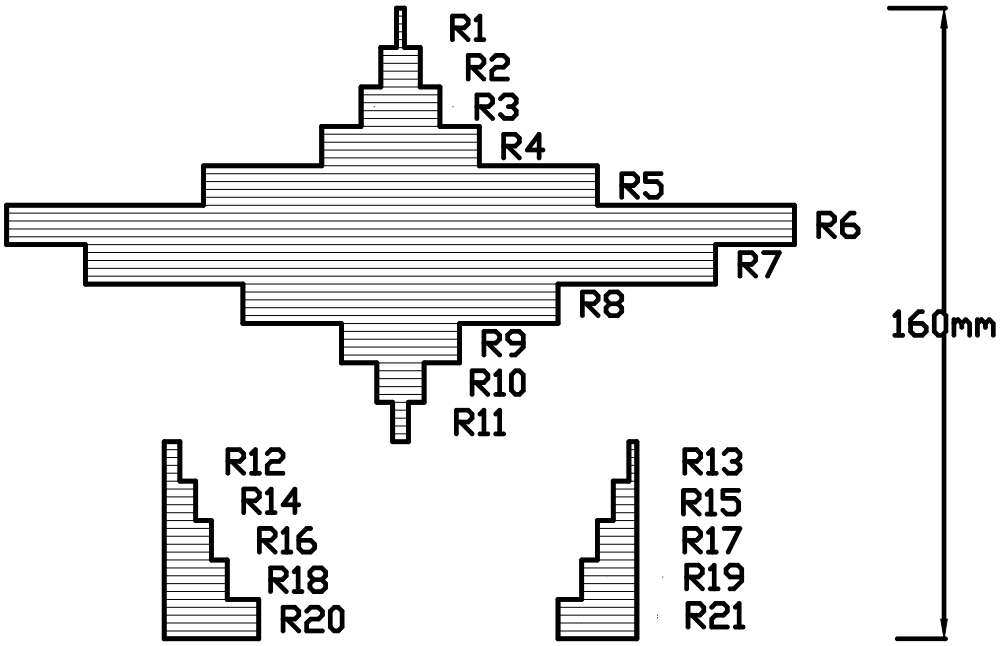

Figure 8.2 A benchmark part with nominal dimensions from 1 to 100 mm

Table 8.3 The scan speed set for different regions

Local Region	Hatch line Length (mm)	Optimized Speed (mm/s)		Local Region	Hatch line Length (mm)	Optimized Speed (mm/s)
R1	1	250		**R12**	2	250
R2	5	241		**R13**	1	
R3	10	198		**R14**	4	218
R4	20	165		**R15**	3	
R5	50	110		**R16**	6	194
R6	100	100		**R17**	5	
R7	80	100		**R18**	8	178
R8	40	128		**R19**	7	
R9	15	178		**R20**	12	160
R10	6	228		**R21**	10	
R11	2	250				

To prove that the SC method works effectively, a benchmark part (Figure 8.2) that has nominal dimensions from 1 to 100 mm (the regions with different hatch line lengths are indicated as R1 to R17 in Figure 8.2) was separately built by the traditional method and the new SC method. In the traditional method, the scan speed was kept constant during the whole process. For the part built by the new SC method, the corresponding scan speed for the local regions with different hatch line lengths from Equation (8.4) is listed in Table 8.3.

The comparison between the dimensional errors of the two parts is presented in Figure 8.3 (a) and (b), which show that with the fixed scan speed, much larger errors are obtained where the nominal dimensions are small. With SC, the errors for the parts with short nominal dimensions are reduced by as much as 40%, from a range of (–0.23 mm, 0.46mm) to (–0.21 mm, 0.25 mm). As can be seen in Figure 8.3, there is little difference in the errors for regions with larger dimensions.

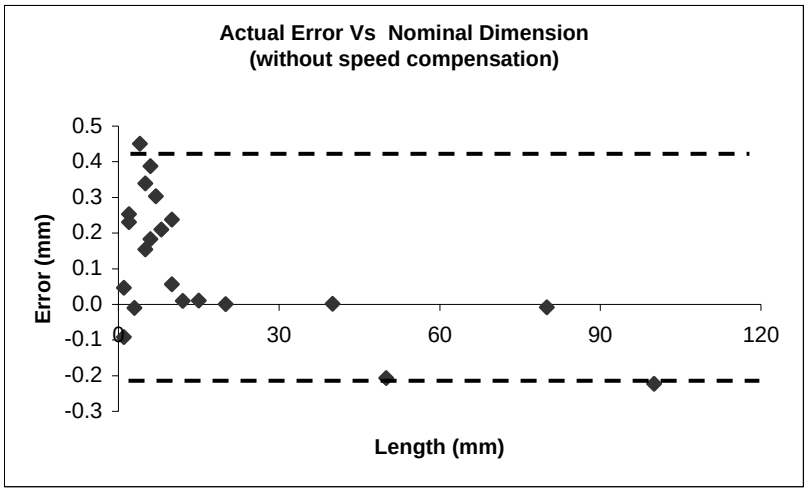

(a)

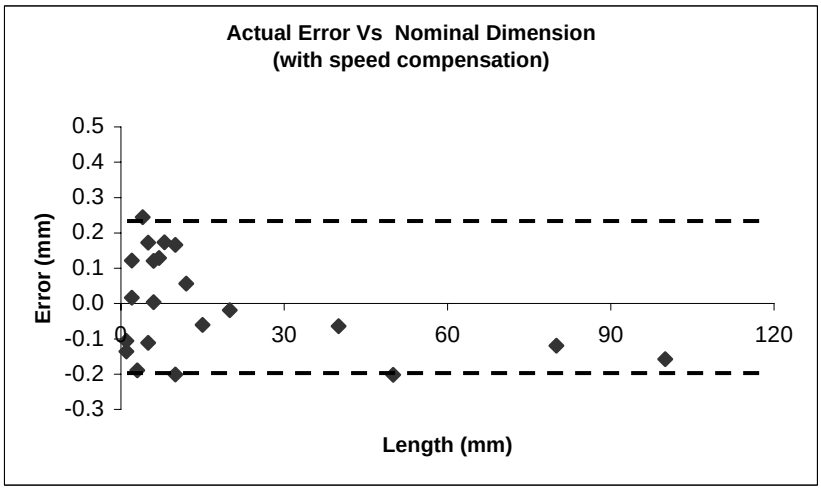

(b)

Figure 8.3 Error comparison by the traditional method (a) and the SC method (b) (The bottom and top dashes represent the positive and negative maximum errors)

8.6 Summary

In this chapter, a speed compensation (SC) method has been proposed to improve the dimensional accuracy. The case study with a benchmark part demonstrates that the new method can generate suitable speed settings for different geometry shapes, so as to increase the dimensional accuracy of the final part effectively. In future work, other process parameters, such as laser power, can be considered independently, or together with the scan speed, for possible further improvement on the dimensional accuracy.

Although this method has been developed based on the DMLS process, it is also applicable to other laser sintering processes. In future work, more experiments can be carried out for other laser sintering techniques.

Chapter 9

Conclusions

The aim of this research is to improve the performance of the DMLS process by optimizing and controlling the process parameters that affect the quality of the built part. The effects of the main process parameters on the sintered part quality, including scan speed, laser power, orientation, layer thickness and hatch space, have been studied based on the developed DMLS system.

9.1 Contributions

The main research contributions reported in this thesis are summarized as follow:

1) An Approach to Calibrate and Compensate the DMLS System

As a laser sintering process, the errors brought by the laser system have been analyzed systemically and the methods to compensate these errors are given, which reduce the possible errors caused by the laser system and improve the part accuracy.

2) An Intelligent Parameter Selection Approach

After fabrication, the four main resulting properties are processing time, mechanical strength, geometric accuracy and surface roughness. By using the experimental method, the effects of different parameters on these resulting properties have been derived qualitatively. The results indicate that the effects of different parameters on the part resulting properties are different from one another. An ideal parameter setting that can satisfy all the requirements does not exist. A feed-forward NN has been introduced to build a mapping between the goals in relation to the process parameters.

An intelligent parameter selection system has been implemented to determine the set of the parameters automatically based on different user requirements. It provides users a proper guidance and helps them to quickly realize their ideas on the requirements for a particular application.

The work in this research is of considerable importance since it derives the relationship between the process parameters and the final quality of the sintered part. The IPS method proposed is a promising tool to improve and control the resulting properties effectively and may make the DMLS process more automatic.

3) Identification and Determination of the Effect of Part Orientation and Geometry on Anisotropy and Heterogeneity

Different hatch directions usually result in different hatch line lengths, which consequently cause significant change in mechanical strength. However, the direct relationship between the hatch direction variation and the mechanical strength, particularly when the hatch line is kept unchanged, has not been investigated. In the experimental method proposed in this study, two groups of experiments were designed. The first group, Group A includes three cases with different orientations and hatch directions. In Group A, the specimens were built by the DMLS machine directly and the lengths of the hatch lines were different. The other group, Group B, was designed to remove the influence of material heterogeneity (caused by short hatch lines) on the mechanical properties. In Group B, a cuboid was first built. After the cuboid was built, it was cut to the standard specimen by using the wire cut electrical discharge machine (EDM). Also in Group B, the lengths of the hatch lines keep unchanged. Based on the experimental results, two findings can be summarized.

Firstly, although both the orientation and hatch direction affect the anisotropy, orientation has greater influence on the part strength. Secondly, the length of the hatch line also affects the part strength. The strength of the built part using short lines is larger than that using long hatch lines.

4) Development of an Approach to Improve the Material Homogeneity in the Sintering Process due to Different Geometric Shapes

During the sintering process, the material properties are heterogeneous even with a strict control on the process environment because of the variations in the geometric shapes. The different sintering time resulting from the change of geometric shapes causes non-uniform local temperature distribution. The change on the material melting time due to the different local temperature distribution affects the sintering rates and consequently the homogeneous properties of the material. Material heterogeneity is considered as a negative property because it is hard to control. Because a 2D geometric shape can be represented as a series of hatch lines that determine the laser scan paths, a series of experiments based on the different length of hatch lines have been designed and used to analyze the effect due to different geometric shapes. It was found that the shorter hatch lines resulted in more serious effects on the material homogeneity. Based on this finding, two methods are proposed to reduce the negative effect of short hatch lines. Firstly, a GA-based hatch direction optimization method has been proposed and used to reduce the number of short hatch lines. Next, a speed compensation method has been adopted to further reduce the effect of residual short hatch lines by dynamically adjusting the laser energy through controlling the scan speed. The methods given in this study have been proven to be effective in improving the part homogeneity.

Current research has been based on a developed Cu-based material under a specific working condition, but the methods mentioned are also applicable to other selective sintering laser process with different material systems because of similar working principles.

9.2 Future work

From the research work in this thesis, the following areas are suggested to further improve the part quality:

1) Study of the effect of material properties

The material property has an important influence on the resulting properties of the sintered part. Important material parameters, such as particle size, shapes, the content proportion of the binder and structure material, etc. should be optimized together with the process parameters studied in this research.

2) Development of the proposed IPS system by including other materials and RP technologies

Currently, the focus of the IPS system has been on the developed Cu-based material system. But it is applicable of other material systems such as metal, ceramic, polymer, sand, ABS as well as in other rapid prototyping systems using laser source in order to further perfect the IPS system. Different materials and RP technologies can change the part quality significantly. By including the factors of the different materials and RP technologies, the IPS system can more comprehensively cater to the different requirements and applications.

3) Improving the dimensional accuracy by considering the laser power in the speed compensation (SC) method

The proposed SC method only uses scan speed to compensate the neighboring effect. In the future work, other process parameters, such as laser power, should be considered together with the scan speed to further improve the dimensional accuracy.

4) Further mechanical part samples need to be tested to improve and verify the optimization ability with the algorithm developed

In this study, experimental data based on relatively simple test parts (in terms of material and geometry) were used to verify the algorithm and the underlying physics. More complex parts should be built to improve and verify the developed methods for future work.

Bibliography

1. Aditad, V. and Jack, B., “Process Maps for Laser Deposition of Thin-Walled Structures”, Solid Freeform Fabrication Proceedings, 1999, pp. 383-392
2. Agawals, M.K., Bourell, D.L., Beaman, J.J., Marcus, H.L. and Barlow, J.W., 1995, Direct selective laser sintering of metals. Rapid Prototyping Journal, Volume 1, Number 1, pp.26-36.
3. Ahn, S. H., Montero, M., Odell, D., Roundy, S., and Wright, P. K., “Anisotropic Material Properties of Fused Deposition Modeling (FDM) ABS”, Rapid Prototyping Journal, Vol. 8, (no. 4), 2002, pp. 248-257.
4. Amol G. and Richard C., Optimization of SLS Process Parameters using D-Optimality, Solid Freeform Fabrication Proceedings, 2003, pp. 348-362.
5. Andrew, C. L., David, W. R., The Effect Of Layer Orientation on The Tensile Properties of Net Shape Parts Fabricated in Stereolithography, Solid Freeform Fabrication Proceedings, 2003, pp. 289-300.
6. Andre L. Solidiform Inc, personal communication, June,1997.
7. ASTM, Standard Test methods for tension testing of metallic materials. Annual Book of ASTM Standards, ASTM Designation: E8-99, 1999.
8. Badrinarayan, B. and Barlow J.W., 1995, Effect of Processing Parameters in SLS of Metal-Polymer Powders, Solid Freeform Fabrication Proceedings, pp. 55-63.
9. Beaman, J. J, “Solid Freeform Fabrication, A New Direction in Manufacturing”, Kluwer Academic Publishers, Boston, MA, 1997.

10. Berzins, M., Childs, T. H. C., Dalgarno, K. W. and Stein G., "Densification and distortion in selective laser sintering of polycarbonate parts", Solid Freeform Fabrication Symposium, University of Texas, Austin, TX, pp. 196-203, 1995.
11. Box, G. E. P., and Draper, N. R., Empirical Model Building and Response Surfaces, John Wiley & Sons, New York, NY, 1987.
12. Cheng, W., Fuh. J. Y. H., Nee, A. Y. C., Wong, Y. S., Loh, H. T. and Miyazawa, T., "Multi-objective optimization of the part-building orientation in stereolithgraphy", Rapid Prototyping Journal, Vol. 1, No. 4, 1995, pp.12-23.
13. Choi S.H., Samavedam V., Visualisation of rapid prototyping, International Journal of Rapid Prototyping. 2001, v7 n2: 99-114.
14. Childs, T. H. C., Ryder, G. R. and Barzins, M. "experimental and theoretical studies of selective alser sintering", Rapid Product Development, Chapman and Hall, pp. 132-141, 1997.
15. Chiu, W K. Tan, S T, "Using dexels to make hollow models for rapid prototyping", Computer-Aided Design. v 30 n 7 Jun 1998. p 539-547.
16. Clemson University, Build-time estimate program "Slitime" released by Clemson University, Clemson, South Carolina, 1994.
17. Corbel, S., Hinczewski, C. and Chartier, T., Mechanical Properties of Ceramic Parts Made by Stereolithography and Sintering Process, European conference on rapid prototyping and manufacturing, pp. 115-123, 1999.
18. Cormier, D., Unnanon, K. and Sanii, E., "Specifying non-uniform cusp height as a potential aid for adaptive slicing", Rapid Prototyping Journal, Vol. 6, No. 3, 2000, pp. 204-211.
19. Dai, K., Crocker, J., Shaw, L., and Marcus, H., "Finite Element Analysis of the SALDVI Process", Solid Freeform Fabrication Proceedings, 2000, pp. 393-398.

20. David C.T., Richard H.C., Optimizing Part Quality with Orientation Solid Freeform Fabrication Proceedings, 1995, pp. 362-368.
21. DELTRONIC Corp, Deltronic MPC-5 user manual, CA, 1998.
22. Dolenc, W. and Makela, I., “Slicing procedure for layered manufacturing techniques”, Computer-Aided Design, Vol. 26, No. 2, 1994, pp.119-126.
23. Frank, D., Fadel, G., "Expert system based selection of the preferred direction of build for rapid prototyping processes", Journal of Intelligent Manufacturing, 6, 339-45,1995.
24. Frigon, N. L., and Mathews, D., Practical Guide to Experimental Design, John Willey &Sons, Inc Press, 1997, pp.137.
25. Fu, L.M., Neural Networks In Computer Intelligence, McGraw-Hill, Inc. Press, 1994.
26. German, R. M., Liquid Phase Sintering, Plenum Press, New York, 1985.
27. German, R.M., Powder Metallurgy Science, Second Edition, Metal Powder Industries Federation Press, Princeton, NJ, 1994.
28. Gibson, I. and Shi, D. P., Material Properties and Fabrication Parameters in Selective Laser Sintering Process, Rapid Prototyping Journal, v 3 n 4 1997, p 129-136.
29. Guduri, S., Crawford, R.H. and Beaman, J.J., "Direct generation of contour files from constructive solid geometry representations", Solid Freeform Fabrication Proceedings, Austin, TX, 1993, pp. 291-302.
30. Haase. P, “selective laser sintering of metal powders”, MS thesis, Univ. of Texas at Austin, 1989.
31. Haykin, S., Neural Networks, A Comprehensive Foundation, Prentice Hall International, Inc. Press, Second Edition,1999, p. 2 & p. 167.

32. Instron Corp, Manual of Instron model 8501 dynamic testing system, US, 1990.
33. Isaac, M. D. and Ori, I., "Engineering Mechanics of Composite Materials", Oxford University Press, Inc., 1994.
34. Jacobs, P.F., "The Effects of Shrinkage Variation On Rapid Tooling Accuracy", Materials & Design. v 21 n 2 Apr 2000. p 127-136.
35. Jacobs, P., Rapid Prototyping & Manufacturing: Fundamentals of Stereolithography, SME, MI, 1992.
36. JESL Corp, Instructions of JSM-5500 Scanning Electron Microscope, Japan, 1999.
37. Kamash, T., and Flynn, D., Build Time Estimator for Stereolithography Machines – A Preliminary Report, report released by Prototype Express, Schaumburg, IL,1995.
38. Kamesh T., Georges F., Amit B., and Nadim A., "Efficient slicing for layered Manufacturing," Rapid Prototyping Journal, Volume 4, Number 4, 1998.
39. Kandis, M. Buckley and Bergman T. L., "Observation, Prediction and correlation of geometric shape evolution induced by Non-isothermal sintering pf polymer powder", ASME J, Heat Transfer, 119, pp. 824-831, 1997.
40. Kandis, M., Buckley, C. W. and Bergman T. L., "An engineering model for laser-induced sintering of polymer powders", Journal of Manufacturing Science & Engineering, Transactions of the ASME. v 121 n 3 1999. p 360-365
41. Kechagias, J., Anagnostopoulos, V., Zervos, S., and Chryssolouris, G., Estimation of Build Times in Rapid Prototyping Processes, Proceedings of the 6th European Conference on Rapid Prototyping & Manufacturing, July 1997 Nottingham, UK, 137-148.
42. Kruglinski, D. J., Inside Visual C++, Microsoft Press, 4th Edition, 1997.

43. Kulkarni, P. and Dutta, D., “Adaptive slicing for parametrizable surfaces for layered manufacturing”, Proceedings of ASME Design Automation Conference, Boston, MA, 17-20 Sep. 1995, pp. 211-217.
44. Laoui, T., Froyen, L., Kruth, J.P., "Influence of powder parameters on the selective laser sintering of tungsten carbide-cobalt", Proceedings of the 7th European Conference on Rapid Prototyping & Manufacturing, Aachen, Germany, July 7-9, 1998, pp. 271-279.
45. Lin, F., Sun, W., and Yan, Y., A Decomposition-accumulation Model for Layered Manufacturing Fabrication, Rapid Prototyping Journal. v 7 n 1, 2001, p 24-31.
46. Manetsberger, K., Shen, J., and Muellers, J., “Compensation of Non-Linear Shrinkage of Polymer Materials in Selective Laser Sintering”, Solid Freeform Fabrication Proceedings, pp. 346-356, 2001.
47. Manriquez-Frayre, J. A., and Bourell, D. L., “Selective Laser Sintering of Cu-Pb/Sn Solder Powders”,The University of Texas at Austin, Solid Freeform Fabrication Proceedings, 1991, pp. 236-244.
48. Matthew, W., “Galib: A C++ Library of Genetic Algorithm Components”, http://lancet.mit.edu/ga/, 1999.
49. McClurkin, J.E., and Rosen, D.W., “Computer-aided build style decision support for stereolithography,” Rapid Prototyping Journal, Volume 4, Number 1, 1998, pp. 4-13.
50. Miller, D., Deckard, C., Williams, J., “Variable beam size SLS workstation and enhanced SLS model” Rapid Prototyping Journal. v 3 n 1 p 4-11, 1997.

51. Myers, Raymond H. and Douglas C. Montgomery. Response Surface Methodology: Process and Product Optimization Using Designed Experiments. New York: John Wiley and Sons, 1995.
52. Nelson, J.C., “Selective laser sintering: a definition of the process and an empirical sintering model”, PhD dissertation, Univ. of Texas, Austin, TX, 1993.
53. Nelson, J., Xue, S., Samuel. Barlow, J. W., Beaman, J. J., Marcus, H. L., Bourell, D. L., “Model of the selective laser sintering of bisphenol-A polycarbonate” Industrial & Engineering Chemistry Research, v 32 n 10, pp. 2305-2317,1993.
54. Nelson, J.C., McAlea, K., amd Gray, D., "Improvements in SLS Part Accuracy", Solid Freeform Fabrication Symposium Proceedings, The University of Texas, Texas, pp. 159-169, 1995
55. Nikolay K. T., Maxim K. A., Andrey V. G., Victor, I. T., Tahar L. and Ludo F., “Mechanisms of selective laser sintering and heat transfer in Ti powder”, Rapid prototyping journal, V9, N5, pp. 314-326, 2003.
56. Parker, D.B., 1974, Beyond regression, new tools for prediction and analysis in the behavioural science, Ph.D. thesis, Harvard University.
57. Qiu D., Langrana N.A., Danforth S. C., Safari A., and Jafari M., Intelligent Toolpath for Extrusion-based LM Process, Rapid Prototyping Journal, v 7 n 1, 2001, p 18-23.
58. Richard, H. C., Computer Aspects of Solid Freeform Fabrication Geometry, Process Control, and Design, Solid Freeform Fabrication Proceedings, 1993, pp. 102-112.
59. Rajan, V.T., Vijay S., Konstantinos A. T., 2001 The Optimal Zigzag Direction for Filling a Two-dimensional Region, Rapid Prototyping Journal, v 7 n 5 p 231-241.

60. Rock, S.J. and Wozny, M.J., "A flexible file format for solid freeform fabrication", Solid Freeform Fabrication Proceedings, Austin, TX, 1991, pp. 1-12.
61. Roman, S. Access DatabaseDesign & Programming, 2nd edition. O'Reilly & Associates,1999.
62. SCANLAB GMBH, Installation and Operation, PC Real Time Control Board RTC2, for Scan Head and Laser Control in Time, 1998.
63. Shapour, A., Balakumar, B., James, D., Keith, H. and Gregory, W., An Engineer's Guide to MATLAB Edward B. Magrab, Prentice Hall, 2000.
64. Stuttgart Neural Network Simulator (SNNS) user manual, version 4.1, University of Stuttgart. Institute for Parallel and Distributed High Performance Systems (IPVR), 1995.
65. Subramanian, P.K., Vail, N.K., Barlow, J.W., and Marcu, H.L., Anisotropy in Alumina Produced by SLS, Solid Freeform Fabrication Proceedings, 1994, pp. 330-338.
66. Suh, Y.S. and Wozny, M.J., “Adaptive slicing for solid freeform fabrication processes”, Solid Freeform Fabrication Symposium 1993, University of Texas, Austin, August 1993, pp. 404-410.
67. Sun, M. M., and Beaman, J. J., 1995, ‘‘A Three Dimensional Model for Selective Laser Sintering,’’ Proceedings of Solid Freeform Fabrication Symposium 1995, pp. 102–109.
68. Synrad Inc., “Series Lasers, Operation and Service Manual”, Japen, 1999.
69. Tang, Y. X., Loh, H. T., Fuh, Y. H. J., Wong, Y. S., Lu, L., Ning, Y., amd Wang, X.H., “Accuracy Analysis and Improvement for Direct Laser Sintering”, SMA Annual Symposium 2004, January 2004, Singapore.

70. Tontowi, A.E. and Childs, T.H.C., Density Prediction of crystalline Polymer Sintered Parts at Various Powder Bed Temperatures (Selective Laser Sintering Case), Rapid Prototyping Journal, Vol.7, No.3, 2001, pp.180-184.
71. Thümmler, F., and Oberacker, R., Introduction to Powder Metallurgy, Institut of Materials, London, 1993.
72. Tsai S. W. and Wu E. M., A general theory of strength for anisotropic materials, journal of composite materials, 5:58-8-, 1971.
73. Tyberg, J. and Bohn, J. H., Local adaptive slicing, Rapid Prototyping Journal, Vol. 4, No. 3, 1998, pp.118-127.
74. Vuyyuru, P., Kirschman, C., Fadel, G.M., Bagchi, A. and Jara-Almonte, C., "A NURBS based approach for rapid prototyping realization", proceedings pf Fifth International Conference on Rapid Prototyping, Dayton, OH, 1994, pp. 229-40.
75. Werbos, P.J., 1985, Learning logic. Technical Report TR-47, Cambridge, MA.
76. Weissman, E. M., and Hsu, M. B., (1991), " A finite element model of multi layered laser sintered part"' Solid Freeform Fabrication Proceedings, Univ. of Texas at Austin, TX, pp. 86-93.
77. Whitehouse. D.J., Handbook of Surface Metrology, Institute of physics publishing, Bristol, UK, 1994.
78. Williams, J.D., and Deckard, C.R., "Advances in modeling the effects of selected parameters on the SLS process," Rapid Prototyping Journal, Volume 4, Number 2, 1998, pp. 90-100.
79. Williams, J.D., Miller, D., and Deckard, C.R, 1996, ''Selective Laser Sintering Part Strength as Function of Andrew Number, Scan Rate and Spot Size,'' Proceedings of Solid Freeform Fabrication Symposium 1996, pp. 549–557.

80. Willems, N., Easley, J. T. and S. T. Rolfe. Strength of Materials. pp. 72-73. New York: McGraw-Hill. 1981.

81. Wohler, RP report, 2001, Volume 7, P7.

82. Wang, X. W., “Calibration of shrinkage and beam offset in SLS process” Rapid Prototyping Journal. v 5 n 3 1999. p 129-133.

83. Xu, F., Wong, Y. S., Loh, H. T., Fuh, J. Y. H. and Miyazawa, T., “Optimal orientation with variable slicing in stereolithgraphy”, Rapid Prototyping Journal, Vol. 3, No. 3, 1997, pp.76-88.

84. Yu, G.B., and Noble, D., “The development of a laser build-time calculation program using stereolithographic apparatus (SLA)”, Proceedings of the 2nd European Conference on Rapid Prototyping and Manufacturing, The University of Nottingham, 15-16 July 1993.

85. Zhang, Y. W. and Faghri, A., "Melting and Resolidification of a Subcooled Mixed Powder Bed with Moving Gaussian Heat Source," ASME J. Heat Transfer, Vol. 120, No. 4, pp. 883-891, 1998.

86. Zhang, Y. W., Faghri, A., Buckley, C.W., and Bergman, T.L., “Three-Dimensional Sintering of Two-Component Metal Powders with Stationary and Moving Laser Beams”, ASME J. Heat Transfer, Vol. 122, No. 1, pp. 150-158, 2000.

87. Zalzala, A. M. S. and Fleming, P. J., “Genetic Algorithms in Engineering systems”, London, The Institution of Electrical Engineers, 1997.

88. Zeng, D. L. Powder Metallurgy Materials. Powder Metallurgy Press., Peiking, 1989.

89. Zhu, H. H., “Material and processing on direct laser sintering of Cu-based metallic powder”, PH.D thesis, Natoional Univ. of Singapore, Singapore, 2004.

90. Ziemian, C. W. and Crawn III, P. M., “Computer aided decision support for fused deposition modeling”, Rapid Prototyping Journal, Vol. 7, No. 3, 2001, pp.138-147.

List of Related Publications

Journal publication

1. Y. Ning, J.Y.H. Fuh, Y.S.Wong and H.T. Loh, “An intelligent parameter choosing system for the Direct Metal Laser Sintering (DMLS) Process”, International Journal of Production Research, Volume 42, Issue 1, pp183-200, 2004.

2. Y. Ning, Y.S. Wong and J.Y.H. Fuh, “An Approach to Minimizing Geometric Shape Effect on Part Accuracy in Selective Laser Sintering”, IEEE Transactions on Automation Science and Engineering, under revision (conditionally accepted), 2004.

3. Y. Ning, Y.S.Wong and J.Y.H. Fuh, **“**Effect and Control of Hatch Length on Material Anisotropy and Heterogeneity in Selective Laser Sintering”, Proceedings of the Institution of Mechanical Engineers Part B -Journal of Engineering Manufacture (IMechE), Accepted, 2004.

Conference publication

1. Y. Ning, J.Y.H. Fuh, Y.S. Wong and H.T. Loh, "Application of Feed-forward Neural Network to Predict resulting properties from Direct Metal Laser Sintering Process ", Proceedings of the 30th International Conference on Computer & Industrial Engineering, June 28-July 2,2002, Tinos Island, Greece.

2. Y. Ning, J.Y.H. Fuh, Y.S. Wong and H.T. Loh, "Process Parameter Optimization Using a Feed-forward Neural Network for Direct Metal Laser Sintering Process", Proceedings of the International Conference on Manufacturing Automation (ICMA 2002), December 10-12, 2002, Hong Kong, China.

3. Y. Tang, H. T. Loh, J. Y. H. Fuh, Y. S. Wong, L. Lu, Y. Ning, X. Wang, “Accuracy Analysis and Improvement for Direct Laser Sintering”, SMA Annual Symposium 2004, January 2004, Singapore.

Appendix

(i) Calculated Calibration Factor K_{xave}^{1}

L / *y*-axis	80	70	60	50	40	30	20	10
-80	265.66	265.73	265.80	265.73	265.46	265.80	265.67	265.44
-70	265.51	265.70	265.80	265.70	265.79	265.79	265.73	265.52
-60	265.64	265.71	265.63	265.64	265.82	265.76	265.81	265.63
-50	265.60	265.70	265.76	265.81	265.79	265.83	265.57	265.68
-40	265.56	265.59	265.77	265.70	265.81	265.64	265.69	265.60
-30	265.61	265.75	265.74	265.77	265.64	265.83	265.72	265.76
-20	265.67	265.57	265.52	265.74	265.79	265.80	265.68	264.68
-10	265.48	265.67	265.80	265.71	265.76	265.78	265.26	265.76
0	265.77	265.55	265.43	265.63	265.81	265.77	265.81	265.76
10	265.61	265.69	265.72	265.72	265.71	265.79	265.35	265.71
20	265.77	265.78	265.68	265.65	265.63	265.75	265.64	265.73
30	265.75	265.76	265.60	265.46	265.79	265.82	265.80	265.49
40	265.66	265.73	265.72	265.75	265.78	265.74	265.75	265.73
50	265.76	265.76	265.48	265.63	265.63	265.77	265.68	265.76
60	265.82	265.67	265.81	265.81	265.77	265.72	265.57	265.65
70	265.69	265.82	265.69	265.72	265.76	265.80	265.57	265.20
80	265.61	265.69	265.66	265.77	265.65	265.80	265.80	265.36
							K_{xave}^{1} = 265.69	

(ii) Calculated Calibration Factor K_{yave}^{1}

L / *x*-axis	80	70	60	50	40	30	20	10
-80	264.67	264.75	264.37	264.30	264.55	265.46	240.30	271.94
-70	264.39	264.57	264.00	264.00	264.38	264.59	266.16	267.15
-60	264.32	264.18	264.30	264.03	264.15	264.81	264.97	265.99
-50	264.23	264.42	264.30	264.22	264.56	264.66	265.39	264.00
-40	264.31	264.24	264.03	264.43	264.05	264.13	264.32	264.58
-30	264.18	264.34	264.29	264.48	263.93	264.80	265.15	266.05
-20	264.25	263.99	264.08	264.26	264.26	264.42	264.49	264.05
-10	264.13	264.35	264.35	264.55	264.15	264.51	264.05	264.45
0	264.27	264.49	264.33	264.35	264.03	264.26	264.18	264.50
10	264.38	264.43	264.42	264.34	264.09	264.79	264.67	265.91
20	264.32	264.73	264.08	264.61	264.06	264.49	265.15	265.97
30	264.18	264.61	264.21	264.57	264.27	264.15	265.22	264.91
40	264.31	264.54	264.24	264.42	264.52	264.76	264.44	265.98
50	264.27	264.54	264.36	264.56	264.51	264.50	264.77	264.21
60	264.27	264.54	264.01	264.41	264.40	264.80	264.37	267.50
70	264.34	264.66	264.38	264.73	264.87	264.60	264.74	264.50
80	264.22	264.55	264.35	264.05	264.30	264.36	264.89	268.51
							K_{yave}^{1} = 264.64	